ISBN 978-82-471-1213-7 (printed ver.)
ISBN 978-82-471-1214-4 (electronic ver.)
ISSN 1503-8181

NTNU
Norwegian University of
Science and Technology

Theses at NTNU, 2008:259

NTNU
Norwegian University of
Science and Technology

Thesis for the degree of
philosophiae doctor
Faculty of Engineering Science and Technology
Department of Marine Technology

Doctoral Theses at NTNU, 2008:259

Mateusz Graczyk

Experimental Investigation of Sloshing Loading and Load Effects in Membrane LNG Tanks Subjected to Random Excitation

Mateusz Graczyk
Doctoral Thesis

Mateusz Graczyk

Experimental Investigation of Sloshing Loading and Load Effects in Membrane LNG Tanks Subjected to Random Excitation

Thesis for the degree of philosophiae doctor

Trondheim, October 2008

Norwegian University of
Science and Technology
Faculty of Engineering Science and Technology
Department of Marine Technology

NTNU
Norwegian University of
Science and Technology

NTNU
Norwegian University of Science and Technology

Thesis for the degree of philosophiae doctor

Faculty of Engineering Science and Technology
Department of Marine Technology

ISBN 978-82-471-1213-7 (printed ver.)
ISBN 978-82-471-1214-4 (electronic ver.)
ISSN 1503-8181

Theses at NTNU, 2008:259

Printed by Tapir Uttrykk

Abstract

Loads and load effects due to sloshing in LNG membrane tanks are investigated. Sloshing is a resonant phenomenon of a violent fluid motion and occurs in partially filled tanks.

In order to determine characteristic design parameters due to sloshing load a multistep procedure needs to be followed. This involves the long-term randomness of sea environment, ship motion in waves, fluid motion and pressures induced in tanks, structural response and assessment of the structural capacity.

Various issues within this procedure are addressed in this work. It is focused on the development of procedures for performing and analyzing sloshing experiments, studying sloshing-induced pressures in tanks as well as investigating structural response of the containment system. Analytical, numerical and experimental techniques are combined.

In current design practice sloshing pressures, given the motion histories of the tank, need to be obtained experimentally. Therefore, an important part of this work is sloshing experiments, performed by means of a sloshing rig at MARINTEK. The rig enables manipulating a tank model so that a ship motion in waves is represented. Pressures on an internal surface of the tank are measured. The tank walls are transparent, hence, visual inspection and video recording are also performed.

The long-term stochastic description of sloshing phenomenon involves an interaction between wave excitation, ship motion and fluid motion. The analysis is focused on determining a simplified method for estimating sloshing response that is sufficiently accurate to correctly identify the critical sea states. Sloshing response is then expressed in terms of an approximate measure which may be analyzed by a usual linear long-term analysis. This approach is also utilized for determining representative conditions for laboratory tests.

The applicability of two statistical models to represent the short-term pressure magnitude is studied and the variability of estimates is discussed. Techniques for representing pressure time histories in a simplified manner are revised and the importance of local effects in time histories is investigated. Moreover, parameters of pressure time-histories that are crucial for structural response are identified. Load duration and rise time as well as its spatial concentration are required for determining the design sloshing load. Qualitative characteristics of pressure in various conditions and filling levels are found. Scaling issues are also investigated with regard to gas compressible effects.

Insulation of membrane LNG tanks is in direct contact with the cargo. Use of non-standard materials and complex structural arrangement make the structural response very different from the response of a steel panel. Sensitivity studies both in terms of temporal and spatial load distribution are performed. Modal composition of the response as well as patterns of static and dynamic responses and their characteristic values are studied. The suitability of simplified methods for dynamic response analysis is assessed.

As the duration of sloshing pressure is similar to the natural period of the structure, hydroelasticity may become important. The effect of the fluid-structure interaction is assessed by an analytical method. This is done by utilizing a simplified structural and hydrodynamic representation.

The effect of the global behaviour of LNG membrane ships on the tank pressure is also considered. Hull elasticity and nonlinear effects are assessed by investigating the vertical bending moment and the vertical acceleration.

Acknowledgements

This work has been performed under supervision of Prof. Torgeir Moan. I would like to thank him for the professional guidance and support.

A number of other scientists from both the Department of Marine Technology, the Centre for Ships and Ocean Structures, and MARINTEK helped me at different stages of this work. I want to thank Prof. Arvid Næss and Prof. Odd Faltinsen for their valuable discussions on statistical and hydrodynamic analyses, respectively.

I wish also to thank Dr. Olav Rognebakke and Joachim Allers for assistance with preparing experiments and Dr. Jan Roger Hoff for helping me develop tools for analysing experimental data.

Many thanks go to colleagues and friends at the department and at the Centre who made the studies something more than just hard work.

I want also to express my gratitude and love to my wife Barbara and daughter Maja, who accepted my absences from home-life, but also supported and motivated in the moments of doubt.

My research was supported financially by the Research Council of Norway and the Centre for Ships and Ocean Structures.

Mateusz Graczyk

Trondheim, 09.09.2008

Contents

I Theoretical background **1**

1 Introduction **3**
1.1 Background . . . 3
1.1.1 Characteristics of natural gas and transport solutions . . . 3
1.1.2 History, characteristics and prospects for gas shipping . . . 4
1.1.3 Tank systems for gas transport . . . 6
1.1.4 Structural issues of LNG carriers . . . 8
1.2 Objective and outline of the thesis . . . 11

2 Analysis of sloshing in LNG tanks **15**
2.1 The sloshing phenomenon . . . 15
2.2 Analysis of sloshing in membrane tanks . . . 20
2.3 Sea climate variability . . . 20
2.4 Analysis of ship response . . . 24
2.5 Fluid motion and pressures in a tank . . . 27
2.5.1 Analytical methods . . . 27
2.5.2 Numerical methods . . . 29
2.5.3 Experimental methods . . . 31
2.5.4 Post-processing of experimental results . . . 35
2.6 Structural response . . . 37

3 Concluding remarks **45**
3.1 Original contributions . . . 45
3.2 Recommendations for further work . . . 47

References **56**

A Sloshing experiments **57**

B Post-processing of experimental results **63**

C Frequency of compressible oscillations of a gas pocket **67**

II Articles **71**

Part I

Theoretical background

Chapter 1

Introduction

1.1 Background

1.1.1 Characteristics of natural gas and transport solutions

The production of the natural gas is the third biggest among energy sources, after oil and coal. However, in this decade gas production is expected to exceed coal production (RINA, 2004; Gastech, 2005; RINA, 2006).

The natural gas is a gaseous fossil fuel obtained by exploring oil fields or separate natural gas fields. It is also found in smaller quantities in coal beds. The natural gas consists of approximately 95% methane, (CH_4), with small amounts of other hydrocarbons - ethane (C_2H_6), propane (C_3H_8) and butane (C_4H_{10}) as well as nitrogen (N_2). The gas is colourless, odourless, non-toxic, non-carcinogenic and lighter then air (approx. 50% density of air).

Since the location of the natural gas reserves and production areas do not overlap with those where the consumption is largest, a need of transporting the gas arises. Concentration of worldwide natural gas reserves is presented in Figure 1.1. The consumption is largest in USA, Japan and Europe.

There are two common ways of long distance transport of natural gas: by pipelines (currently approximately 75% of volume) or by vessels. The latter method presently refers only to transportation of the gas in the liquid form (Liquefied Natural Gas - LNG) but new solutions emerge. They include gas transport in liquid pressurized form (Pressurized Liquefied Natural Gas - PLNG), in pressurized form (Pressurized Natural Gas - PNG, or Compressed Natural Gas - CNG) or in solid form, as pellets (Natural Gas Hydrate - NGH). Other solutions are to produce the electricity (HVDC) or Gas-to-Liquids (GTL) technology allowing transformation of the gas by chemical gas conversion processes into hydrocarbon liquids suitable for shipping via conventional tankers, methanol for shipping in bulk chemical carriers or pressurized LPG type liquids.

Choice of the solution is dependent on economic conditions, specifically on the distance to the market and production capacity. In some cases the natural gas cannot be profitably utilized. Then it is often re-injected into the ground for later recovery (Underground Gas Storage - UGS). This solution facilitates oil pumping by keeping

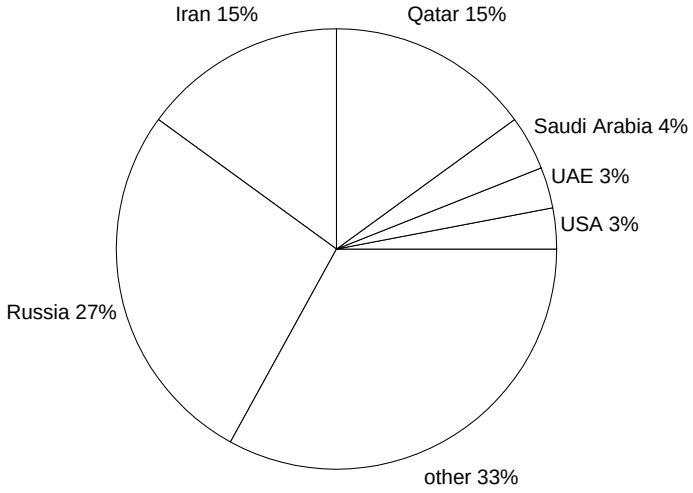

Figure 1.1: Worldwide reserves of the natural gas.

underground pressures higher. Burning the gas (so-called flared gas) is now forbidden in many countries. This is waste of the resources and an environmental danger due to the greenhouse effect.

Shipping the natural gas in liquefied form is economically the most effective method of long distance overseas transportation. Liquefied natural gas (LNG) is obtained by the process of cooling the natural gas down to a temperature of -163°C approximately at atmospheric pressure. The liquid obtained has density of 0.42t/m^3. The volume in liquefied state is reduced by a factor of around 600.

LNG is environmentally friendly, but commonly considered to be scary. It is non-explosive but flammable when mixed with air with 0.05-0.15 fraction of methane. If released into the air, the liquid immediately warms up and converts back to the gas. The gas is initially colder and heavier than the air, so it freezes water vapour in the air, which can create an icy fog. As the gas warms up, it dissipates and rises harmlessly into the air. LNG is cryogenic, thus contact with a non-cryogenic material, such as hull structural elements causes it to become brittle. Exposure to skin causes cryogenic burns.

1.1.2 History, characteristics and prospects for gas shipping

Shipping a gas in bulk is an old concept. Its history and milestones are described in e.g. Curt (2004); Lindemark et al. (2004); Sember and Mumtaz (2005). In 1914 the first barge for feasible gas transport in liquid form was patented. The first dedicated liquefied gas carrier *Herøya* was built in 1949 in the Horten Navy Shipyard. This vessel transported LPG and ammonia in pressurized vertical cylindrical cargo tanks. *Methane Pioneer*, built in 1958, was based on prismatic aluminium tank system of 5000m^3 with balsa insulation. The first commercial LNG vessels, *Methane Princess* and *Methane Progress* of 27400m^3 using the Conch containment system started operating in 1964. The first membrane containment ships *Polar Alaska* and *Arctic Tokyo*

with 71500m^3 were delivered in 1969. The concept of LNG carriers with spherical tanks was originated also in late 1960's. *Ben Franklin* and *El Paso Paul Kayser* vessels at 120000m^3 and 125000m^3, respectively, delivered in 1975 set a size standard maintained for the next 20 years with a small growth to around 133000m^3. A self-supporting prismatic containment system, typical for LPG ships, was first adopted in LNG technology in 1993 in two 83500m^3 ships *Polar Eagle* and *Polar Sun*. LNG carriers presently built have the capacity on a level of approximately 150000m^3.

Gas shipping is under continuous development and change. It applies both to the global gas market and to the ship design and operation as a means of conveyance. Fleet growth, new trade routes, emergence of spot markets, demand for offshore offloading, ship size growth and application of new propulsion systems represent main challenges for the gas shipping, see e.g. RINA (2004); Gastech (2005); RINA (2006).

A significant fleet expansion has taken place in the last few years. The order-book exceeds 50% of the existing fleet, both in terms of number of vessels and total capacity (Mahmood, 2005).

The changes in the global LNG market lead to relocation of typical shipping routes to new sea areas (Magelssen, 2005). Some of the new routes cross areas known for very rough conditions. As compared to a ship operating world wide, shipping in North Sea, North Atlantic or at the Alaskan coast is much more challenging in regard to both strength and operational issues.

Emergence of spot markets and use of ships in short term charters cause that operational flexibility in different conditions and speeds determine the profitability. This can also induce a need for shipping with a partial filling in cargo tanks. Partial filling is very unfavourable when considering sloshing loads in the tanks.

A demand for offshore offloading appears also as an important shipping characteristics transformation. Reasons for this can be a big LNG traffic and resulting security issues and terrorist attack threat. Among the novel solutions the most advanced design works are devoted to floating or gravity based offshore terminals or to outfitting the vessels with regasification facilities. The former solution assumes a traditional berthing and a gas transfer in liquefied state while the latter enable delivery of the cargo in gaseous state to the port by a receiving buoy. Potential problems which have to be faced include partial loading of the LNG tanks and relative motion between the terminal and a ship during offloading operation.

Another trend is designs for LNG Floating Production, Storage and Offloading Systems (LNG FPSO) or its derivatives Floating LNG Plants (FLNG) and Floating Oil and Natural Gas (FONG), (Kernaghan, 2004). The main concept is the integration of well control, processing, storage and offloading on a barge positioned in the vicinity of the field. Such a configuration provides a significant cost reduction.

A demand for an increased ship size appears as it enables taking advantage of the economies of scale. Increasing the size of a standard LNG carrier from about 145000m^3 to 200000m^3 would reduce transportation costs by 15 percent (Sember and Mumtaz, 2005). Designs of a new generation very large LNG carriers with cargo capacities up to 250000m^3 have already been developed.

In order to increase LNG carriers' size, a number of significant changes in the hull shape, internal arrangement and structural solutions have to be performed (Pastoor

et al., 2005). For instance, ship motions for larger hulls may be different from the currently operated carriers.

Parametric roll has as long been only reported for large container vessels. However, it can also be an issue for large LNG carriers (Zhao et al., 2004). Parametric roll is a resonance phenomenon related to a periodic change of stability parameters and occurs in head and following seas. This roll motion may be excited when the wave encounter period is close to half of the rolling natural period and damping is insufficient to dissipate the parametric roll energy to avoid a resonant condition. Sloshing with its natural period of the order of 5-10 seconds can contribute to the parametric roll.

It is economically advantageous to have a minimum number of tanks due to the complexity of manufacturing process and cost of the containment system. On the other hand a limited number of tanks with increasing hull dimensions implies larger tanks and increasing sloshing loads. Hence, ship design needs to be optimized to balance the number of tanks with acceptable sloshing loads, i.e. which exceeds the strength of currently available insulation system. The wave excitation, ship motion, motion of the fluid in the tanks and the resulting pressure needs to be determined.

1.1.3 Tank systems for gas transport

During the four decades of the sea-borne LNG transport only five cargo tank designs have been applied (Harper et al., 2004). The main classification of tank designs distinguishes between self-supporting tanks and so-called membrane tanks.

Main features of self-supporting tanks are that they are independent from the hull and do not directly transmit the fluid loading to the hull plating, but only integrated forces through the supports. The fleet of LNG carriers with independent tanks is dominated by the Moss spherical tank design. An important feature and advantage of this tank system is the possibility of prefabricating the entire tank, which allows the shipyard to construct the hull and the tanks in parallel and then install the entire tanks in the hull. Spherical tanks show a favorable fluid behavior that minimizes sloshing loading by allowing ship acceleration energy to be transformed to a rotation of the bulk LNG.

LNG carriers with the Moss spherical tanks made up the majority of orders until the end of the 1990's. Presently, the membrane system dominates among new constructions. A reason for this fact is the inherent inefficiency of hull space usage in ships with the Moss system, resulting in high tonnage canal fees and a large hull height of such ships, resulting in constraints regarding passing under bridges in terminals.

Membrane LNG tankers are of interest in this work due to their susceptibility to violent fluid impacts on tank structure. Membrane tanks are supported by the hull steel structure. As the LNG is kept at $-163°C$, the steel structure needs to be covered with an insulation system. The insulation is covered with a thin steel membrane which ensures the tightness against both the fluid and gas. Moreover, the containment system has to be capable of withstanding the loads excited by the fluid.

LNG carriers built up to 2006 have the capacity on the level of approximately $150000m^3$. Tanks make up the width between inner walls of the double hull and are separated by transverse bulkheads. There are commonly four tanks over the length.

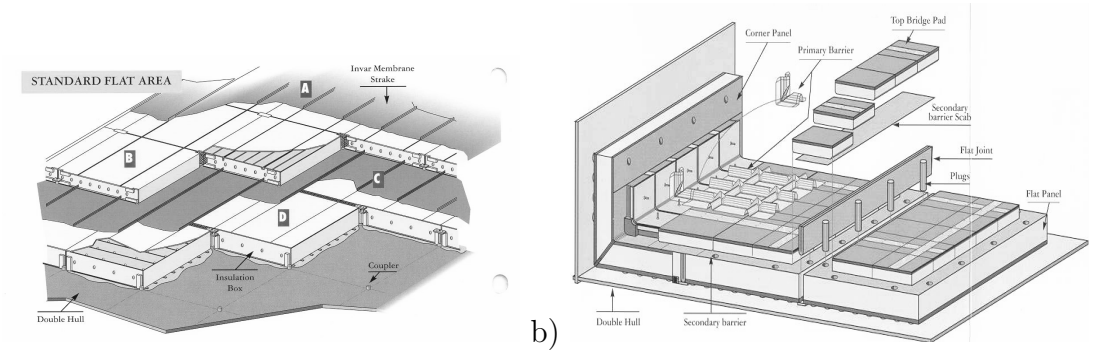

a) b)

Figure 1.2: (a) Flat panel area of the No.96 containment system, (b) corner area of the Mark III containment system (www.veristar.com, 2008).

The first tank is smaller than the other. The tanks are chamfered along all the four, both lower and upper longitudinal edges, but not in a longitudinal cut.

New tank shapes referred to as prism or pyramid has recently been developed (Noble et al., 2004). Larger height and enlarged upper chamfers result in very narrow roof area and hence, reduce the fluid free surface. In this way also the fluid motion in high filling levels and consequently the sloshing loads are reduced as well as the resonance period of the tank is lowered.

The principle of double barrier is applied to a containment system, i.e. two membranes and two layers of insulation are installed in order to increase the reliability of the containment. IMO (1976) requires that the containment should hold any possible damage of the primary barrier resulting in leak of liquid cargo for a period of fifteen days. During this period the temperature of the steel structure should not decrease to the level that the steel becomes brittle.

The membrane LNG tankers are dominated by two containment systems: No.96 and Mark III, invented and patented by GazTransport & Technigaz. Recently, new containment designs have appeared such as CS1 by the same producer and new designs by Korean Gas and OceanLNG (Pastoor et al., 2005).

The No.96 system utilizes the technology and materials used since 1968. This system is shown in Figure 1.2a. The system consists of two layers of plywood boxes (e.g. birch, maple) strengthened internally by means of longitudinal and transverse stiffeners. The boxes are filled with an insulating powder, expanded perlite silicone-treated for waterproofing.

The strength of the box is achieved by means of plywood internal stiffeners running longitudinally; polyurethane transverse spacers are provided for prefabrication purposes. The plywood structure of the boxes is assembled using stainless steel staples.

The boxes are fixed to the double hull by means of an integrated metallic network of U-bars and cross-pieces designed to reduce heat transfer.

Two flat metallic membranes are impermeable to gas and liquid. They are made of 0.7mm thick Invar, an alloy with a 36% nickel content and a very low coefficient

of thermal contraction. The membranes are manufactured as strips and fixed to the insulating boxes by sliding joints to prevent stress concentration.

The Mark III system is shown in Figure 1.2b. The primary insulating material is a reinforced polyurethane foam. The first layer is a 1.2mm thick corrugated stainless steel membrane, attached by tack welding to the weld protection strips embodied in the plywood underneath. The plywood sheet is integrated with a pad of cryogenic foam. They are cut perpendicularly to the surface in order to accommodate the structural forces associated with low temperatures. A secondary membrane of fibreglass fabric and aluminium foil laminate called Triplex is placed beneath the pad. Underneath, there is a prefabricated foam panel and a plywood sheet. A standoff space between panel and hull is held by mastic ropes. The layers are mechanically and adhesively joined to each other and to the hull. The insulation space below the containment system is kept inerted with nitrogen and enables monitoring for the natural gas or water. It also accommodates a tolerance for hull deformations during installation of the panels.

More complex structure including heavy stainless steel angles is applied along the tank edges and in the corners.

A pump tower include LNG loading and discharging facilities such as pumps, pipes and level gauges which are supported by 3 or 4 vertical pipes and a number of bracing members. The pump tower is typically located near the center of the aft transverse bulkhead.

1.1.4 Structural issues of LNG carriers

While the steel hull can be designed according to conventional ship design practice, specific issues related to loading and resistance of the membrane LNG tank need to be investigated. They are related mainly to loads exerted by fluid motion in the tanks (sloshing) and thermal effects due to temperature differences.

Hence, criteria for ultimate and fatigue limit states must be determined both for steel structure and containment system.

A steel hull of the membrane type ship is similar in terms of spatial arrangement and structural design to typical ship types such as oil tankers or bulk carriers. Thus, design criteria for the steel structure with respect to ultimate and fatigue limit states can be treated in the same manner as for seagoing vessels (DNV, 2008). However, some characteristic design and operational features are unique to LNG carriers as discussed subsequently.

Slamming increasingly becomes an issue for LNG carriers when the vessel size increases. Typically the length and breadth increase while draught is limited by constraints associated with the terminals. Hence, the hulls of large LNG vessels have a smaller deadrise angle of the bow flare as well as a smaller natural frequency. Consequently, slamming forces can increase significantly and the hull natural frequency will approach the wave excitation frequency. Due to structural dynamic effects the total response might increase, especially in terms of acceleration in the fore part as well as bending moment and shear forces in the hull. Fatigue loading may also increase. Recent developments regarding such whipping-induced response are for instance de-

scribed by Jensen and Mansour (2003) and Wu and Moan (2005) and references therein.

Based on experimental investigations Zhao et al. (2004) report that for a large LNG carrier the increase of bending moment can reach between 30% and 150%. Bow slamming is found to be most significant in head seas at high forward speed. A big influence of increasing speed on the measured response is observed. Stern slamming is especially significant in following seas with low speed. This issue is also investigated for an LNG carrier of a typical size in the Paper II of this thesis. Here the approach by Wu and Moan (2005) is applied. It is shown that a slamming-induced whipping may increase the wave-induced bending moment by up to 40% for a $138000m^3$ vessel.

Increase of local acceleration due to hull flexibility may affect inertial forces from the cargo on the tank structure. The effect of hull flexibility on the vertical acceleration in the fore part is investigated in the Papers II and III of this thesis. In the critical sea state an increase of the vertical acceleration by 20% is observed.

Fatigue becomes important also in view of operation in more harsh conditions. The effect of wave environment of the vessel operation on the fatigue life of structural elements is studied by Kim and Lee (2005). The authors investigate side longitudinals and report a large influence of service route on fatigue life.

Lindemark et al. (2006) show that the inner hull knuckles are the most critical areas with respect to fatigue due to high stress concentrations, inaccessibility of the structure for inspection and repair as well as the serious possible consequences as cracks in the inner hull may result in contamination of membrane tank insulation by the ballast water.

The main component of loading on the membrane tanks is due to sloshing. This phenomenon is described in more detail in the next chapter.

Limit state criteria for containment systems arise mainly from extreme loading. Failure modes of the Mark III structure include bending of the lower plywood between the resin ropes and shear of the lower plywood just aside the resin ropes. Moreover, the through-thickness compression of the foam just above the lower plywood near resin ropes and just below the upper plywood represent failure modes. The latter is relevant in case of highly concentrated loading only.

In case of the No.96 system the limit state is first reached in the plywood plates of the boxes due to shear and bending under lateral loading as well as buckling and indentation under axial loading.

Another LNG carrier-specific loading in the containment system components is due to the thermal effects. Especially in-plane stresses resulting from the contraction and expansion of the elements are important as the layers continuously extend over large areas. This loading may combine with tension and compression due to the wave excited overall hull bending.

In the Mark III containment system the forces are accommodated in the plywood sheet integrated with a pad of cryogenic foam by the cuts normal to the surface. The special corrugated shape of the membrane accommodates the in-plane force in this layer.

In the No.96 containment system the plywood boxes do not make up the continuous structure. The membrane is made of Invar, the steel with a 36% content of nickel and a very low coefficient of thermal expansion. The surface of the insulation system is not flat because the Invar strips are raised at the edges.

In order to establish design procedures and safety factors for the structure its strength capacity needs to be known. Materials used in the containment system, such as polyurethane foam, plywood, mineral powder and resin ropes are non-standard in marine technology and the information available in literature is limited.

Among recent works, the producer of the containment system presents results of a testing campaign (Chapot, 2002). The experiments include among other things drop tests in cryogenic conditions using liquid nitrogen at -196°C. "Low cycle" fatigue tests are also conducted.

Numerical and experimental investigation of the strength of a containment system is presented by Lee et al. (2004). The limit state is studied numerically by applying conventional volumetric elements which capture a bulk response of the structure and interfacial cohesive elements located along the boundaries where the failure can be expected. Dry and wet drop tests of containment systems' sub-assemblies are reported.

A comprehensive quasi-static testing of representative components and sub-assemblies of the containment systems is presented by Pastoor et al. (2005). Cases tested include: the Mark III sub-assembly both for ultimate static capacity and "low cycle" fatigue as well as No.96 plywood plates for shear, bending, buckling and indentation strength.

Strength criteria of the No.96 containment system are investigated experimentally and numerically by Paik (2006). By a tensile coupon testing a linear stress-strain relationship for plywood is proved. Ultimate strength of the insulation box without the mineral filling and rigidly supported under both static and dynamic loading is calculated by the finite element method. The behavior of the plywood box is nonlinear.

A similar study is presented by Lee et al. (2006) for the Mark III containment system. Ultimate strength under both static and dynamic loading is investigated experimentally by measuring impact force and local structure accelerations during dry drop tests. A limit state is found by a nonlinear FE analysis of a foam specimen and a section of insulation system. Results of the static and dynamic analyses are compared with experiments.

Fibre optic sensors are used to measure strains under static loading, cyclic quasi-static loading and dry drop tests. Horizontal and vertical strains distribution in the foam as well as crack initiation and propagation are investigated. This technique enables better understanding of the structural response and validation of numerical codes.

A similar idea motivates Kim et al. (2006) to develop a structural health monitoring system for a membrane containment system. Fibre optic sensors are also used, capable of measuring strain, temperature and pressure. The response of the containment system to static and dynamic loading, with and without damage, is analyzed and the possibility of predicting damage is investigated.

A separate analysis needs to be performed for the pump tower structure. The hydrodynamic load on the pump tower can be estimated by the Morison's equation, see e.q. Faltinsen (1990).

A key role in design of LNG vessels play sloshing loads and load effects. Responses of interest may be associated with local effects in the containment system and effects in the steel panel supporting the insulation. The global ship response may also be affected by forces from the fluid. It is noted that the standard LNG vessels are largely built based on accumulated engineering experience. If tank dimensions are increased, the sloshing load in severe seas or in partially filled tanks cannot be estimated by a simple extrapolation of parameters and values typical for the today's standard design and operation procedures.

Hence, the gas industry needs rational methods to address the loading. Rules of classification societies have mainly been based on a comparative approach. They require that loads or responses do not exceed those appearing in the ships presently operated. Some attempts have been made to develop an absolute approach (ABS, 2006). Within the present theoretical knowledge and state-of-the-art of the studies devoted to sloshing it is, however, difficult to fully rely on such formulations.

Many investigations devoted to determining sloshing response in the LNG tanks were initiated during the period in which the work in this thesis has been performed. The procedures are presently under constant development.

In order to determine load effects in the tank structure a complex sequence of issues needs to be investigated. This includes a long term variation of the sea environment, ship motion, fluid motion in the tanks, pressures acting on the tank structure and finally structural load effects.

1.2 Objective and outline of the thesis

The main objective of this work is to determine sloshing load effects in membrane LNG tanks with account for the stepwise procedure described above. More specifically, the focus is placed on characteristics of fluid motion in the tank and excited pressures, variability of loading and environmental conditions, as well as structural response of the tank structure. Moreover, the objective is also to develop a procedure for performing and analyzing sloshing experiments. The scope is schematically presented in Figure 1.3.

The thesis is organized as a paper collection. The papers are preceded by a theoretical background (Part I) consisting of an introduction and a description of sloshing in the membrane LNG tanks and the necessary steps of analysis. Issues dealt with in the papers are characterized and linked to the overall set of problems and methodology.

Five papers are presented in Part II. They are listed below in chronological order together with the explanation of co-authors' role.

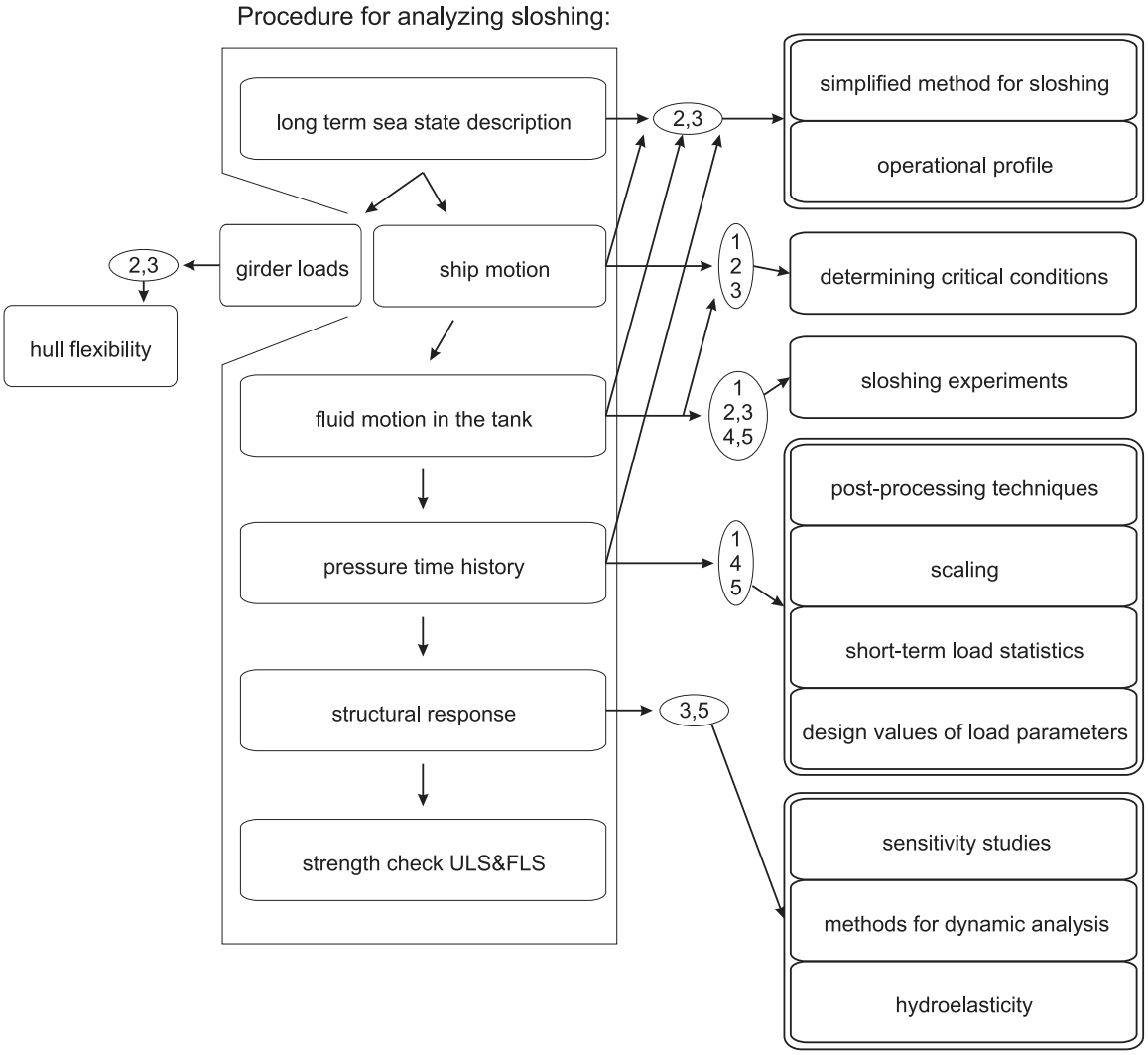

Figure 1.3: Scope of the thesis with indicated paper numbers that deal with particular issues (attached in Part II).

1. Graczyk M., Moan T. and Rognebakke O. (2006) Probabilistic Analysis of Characteristic Pressure for LNG Tanks. Journal of Offshore Mechanics and Arctic Engineering - Transactions of the ASME, 128:133-144.

   Dr Olav Rognebakke performed sloshing calculations with his computer code based on the multimodal method.

2. Moan T., Graczyk M., Shu Z. and Rognebakke O. (2006) Recent Developments of Structural Design of Ships Based on Direct Calculations - with Emphasis on LNG Carriers. In: Proceedings of the International Conference on Ship and Shipping Research, NAV, Genova, Italy.

   The paper was presented by Prof. Torgeir Moan as a keynote paper. Zhi Shu was involved in assessment of operational effects and performed seakeeping calculations with WASIM. Dr Olav Rognebakke performed sloshing calculations with his computer code based on the multimodal method.

3. Graczyk M., Moan T. and Wu MK. (2007) Extreme Sloshing and Whipping-Induced Pressures and Structural Response in Membrane LNG Tanks. Ships and Offshore Structures, 2(3):201-216.

   Dr MingKang Wu described whipping analysis in the paper and performed calculations with his computer code, WINSIR.

   The paper was granted the 2007 Best Paper award by the editorial board of the journal.

4. Graczyk M. and Moan T. (2008) A Probabilistic Assessment of Design Sloshing Pressure Time Histories in LNG Tanks. Ocean Engineering, 35:834-855.

5. Graczyk M. and Moan T. (2008) Structural Response to Sloshing Excitation in Membrane LNG Tank. Submitted for publication.

Moreover, one paper has been published during the Ph.D. studies but is not included in the thesis. This is due to the fact that the paper presents non-definitive stage of analyses and partially overlaps with Paper IV and Paper V. This is:

- Graczyk M. and Moan T. (2007) Assessment of Sloshing Pressure and Response in LNG Tanks. In: Proceedings of the International Conference on Violent Flows, VF-2007, Fukuoka, Japan.

Detailed description of experimental set-up and results of analyses that are not included in the papers, are presented in Appendices.

Chapter 2

Analysis of sloshing in LNG tanks

2.1 The sloshing phenomenon

Sloshing is a violent resonant fluid motion in a moving tank. The condition for the phenomenon to appear is a presence of a free surface. Therefore, in fully loaded ship tanks sloshing is not an issue. The resonant nature of the phenomenon implies that the fluid response becomes violent when the excitation period is close to the natural period of fluid motion.

Sloshing may be considered to comprise many phenomena, among them breaking and overturning waves, run-up of fluid, slamming, two-phase flow, gas cushion, turbulent wake and flow separation.

Sloshing is a highly nonlinear phenomenon. Abramson (1966) classifies mechanisms of the nonlinear effects in fluid motion in the tanks as due to (i) geometry and appearing already for small amplitudes of oscillation and response, (ii) large amplitudes and (iii) coupling and instabilities of various sloshing modes involving essentially different sloshing behavior.

The natural frequency of a fluid with large motion amplitudes depends on the response amplitude. The relationship between amplitude and the period is shown in Figure 2.1. For a given period there may exist either one, two or three values of the amplitude.

Therefore, different patterns of the fluid motion may appear in the tank. Faltinsen et al. (2003) show that even for the tank excitation limited to periodic steady-state longitudinal or diagonal motion a very complex set of response regimes is observed. The regimes include planar and diagonal resonant standing waves, swirling waves moving along tank walls clockwise or counterclockwise as well as square-like resonant standing waves coupling in-phase oscillations of the two lowest modes.

Fluid motion in the not fully filled tank has been investigated for many decades. As sloshing damage was reported in the two first membrane LNG tankers, sloshing related to LNG carriers became a very relevant research area in 1970's and 80's. An important contribution was made by Abramson et al. (1974), DNV (1976) and Cox et al. (1980).

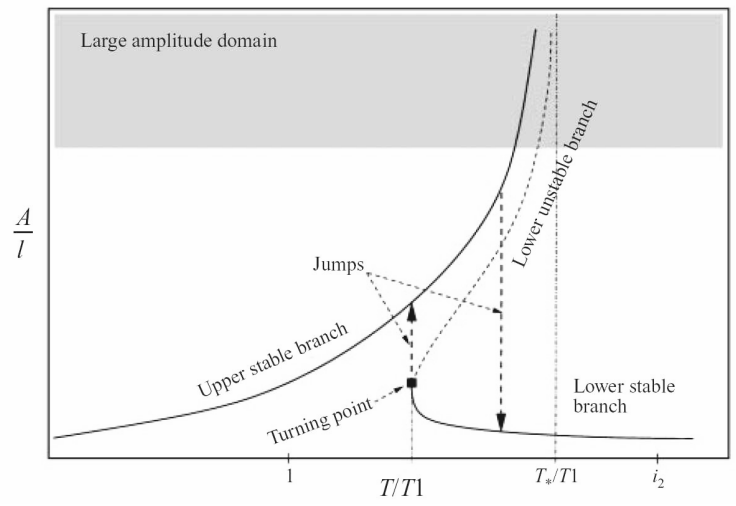

Figure 2.1: Non-dimensional surface elevation vs. the ratio of the period and the first natural period in a rectangular tank (Faltinsen and Timokha, 2001).

Physics of the sloshing phenomenon is extensively investigated in literature. Recently, an extensive survey of sloshing studies have been performed by Ibrahim (2005).

Recently, much interest again in the sloshing problem in LNG tanks has emerged. This is due to the challenges the LNG shipping is facing.

The main publication forum are gas-related conferences, such as International Conference on Design & Operation of Gas Carriers (RINA, 2004), International Conference on Design, Constructon & Operation of Natural Gas Carriers & Offshore Systems, ICSOT (RINA, 2006) and Gastech, see e.g. Gastech (2005). The main contributions are cited abreast with the following description of different aspects of sloshing.

Fluid in the tank subject to sloshing can cause very high pressure on the structure. The structural response is not only dependent on the pressure magnitude. These are also the temporal pattern and spatial pattern of pressure which need to be considered. The pressure may be highly concentrated both in time and space.

There is a number of factors that influence the regime of fluid flow and in consequence the resulting pressures and structural response. The factors are mutually dependent and a distinct evaluation of each particular factor influence would be very cumbersome.

An important factor is the tank geometry. Spherically shaped tanks show very favorable behavior in regard to sloshing. It was found that sloshing loads were modest and composed primarily of global accelerations and hydrostatic effects (Abramson, 1966). This tank geometry allows transformation of ship acceleration energy to a rotational motion of the fluid.

Use of parallel flat walls and 90° edges in a tank design increases significantly importance of violent fluid impacts. Consequently, in the membrane tank system, areas where the most of impacts is expected under rolling motion, i.e. longitudinal

tank edges are chamfered. It results in a reduced free surface area in high filling levels and prevents fluid impacts with a near-parallel free surface on the tank roof.

Sloshing to large extent depends on the tank motion. The tank motion constitutes an excitation of the fluid in the tanks and is caused by external sea loading and the resulting ship motions. The sea–ship system in irregular waves is quite complex itself but for practical applications it can be described by a spectral formulation of the sea combined with deterministic parameters describing ship operation profile. Commonly applied sea state parameters are the significant wave height H_s, the wave zero crossing period T_z and the directional distribution function $f(\theta)$. Ship operation parameters are the wave heading angle β and forward speed U.

How the significant wave height affects the sloshing pressures in the tank is investigated by Pastoor et al. (2004) and Tveitnes et al. (2004). Pressures measured during a 20-year storm and in much more benign sea are compared. For beam sea a reduction of the H_s by 50% results in pressure reduction only of the order of 10-30%.

Actually, the sloshing pressure to a larger extent depends on the wave zero crossing period. As mentioned, sloshing is a resonance phenomenon and the expected most severe sea states are the ones with zero crossing period in the proximity of the lowest natural frequency for the fluid in the tank.

The wave heading angle in the obvious way governs the relative importance of ship motion in particular degrees of freedom. The shape of the prismatic chamfered tank enforces to some extent the motion pattern of the fluid, which makes the sloshing dependent on the direction of excitation.

Speed affects the accelerations experienced by the hull, which has a large influence on the sloshing. Therefore a voluntary speed reduction or a course change is important when sailing in rough conditions. Tveitnes et al. (2004) and Pastoor et al. (2004, 2005) studied the effect of speed reduction on sloshing pressures. Speed reduction from 3/4 of the design speed by 65% to a manoeuvring speed of 5 knots results in the reduction by about 40% in the sloshing impact pressures. In beam waves the reduction is negligible due to the small effect of the speed on viscous damping which governs the ship response in roll.

Ship speed U and wave heading angle β also influence the sloshing response by altering the wave encounter frequency ω_e according to the expression

$$\omega_e = \omega_0 + \frac{\omega_0^2 U}{g} \cos\beta \tag{2.1}$$

where ω_0 is an incident wave frequency. Thus, the parameters cause a shift in the ship motion spectrum peak along the frequency scale.

Fluid behavior in tanks at high and low filling levels exhibits different pattern, see a sketch in Figure 2.2. At the high filling level, where the filling height is approximately 90% of the tank height, the standing wave motion is observed. The amplitude of the wave is limited by the gap between the fluid free surface and the tank ceiling and there is no significant liquid motion in the horizontal direction. Large fluid impacts on the tank roof may appear. Due to small incident angle during the impacts, there is a large probability for a gas cushion creation.

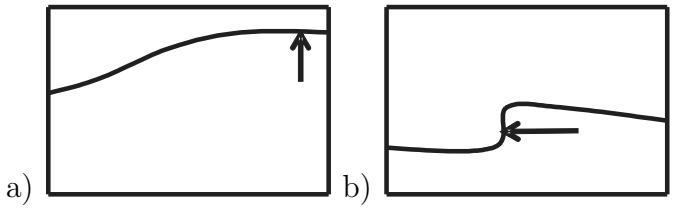

Figure 2.2: Sketch of the sloshing flow pattern for (a) high filling level (b) low filling level.

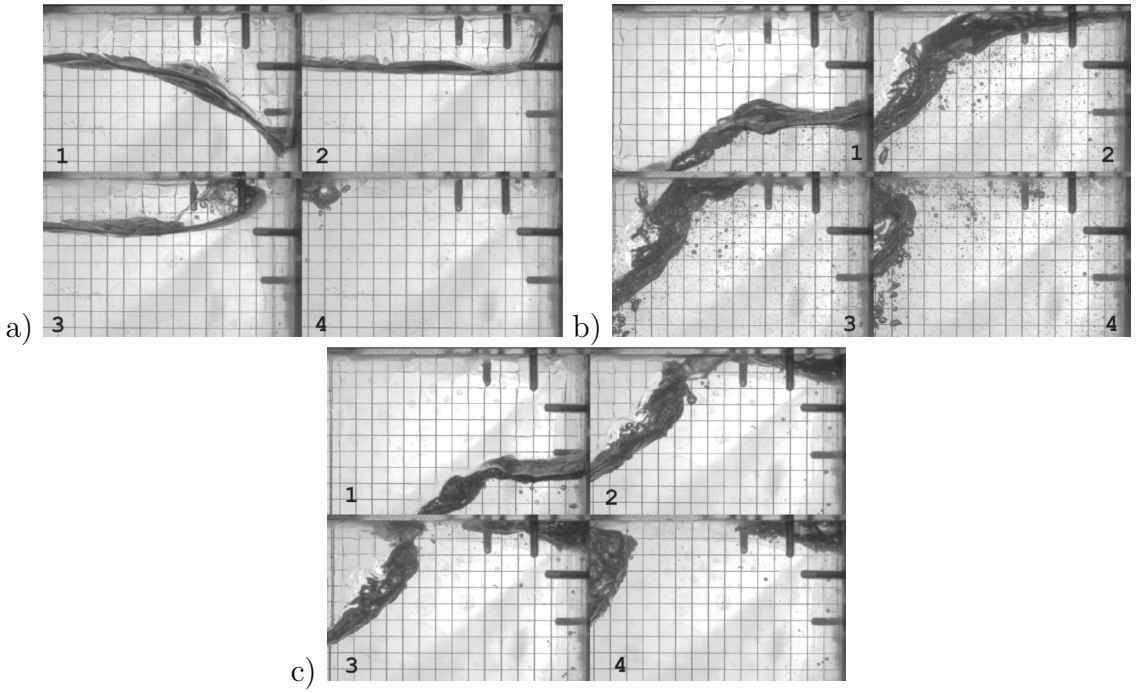

Figure 2.3: Free surface for different fluid impacts on the tank roof for a high filling level: (a) high curvature hydrodynamic impact, (b) hydrodynamic impact with a flat free surface, (c) impact with a gas cushion entrapped (Rognebakke et al., 2006).

At the low filling level, where the filling height is less than 20% of the characteristic horizontal tank dimension another pattern can be observed in form of hydraulic jump or bore, see e.g. (Shin et al., 2003). Hence, impacts appear mainly on the vertical surfaces and the pressures excited are characterized by a different pattern.

Rognebakke et al. (2006) investigate experimentally a shape of the free surface as well as temporal and spatial pattern of the pressure in the impact region for high filling levels. A two-dimensional free surface is captured by means of a high-speed camera. Three types of fluid impacts are presented: (a) a high curvature hydrodynamic impact with a high velocity jet resulting in a very localized pressure, (b) a hydrodynamic impact of a flat free surface resulting in loading on a large area and (c) an impact with a gas cushion entrapped in the tank corner and with a oscillating pressure pattern due to compressible effects. The three forms of the free surface are presented in Figure 2.3.

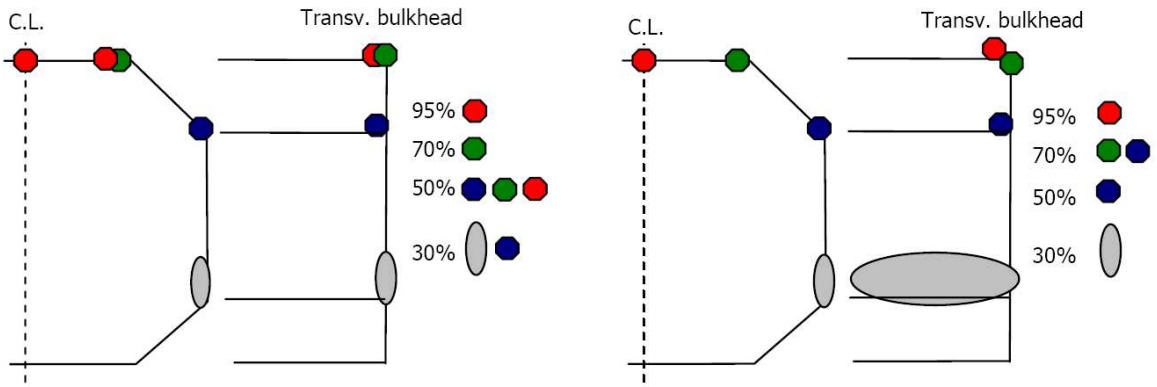

a) b)

Figure 2.4: Main sloshing impact locations in the chamfered prismatic tank (a) for head wave conditions (b) for beam wave conditions (Pastoor et al., 2005).

Locations subject to the highest sloshing loading need to be identified for the relevant LNG tank. This information is needed in performing sloshing experiments due to the economical and technical limits in the number of pressure sensors that can be used. Based on sloshing tests with various filling levels and wave heading angles, see e.g. Pastoor et al. (2005) and Zalar et al. (2005) the most exposed locations inside the tank are determined as shown in Figure 2.4.

It is observed that the tank roof is most exposed in the higher filling levels and in head seas, while the upper chamfer corners are most exposed in 50-70% filling levels and beam seas. In this range (50-90%) the critical locations are well defined. For lower filling levels the lower corner of the upper chamfer as well as the tank walls and the edge with bulkhead are most exposed. However, the critical locations are not that easily defined.

Qualitative comparisons of sloshing load in various filling levels are reported in the literature. It is shown both by numerical and experimental studies that sloshing pressure magnitude is larger for low filling levels than for high filling levels, see e.g. Kim et al. (2002); Zalar et al. (2005).

Pastoor et al. (2004) and Tveitnes et al. (2004) investigate temporal characteristics of pressure peaks and make a qualitative comparison of peaks' pattern in various filling levels. In a low filling level a hydraulic jump is often impacting the tank wall. In this situation the authors report that the pressure duration is longer than the impact of a standing wave on the tank roof for high filling level. The same conclusion is drawn by Lee et al. (2004).

Spatial concentration of pressure is investigated by Kim et al. (2002) for filling levels between 16-96%. In Kim et al. (2003) the studies are further complemented by 3-dimensional calculations. Tveitnes et al. (2004) investigate the problem experimentally for filling levels at 50-95% in head and beam sea. The studies show that the pressures for low filling levels act over a larger area than in high filling levels.

Consequently, the ratio of averaged pressure to maximum pressure can be 3 times higher for the low filling level.

Similar results are obtained by analyses performed in this work. A quantitative comparison of loading parameters for two various filling levels is presented in the Paper IV.

2.2 Analysis of sloshing in membrane tanks

In order to determine load effects in the tank structure the complex system of mutually interacting elements needs to be investigated. The system includes sea environment, ship response in waves, fluid motion in the tank and tank structure response. A stepwise approach is then required to determine the pressures and load effects which is checked by the proper strength criteria. The approach is well illustrated in the Paper II of this thesis.

The analysis covers a sequence of issues. Firstly, a long term variation of the sea state needs to be determined. Then, ship motion in a stochastic seaway is analyzed considering also operational criteria and the effect of avoiding heavy weather. Fluid motion in the tanks needs to be determined and pressures acting on the tank structure found. Structural load effects can then be determined and compared to the respective resistance. A feedback effect of sloshing loading on the ship motion should also be included. In order to optimize the accuracy and efficiency of the estimates of load effects, analytical, numerical and experimental approaches are commonly combined.

2.3 Sea climate variability

A sea surface elevation may be represented by a stationary random process in short time (practically of the order of a few hours). The basic model to represent ocean wave elevation is the Gaussian distribution (Ochi, 1990):

$$f(x) = \frac{1}{\sigma\sqrt{2\pi}} e^{-\frac{(x-\mu)^2}{2\sigma^2}}, \tag{2.2}$$

where μ is the mean and here $\mu = 0$, σ is the standard deviation. If the process is assumed to be narrow-banded the individual maxima are Rayleigh distributed (Ochi, 1990):

$$f(x) = \frac{x}{\sigma^2} e^{-\frac{x^2}{2\sigma^2}}, \tag{2.3}$$

$$F(x) = 1 - e^{-\frac{x^2}{2\sigma^2}}. \tag{2.4}$$

The irregular sea states may be represented with a spectral formulation. The spectra are expressed in terms of the significant wave height H_s, a characteristic wave period, e.g. T_p or T_z and the directional distribution function $f(\theta)$. The most commonly applied spectra are Pierson - Moskowitz, representing fully developed sea states and JONSWAP, capable of representing also not fully developed sea states, see e.g. in Ochi (1998).

A probabilistic nature of the sea environment in a long-term period is specific for each geographical region. Models for the long-term variability are expressed in form of scatter diagrams, i.e. a joint probability density function of H_s and, commonly, a characteristic wave period, T_p or T_z, as originated by Battjes (1972).

The long-term variability of the sea environment needs to be considered in order to determine characteristic design values with a given return period. In case of sloshing studies the ship response is a transitory step towards determining fluid motion and excited pressures. These three issues are coupled in the sense that the long-term sloshing response in the tank is an effect of the sea state severity over the time period of interest, ship motion in given sea condition as well as fluid motion in the tank under given ship motion. Therefore, the long-term response of a fluid in a tank is coupled with the sea excitation and ship response. Hence, the analysis of these steps needs to be combined.

A full long-term analysis consists in a summation of the short-term probabilities of exceedance in all possible combinations of variables that influence the response

$$F_R(r) = \int_{H_s}\int_{T_z}\int_{U}\int_{\beta} F_{R|H_s,T_z,U,\beta}(r|h_s,t_z,u,\beta) \;\; f_{H_s,T_z}(h_s,t_z)\cdot$$

$$f_{U,\beta|H_s,T_z}(u,\beta|h_s,t_z) \;\; \frac{\overline{T_z^R}}{T_z^R(h_s,t_z,u,\beta)} \;\; \mathrm{d}\beta \; \mathrm{d}u \; \mathrm{d}t_z \; \mathrm{d}h_s \tag{2.5}$$

where H_s, T_z, U and β are significant wave height, wave zero crossing period, speed and wave heading angle, respectively. The terms of the integrand represent, respectively, the short term cumulative probability distribution of response, probability of the sea states' occurrence, distribution of operational parameters and relative number of peaks in particular sea states. $\overline{T_z^R}$ is the average response zero crossing period.

Physically, performing the summation is only possible for linear phenomena which can be analyzed in frequency domain. The full long-term analysis of the vertical ship acceleration is reported in the Paper II of this thesis.

Sloshing phenomenon is highly nonlinear and may not be analyzed in the frequency domain. Moreover, a full understanding of the interacting phenomena during the violent motion in the tank is still lacking and therefore, the most reliable approach for obtaining sloshing pressures is based on costly laboratory tests. Large number of test cases is required due to many variables affecting the sloshing response and due to a limited repeatability of results for a given input. All these factors make the full long-term approach not feasible for sloshing analysis.

Several simplified methods has been developed, among them the response surface approach, see e.g. Videiro and Moan (1999) and the contour line approach (Haver, 1987; Winterstein et al., 1994). These methods enable predicting load- and response-maxima corresponding to a prescribed return period without having to carry out a full long-term analysis.

As these both approaches require determining the short-term responses in several sea states, it may be still quite time-consuming for nonlinear problems. Another simplified approach may then be used; it consists in conditioning the wave episode upon the response (Dietz et al., 2004). This method is not utilized herein.

The response surface concept and the contour line concept are based on the fact that the long-term response is only slightly larger than the short-term response in the critical condition. In analysis by the response surface approach a few conditions that contribute most to the long-term extreme are considered. The contribution from a given condition is assessed based on its coefficient of contribution:

$$C_R(r) = \frac{PoE^{\,i}(r)}{PoE^{LT}(r)}, \tag{2.6}$$

where $PoE^{LT}(r)$ is the probability of exceedance in long-term and $PoE^{\,i}(r)$ is the probability of exceedance in a given condition. The coefficient of contribution needs to be determined in advance by a simplified analysis.

In the contour line approach the environmental and response long-term analysis are decoupled. The contour lines represent the sea states with the same probability of occurrence and hence, a set of the critical conditions for a given return period. The life-time estimates are calculated by the short-term analysis of the response in one of these critical sea states. In order to represent the life-time response by the short-term extreme, one of the following methods (or a combination of them) needs be applied: sea state duration or significant wave height can be artificially increased, a characteristic short-term value may be calculated for a higher quantile of the response or this may by multiplied by a correction factor.

The contour line method can be extended to cover load effects which depend on operational parameters, as vessel speed and heading angle. The critical conditions will then determine a multidimensional contour surface (Baarholm and Moan, 2002).

The suitability of the contour line approach to the sloshing analysis has not been proven. However, this approach has been successfully applied in other nonlinear problems, e.g. Baarholm and Moan (2001) has proven its feasibility in analyzing wave bending moment. Due to the lack of other effective tools this is commonly adopted to analyzing sloshing, see e.g. Pastoor et al. (2004) and Lee et al. (2004).

Uncertainty is related to the choice of the representative conditions (sea states and operational parameters) as well as a way of representing the life-time response by the short-term extremes. As mentioned above, the critical sea states are commonly assumed to be located along the contour line with a given return period. Supplementary analyses based on analytical, numerical and experimental methods are performed in order to qualitatively compare sloshing severity.

Baarholm and Moan (2001) show that the long-term estimate of a linear hull bending moment exceeds the short-term response in the critical sea state by 10-20%. Larger discrepancy applies for the nonlinear bending moment. The proper factor or quantile may be strongly dependent on the phenomenon characteristics, specifically on the shape parameter of the statistical model, characteristic period and return period of interest. For example, the nonlinear bending moment in the merchant ships can be described by the Weibull model with the shape parameter in range 1.3-3.0 (Wang and Moan, 2004), while the sloshing pressure in LNG tank by the same model with the shape parameter in range 0.53-0.83 (see Paper IV of this thesis).

Valsgård et al. (2006) investigate how the long-term estimate of the extreme value may be represented by a short-term estimate for Weibull distributed responses with

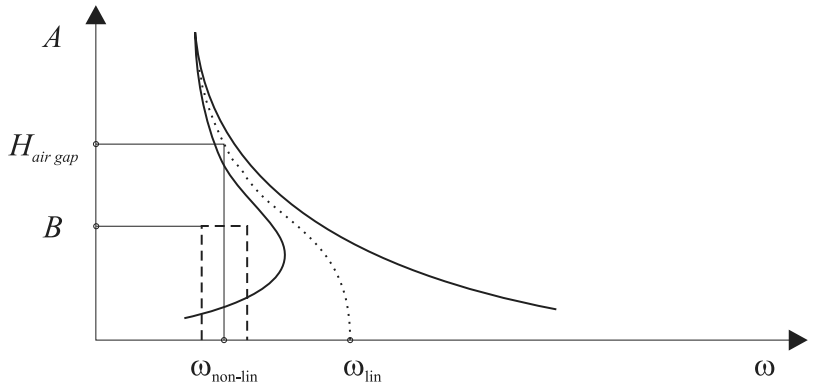

Figure 2.5: The sloshing frequency-amplitude relationship for high filling levels (solid line) and the simplified realtionship for the quasilinear frequency-domain method (dashed line).

different values of the shape parameter. The authors compare an approximate long-term estimate to a short-term response and show that for phenomena characterized by such low values of the shape parameter it is difficult to represent the long-term extreme value estimate by short-term estimates.

Therefore, the suitability of the contour line approach for sloshing analysis needs to be investigated and the proper factor or quantile needs to be determined.

In order to investigate this issue a simplified measure for sloshing response needs to be found so that a full long-term analysis of this measure can be performed. This measure may be the statistical characteristics of the horizontal acceleration of the tank. A concept similar to those presented by Hoff (2004) and Lee et al. (2004) and based on the idea of RAO for linear systems is presented in the Paper I of this thesis. The sloshing "transfer function" relates a quantity representing the sloshing response to the excitation in a simplified form. The simplified relationship provides a constant value B in the vicinity of the tank natural frequency and zero otherwise. This is schematically presented in Figure 2.5. This relationship is combined with the "load" spectrum of the horizontal acceleration. The resulting measure, interpreted as the quasi-RMS, is calculated by integrating the acceleration spectra in the range corresponding to the tank natural frequency.

As may be observed from Figure 2.5, nonlinearities in the sloshing response play an important role in the method presented. In the Papers II and III a further development of this method is presented. A different method of determining the proper integration range of the spectra is applied such that the eigenfrequencies are covered more accurately. The bandwidth of the integration is extended in the Paper II, i.e. the integration in the $1/2^{\text{th}}$ octave band around ω_{lin} is performed. In the Paper III a shift of the integration range towards the nonlinear frequency $\omega_{\text{non-lin}}$ and a narrow integration range ($1/12^{\text{nd}}$ octave band) is imposed for a high filling level. The natural frequency $\omega_{\text{non-lin}}$ is approximated by $\beta \cdot \omega_{\text{lin}}$, where β is a constant. β in range 0.8-0.9 is applied.

For a low filling level the importance of secondary resonances becomes apparent. This means that higher modes contribute to the response. A multiple range of integration, corresponding to a few eigenfrequencies is chosen in this case.

This formulation makes it possible to perform a full long-term analysis and in this way validate the simplified approaches. Results of a long-term analysis of the quasi-RMS are presented in the Paper III. The approach based on the coefficient of contribution is applied and the suitability of the contour line approach is investigated.

It is found that sea states with a low H_s may contribute much to the long-term sloshing response. This large contribution is caused by two factors: (i) large sloshing induced pressures when the excitation frequency is close to the fluid resonance, even in small waves, and (ii) a large probability of occurrence of sea states with low H_s. Large contribution of benign sea states to the long-term response may limit the applicability of the contour line approach, as long as it is based on a common set of variables (significant wave height, wave period and possibly speed and heading).

The applied method of investigating ship acceleration spectra appears to be an effective tool for determining the critical sea states. However, the results appear to be very sensitive to the applied estimate of the natural frequency and before the method can be applied for determining the long-term sloshing response the present investigation must be complemented with further studies.

As mentioned, an operational profile of a ship affects the long term response. In practice, when sailing in severe sea states, ship responses is usually limited by reducing speed and changing the course. These actions are generally made based on observations of the waves and vessel's responses and according to certain operational limiting criteria such as slamming, green water and vertical acceleration. The heavy weather manoeuvering model may be described as in Guedes Soares (1990). In the estimation of the extreme ship responses, the speed and wave heading angle need to be determined conditional on the severity of the sea state.

The shipmaster has also an advanced knowledge of what kind of sea states are ahead on the planned route and which actions should be adopted to avoid running into severe sea states. This effect is observed by Olsen et al. (2006) who reported that sea states encountered by ships operating in a given sea regions are significantly less severe than the weather conditions observed in these regions. Therefore, the scatter diagram representing the long-term sea state variability needs to be modified in accordance with a realistic operational profile.

Effect of avoiding a heavy weather on the long-term ship responses is investigated in the Papers II and III of this thesis.

2.4 Analysis of ship response

Wave induced motions and loads can to some extent be described by linear theory. Ship motion can then be analyzed in the frequency domain by means of the response amplitude operator, RAO or $H(\omega)$.

Ship motion response amplitude operators may be obtained by different methods. RAOs may theoretically be determined by analytical methods. In practice, however,

this approach can only be applied to very simple hull shapes consisting of the basic geometric figures. Numerical methods are in common use. They are usually based on the potential theory in combination with a strip theory or a 3D panel approach.

Approaches based on strip theory ware developed by Gerritsma and Beukelman (1964) for heave and pitch motions and by Salvesen et al. (1970) for heave, pitch, sway, roll and yaw motions. Such a method approximates a three-dimensional hydrodynamic solution by a set of two-dimensional problems. The main idea consists in dividing the hull into a number of strips, solving the 2D problem in each of them and integrating results along the hull. Although there is an increasing interest in applying fully 3D schemes, strip theories are still widely in use, as reported by the Load Committee of the recent ISSC (Temarel et al., 2006).

Ship motion RAOs, $H(\omega)$ obtained for each degree of freedom are combined with a sea spectrum $S(\omega)$ and constitute the ship motion representation in frequency domain, $S_{ship}(\omega)$

$$S_{ship}(\omega) = |H(\omega)|^2 S(\omega). \tag{2.7}$$

The ship motion is successively transformed to the tank coordinate system. In order to do so, tank subject to the most severe sloshing has to be chosen. As the accelerations are largest at the forward part of the ship, most forward tanks are commonly subject to sloshing analysis. If the most forward tank is of the same size as the others, this tank should be used in the analysis, otherwise the second tank should be analyzed (Lee et al., 2004; Pastoor et al., 2004; Zalar et al., 2005).

Forces excited by the fluid in tanks affect the ship dynamics. Due to technical complexity of modeling this coupling effect in experiments, the feedback from the sloshing-induced forces to the global ship loading is commonly not accounted for. However, a growing interest in this issue is recently observed.

The sloshing-induced forces and moments integrated over the whole tank are not dependent on local phenomena that likely occur in the impact area. Therefore, contrary to the analysis of the local pressures in the tank, numerical approaches are capable of accurate predicting the global effects such as integrated forces and moments.

The same problem as for passive anti-rolling tanks needs to be solved here. Therefore, findings in both these fields of interest are considered herein.

Kim (2002) solves the coupled sloshing problem in anti-rolling tanks by applying the finite difference method for internal problem and a time domain approach based on the potential theory for the external problem. A large effect of internal flow on the ship motions is reported in terms of both amplitude and the peak frequency of response. Qualitative comparison with experiments is presented.

Rognebakke and Faltinsen (2003) study the coupling effect both experimentally and numerically. The authors perform a two-dimensional analysis of a tank moving in one degree of freedom (sway) with a small amplitude. Simulation of sloshing is based on the multimodal method of Faltinsen and Timokha (2001). The external flow is modeled by the boundary element method and solved in frequency domain. The internal flow is solved in time domain. The convolution integral is included in

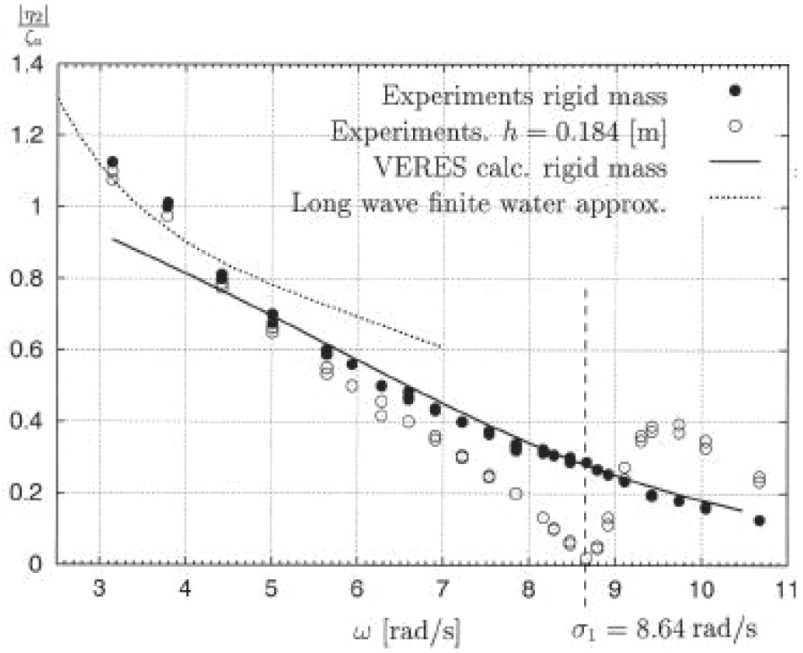

Figure 2.6: Effect of sloshing loads on sway motion. h denotes the filling height such that $h/L = 0.49$, where L is the tank length (Faltinsen and Rognebakke, 2000).

the equation of motion in order to study an arbitrary motion and transient effects. However, it is shown that when the tank behavior in the regular sea is investigated, the motion is almost linear and sinusoidal when a steady-state is reached. This fact means that higher harmonics are filtered out by the system and there is no need for the convolution formulation.

A large influence of the fluid motion in the tanks on the ship motion is observed and a comprehensive analysis of the physical effects is presented. For excitations with a frequency similar to the natural tank frequency the sloshing force and the wave excitation force are out of phase so they counteract each other. For higher excitation frequencies the forces act in phase and the total ship response is enlarged, Figure 2.6.

Various combinations of filling level and number of tanks are investigated. Both linear and nonlinear sloshing models are applied to simulate the internal loading. A good accuracy is observed for the nonlinear model; however, a problem with determining the proper damping in the fluid is reported. As no impacts are observed on the tank roof, the Keulegan damping due to dissipation of energy in the viscous boundary layer is applied. The authors conclude that this damping level is too low and such effects as a spray formation and transition to turbulent flow in the boundary layer can be important. If heavy impact occurs on the tank roof, the damping can be calculated more rationally.

Gaillarde et al. (2004) present an experimental study of coupling between sloshing and ship motion considering motions in 6 degrees of freedom. The authors analyze two different ship models with internal tanks subjected to irregular waves. Different

combinations of speed, wave heading angle, tank filling level and sea parameters are tested. Measurements of the ship motions including accelerations, mooring forces, fluid free surface elevation in the tanks and tank support reaction forces provide valuable data for validation of numerical codes.

A large effect of coupling on the ship motion is observed. Moreover, the second order force on a moored ship and speed variation for the ship with forward speed are observed to be much affected by the internal flow. A numerical method for calculating linear sloshing by the potential theory and for coupling the internal loading with ship motion is also proposed.

Lee et al. (2007) use the experimental results by Gaillarde et al. (2004) for a validation of two numerical approaches based on the frequency domain formulation and on the time domain formulation, respectively. Sloshing simulations are performed by a commercial software based on the potential theory in the former approach and by the own code based on the finite difference method in the latter approach. Frequency domain software based on the linear potential theory is used for the external flow in both approaches. A convolution formulation is used in the time domain approach. Motion in two degrees of freedom, sway and roll due to irregular wave excitation is investigated. Spectra and transfer functions of the ship response with and without the coupling effect are presented. The results show a qualitative agreement with experiments.

Kim et al. (2007) study coupling effects of ship motion and sloshing. Ship motion is solved in the frequency domain and the convolution formulation is used. Fluid motions in a tank along with the global forces and moments are calculated by a finite difference code. The method is applied in an analysis of a sway motion of a box-type barge with rectangular tanks and roll motion of a merchant ship with rectangular anti-rolling tanks. A good agreement with experiments in terms of natural frequency of the motion is observed. The magnitude of motion shows a qualitative agreement.

All these investigations demonstrate that the coupling effect is very important in determining global loads on a ship and the resulting ship motions. More studies are needed in order to develop a comprehensive model that could provide a motion input for sloshing analysis.

2.5 Fluid motion and pressures in a tank

2.5.1 Analytical methods

The sloshing phenomenon has been widely investigated. A comprehensive review of available analytical and numerical methods as well as historical development can be found e.g in Ibrahim (2005).

Sloshing in regular tank shapes were studied already by Lamb in his classical book *Hydrodynamics* in 1895. Abramson (1966) presents an extensive survey of sloshing theories up to 1966 with a special focus on applications within the space vehicle technology. Three-dimensional solutions are presented for various tank shapes including

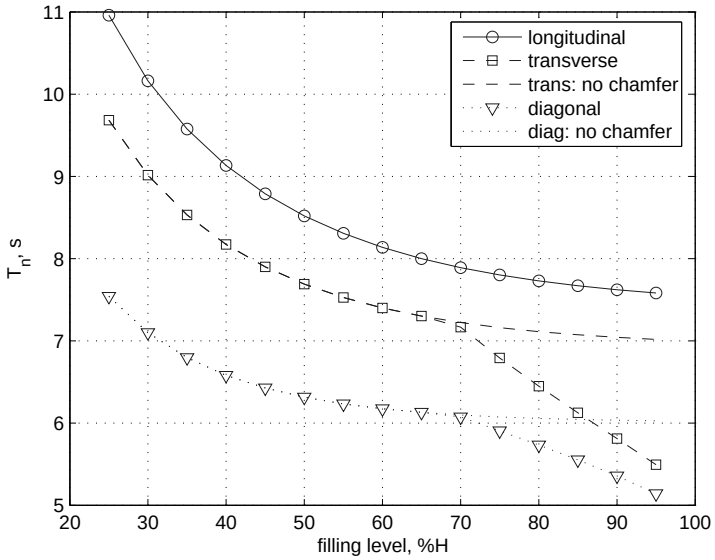

Figure 2.7: Linear eigenfrequencies for a typical LNG tank. Tank dimensions presented in Table A.1, the first series of experiments.

rectangular, cylindrical, circular sector-compartmented, spherical, toroidal and conical tanks for different modes of excitation.

Linear sloshing solution is valid for a small excitation amplitude and frequency distant form the fluid natural frequency. It can be obtained in analytical form by potential theory, for a regular tank geometry.

Natural frequencies of the fluid free oscillations in the rectangular tank are expressed by

$$\omega_{mn} = \sqrt{\pi g \sqrt{\frac{m^2}{a^2} + \frac{n^2}{b^2}} \ \tanh\left(\pi h \sqrt{\frac{m^2}{a^2} + \frac{n^2}{b^2}}\right)}, \tag{2.8}$$

where a, b and h denote the tank length, breadth and the fluid depth, respectively. The eigenfrequencies of the first modes in two directions parallel to the symmetry axes and in the diagonal direction are obtained by inserting $(m = 1, n = 0)$, $(m = 0, n = 1)$ and $(m = 1, n = 1)$, respectively.

The application of the linear theory is very limited. In this work the linear natural frequency is to some extent utilized in determining an approximate measure for sloshing response, as described in Section 2.3. This measure is applied in Paper I, II and III of this thesis for preparing experiments and specifically for determining sea states with critical sloshing response as well as for validating approximate methods for long-term sloshing response. Eigenfrequencies for a typical LNG tank based on linear theory are presented in Figure 2.7. The eigenfrequencies for the chamfered tank shape are calculated in a simplified way by modifying the tank breadth, b.

A general method for nonlinear sloshing is proposed by Moiseyev (1958). Based on this theory a solution for nonlinear sloshing in vertical cylindrical tank is described by Hutton (1963) and for a two-dimensional rectangular tank by Faltinsen (1974). In the

latter, the solution up to the third order is developed for sway and roll oscillations. The problem is solved by application of potential theory. The response of order $\mathcal{O}(\epsilon^{1/3})$ is assumed, with the tank length and filling height both of $\mathcal{O}(1)$ and excitation amplitude of $\mathcal{O}(\epsilon)$, where ϵ is small.

The analytically-based multimodal approach is presented by Faltinsen et al. (2000). The method is capable of determining the solution for nonlinear sloshing of an incompressible fluid with irrotational flow in a rectangular tank. The free surface elevation and velocity potential are expanded in generalized Fourier series by a set of natural modes. The generalized coordinates of the free surface elevation and the velocity potential are found by a coupled system of nonlinear ordinary differential equations. Use of the method is limited to tanks with vertical walls at the free surface, not too small water depth and excludes overturning waves and heavy impacts on the tank ceiling.

The multimodal approach is further developed by Faltinsen and Timokha (2001). An adaptive procedure based on the inter-modal ordering of the generalized coordinates of the free surface elevation is applied. The approach enables describing sloshing resonant response when the excitation is not very small and the fluid depth is close to the critical depth or small.

The multimodal approach is further combined with a local slamming analysis by Rognebakke and Faltinsen (2000). Damping caused by impacts on the tank roof is calculated by relating the energy loss to the total energy in the fluid. The energy loss is estimated based on the Wagner theory with corrections from similarity solution for the chamfered tank ceilings, where the angle between the structure and the fluid surface can be large.

Development of the multimodal approach for three-dimensional problems is presented by Faltinsen et al. (2003). Different regimes of response in the stable and unstable form and their frequency domains are presented. A contribution of higher modes and effect of decreasing fluid depth is investigated.

The authors study also an effect of different breadth-to-length ratio in tanks with near-square base Faltinsen (2005). With the varying ratio, steady-state wave regimes are conserved but the frequency domains, where these wave regimes are stable, change much.

Although many of the hydrodynamic phenomena contributing to sloshing are well described by analytical formulations, the complete problem is too complex to be solved by analytical methods. Therefore, much attention is devoted to other, numerical and experimental studies.

2.5.2 Numerical methods

The fluid flow can in the general case be described by the Navier-Stokes equations. If viscosity is neglected the Euler equation applies. By further assuming incompressible fluid and irrotational flow the governing equation becomes the Laplace equation. The numerical methods discretize partial differential equations to obtain the system with a finite number of unknowns. This is often performed by meshing a flow domain. The Lagrangian description assumes following the fluid particles, while in the Eulerian

description the computational domain is fixed with respect to a reference frame. The hybrid solution, combining the both approaches can also be used. A separate group of methods are meshless approaches.

A number of numerical schemes is applied in the hydrodynamic computations. The principle of the finite element method (FEM) is to subdivide the domain into a number of discrete volumes (in 3D) or areas (in 2D). A Lagrangian description is commonly used. The solution over the elements is assumed to be in a prescribed functional form scaled by nodal values. The solution is not exact and does not satisfy the differential equations. The result is then obtained by minimizing the residual. For problems with large distortions of the free surface, big deformations of elements may require regridding. An example of applying FEM for sloshing simulations is presented by Kim et al. (2002).

A special type of the finite element method is the boundary element method (BEM). Here, a fluid velocity potential is represented by singularities distributed over the fluid domain boundaries. By using boundary conditions, density of the singularities is determined. The potential flow has to be assumed, the fluid is inviscid and incompressible and the flow is irrotational. The BEM is applied in a sloshing study by Faltinsen (1978).

The principle of the finite difference method (FDM) consists in replacing the partial derivatives of the governing equations by algebraic difference quotients in order to obtain a system of algebraic equations. The method is commonly based on the Eulerian approach and a structured grid.

In the finite volume method (FVM) one calculates values of the fluid flow variables averaged across the fluid domain. The discretization of governing equations is done by integration over each element and subsequently approximating the values on its boundaries. This method is also based on the Eulerian approach, however an unstructured grid can be utilized.

Methods for solving the fluid flow are commonly combined with methods for predicting the free surface based on either surface tracking or surface capturing principle. The most common is the Volume of Fluid (VoF) method. Its principle is to discretize a fluid surface by storing only fluid fraction in each computational cell instead of an exact interface. Cells placed within a fluid domain have a volume fraction equal to unity, ones placed beyond a fluid domain - zero, and ones which contain an the interface - a fraction of unity. By evolving the volumes in time with solution of the advection equation the interface is tracked. Its reconstruction is performed by special algorithms. An example of VoF application for sloshing simulations is presented by Loots et al. (2004).

Among meshless methods, Smoothed Particle Hydrodynamics (SPH) is a promising method for sloshing flow modeling, see e.g. Landrini et al. (2003). In the SPH method, the fluid field is represented as a number of particles interacting with each other through evolution equations. The particles can be arbitrarily scattered over the fluid domain leading to a completely grid-free method. The interaction terms follow from the discretization of mass- and momentum-conservation equations by sampling through a kernel function. They can be computed independently of each

other, which ensures the efficiency of the method through parallelization of calculations. The method is robust even for large free surface fragmentation and folding.

However, a full understanding of all the interacting phenomena is still lacking and limits the reliability of numerical results. The application of numerical methods is moreover limited by the computational expenses that has to be incurred in order to cover a fluid domain with sufficient temporal and spatial accuracy, in a long enough simulation time.

2.5.3 Experimental methods

The most reliable description of the fluid motion and sloshing-induced loads in a ship tank is so far available by experiments. The experiments are performed on models that represent a cargo tank installed on board an LNG carrier in a seaway. The input motion of the tank is provided by a special rig. The measured quantity is pressure excited on the structure by the fluid.

A testing campaign is performed in the framework of this Ph.D. work. The experimental procedure and set-up is presented in Appendix A.

Laboratory tests are expensive in terms of required facilities. Moreover, although most reliable, they are also saddle with uncertainties that result form both physical limitations and lack of well determined post-processing procedures.

Excitation of the tank in all degrees of freedom (DOF) influences the response of the fluid. However, until 2005-2006 sloshing rigs could perform motions in 2- or 4-DOFs (surge+pitch and/or sway+roll). The importance of the excitation in all 6 DOF is shown by Gavory (2005). By comparing experimental results registered during the tests on a 4- and 6-DOF rig the author shows that incorporation of the heave and yaw motions in low filling level experiments increases the maximum average pressure estimates by 42%. An inverse trend is observed for high filling level. A decreases of the average pressure estimates by 16% is observed.

The quality of obtained results is limited both technically and economically. There is a trade-off between the spatial resolution of pressure and sensed area as well as between sampling frequency and the test duration.

The first issue is related to a physical limitations of fitting sensors in the model, available number of sensors and logging channels as well as an intention to limit the amount of logged data. The spatial resolution of pressure measured by a matrix of sensors may reach an order of a few millimeters model scale. In typically scaled tanks (between 1:70 and 1:20, usually 1:50) a resolution of a few tens of centimeters full scale is only available. Hence, the pressures need to be spatially interpolated between measured values.

Moreover, such a high resolution may only be applied on a limited tank surface area. The results obtained may not provide a full overview over excited pressures in various tank regions. Therefore a test campaign needs to be preceded by experiments with a large sensed area even at the cost of spatial resolution of registered pressures. This makes it possible to determine regions where high pressures are likely to occur.

The temporal resolution is mainly limited by the amount of logged data. A 43-minutes' run (corresponding to a 5 hours' duration scaled as 1:50 by the Froude

law) sampled with a frequency of 20kHz may provide approximately 0.5GB data for each pressure sensor. Thus, the sampling frequency is commonly kept as low as possible and pressures need to be temporarily interpolated between the measured values. Richardson et al. (2005) show that the frequency of about 20kHz is a limiting value to assure a good accuracy for the model scaled as 1:50.

Other physical limitations are related to modeling the tank structure that is flexible and possibly corrugated on its surface as well as the gas and liquefied gas characterized by physical parameters which are difficult to represent in laboratory conditions. These issues are related to problems associated with the post-processing procedures and specifically lack of a consistent scaling formulation.

As mentioned, sloshing experiments are performed on models commonly scaled as between 1:70 and 1:20. Very few full scale measurements have been performed, those carried out up to 1980 are reported by Cox et al. (1980). Pastoor et al. (2005) report that a new full-scale test campaign is planned.

An appropriate scaling law has to be determined. The scaling problem related to sloshing is investigated by Abramson et al. (1974) where different effects that possibly influence scaling of sloshing pressure are examined. Among them surface tension, viscosity, compressibility, cavitation and wall elasticity are investigated analytically by comparing magnitudes of their dimensionless formulations. In a more general way the scaling problem is treated by Faltinsen (2005).

The most frequently applied scaling formulation assumes geometric and Froude number similitude. The Froude number is defined as

$$F_n = \frac{V}{\sqrt{gL}}. \tag{2.9}$$

V and L are characteristic tank velocity and length, respectively. This implies that the pressure, p is scaled as

$$\frac{p_p}{p_m} = \frac{\rho_p L_p}{\rho_m L_m}, \tag{2.10}$$

where the subscripts p and m relate to prototype and model, respectively, L denotes characteristic length and ρ fluid density. The time, t is scaled as

$$\frac{t_p}{t_m} = \sqrt{\frac{L_p}{L_m}}. \tag{2.11}$$

Froude scaling applies under the following assumptions: incompressible fluid, rigid tank, no viscosity, no surface tension and a zero density ratio between gas and liquid.

Among these assumptions the most attention is devoted to the problem of compressibility. The compressibility is important for media with a low speed of sound. As the speed of sound of the liquefied natural gas is high, this issue becomes interesting when the gaseous fraction is apparent in the impact region. This is very likely to occur during sloshing in LNG tanks. First of all, the fluid is boiling, which means that bubbles are formed inside the bulk of the liquid. A gas cushion may also be entrapped in the impact region. Moreover, the bubbles may be generated when the cushion collapses.

When the fluid compressibility is important the relationship between the gas pressure and gas density as well as between the gas density and fluid density need to be incorporated. The scaling formulation valid for impact events with a gas cushion entrapped is derived by a simplified analysis with a linearized adiabatic pressure-density relationship by Faltinsen (2005). It is shown that the pressure is scaled as

$$\frac{p_p}{p_m} = \sqrt{\frac{\rho_p \; L_p \; p_p^a}{\rho_m L_m p_m^a}}, \tag{2.12}$$

where p^a is the pressure in the tank. The time is scaled as

$$\frac{t_p}{t_m} = \frac{L_p}{L_m}\sqrt{\frac{\rho_p \; p_m^a}{\rho_m p_p^a}}. \tag{2.13}$$

Pressure time histories of the impacts with entrapped gas cushion consist of a pressure peak followed by distinct oscillations that are caused by the gas compressible effect, while hydrodynamic impacts have a regular, nearly triangular or trapezoidal temporal pattern.

By examining experimental results it is observed that hydrodynamic and gas-cushioned impacts occur randomly in the fluid and should be described by Froude and compressible scaling law, respectively. In practice it is hard to distinguish between impacts of the different types and the Froude scaling is commonly applied.

Application of the two scaling laws yields significantly different results. In model tests the LNG is normally represented by water and the same, atmospheric tank pressure p^a is applied. For a model scaled by 1:50 the Froude scaled impact pressure is larger than the pressure scaled by the compressible law and time is shorter, both by the factor of 4.60. The difference can be reduced by further modifying p^a and/or ρ. The results converge to the same value when the similitude of the Euler number defined as

$$Eu = \frac{p^a}{\sqrt{gV^2}} \tag{2.14}$$

is satisfied.

It should be noted that the commonly cited conservatism of the Froude scaling concerns only pressure magnitude. Conservatism of the temporal characteristics is dependent on these characteristics related to the natural period of the structure. This issue is investigated in Paper V.

Different approaches to this problem are proposed in the literature. Lee et al. (2004) run the tests in atmospheric pressure with water and combine the two Froude and compressible scaling laws. They make an attempt to distinguish between physical phenomena governing each impact by inspecting temporal distribution of the time history.

The scaling law may be further explored by performing model tests in various scales as well as with different fluid and gas densities and pressures. Pastoor et al. (2005) and Richardson et al. (2005) report sloshing tests with various gas densities

and pressures. The results indicate that water-based experiments can be overly conservative. The authors report a large effect of the gas-liquid density ratio on measured pressures and rise time, but a conclusive answer is still not known.

From the fact that LNG is transported in the ship tank as a boiling liquid it follows that the vapor pressure p^v is approximately equal an ambient tank pressure p^a. In case of model tests performed with water in room temperature, vapor pressure is much lower than the pressure in the free surface. The amount of vapor bubbles increases in the boiling liquid. The cavitation number

$$Ca = \frac{p^a - p^v}{0.5\rho V^2} \tag{2.15}$$

needs to be preserved.

The tank walls are represented in the laboratory tests as flat surfaces while the membrane may be corrugated, as in the Mark III system. Such corrugations may cause cushioning of pressure. Shin et al. (2003) investigate this problem by comparing pressures measured on the corrugated and flat structures dropped on the liquid nitrogen. The results show a pressure reduction of the order of 50-75% for small incidence angles which encourage cushion creation. This issue is also investigated by Chung et al. (2006).

Another effect of the gas compressibility in a cushion may also be expected. If the LNG itself is assumed incompressible, this assumption needs to be related to a time scale of events. This means that if a structural response with a high frequency, say above 1000Hz, occurs the assumption is no longer valid. Moreover, the frequency of the gas compressible oscillations may affect the contribution of particular modes of the structural response. This is the case when this frequency is similar to the eigenfrequencies of the membrane structure.

The natural frequency of the compressible gas oscillations has been examined and reported in Appendix C. The effect of gas cushions creation on the pressure magnitude is not investigated.

Commonly, the tank walls in model tests are rigid. This implies that fluid-structure interaction is not accounted for. When the fluid-structure interaction matters during the impact the flexible walls should in principle be applied. The problem of hydroelasticity is described in more detail in Section 2.6 and investigated in the Paper V of this thesis.

If hydroelasticity matters, the material elastic properties of the walls should represent the elastic properties of the membrane tank structure. It means that in addition to the geometrical scaling of structural elements and Froude scaling of their eigenfrequencies, the scaling of the frequency has to reflect the hydroelastic behavior. Faltinsen (2005) shows that if the structure can be represented by a beam of constant thickness the frequency should be scaled as

$$\frac{\omega_p}{\omega_m} = \sqrt{\frac{\rho_m L_m^5 \; E_p \; I_p}{\rho_p \; L_p^5 \; E_m I_m}} \tag{2.16}$$

in order to satisfy the latter issue. L denotes length of the beam and EI its bending stiffness. In model tests the complex tank structure needs to be simplified by using

materials with different properties or a modification of through-thickness dimension. This fact obviously introduces uncertainties.

2.5.4 Post-processing of experimental results

Post-processing techniques are applied in order to extract the necessary information to determine a representative structural loading.

Temporal and spatial characteristics of the pressure may be equally important as its magnitude; this is presented in more detail in Section 2.6. The pressure exerted on a structure by the impacting fluid may have a complex time history and spatial extent. In order to effectively utilize pressures as input to the structural analysis they need to be simplified, i.e. described in terms of a few well-defined parameters. Storing values of these parameters instead of the whole pressure time histories limits amount of data significantly.

The pressure magnitude is one of these parameters. In determining the short-term variability of pressure magnitude it is necessary to observe that the time histories of gas-cushioned impacts include secondary oscillations following the maxima. Including these maxima violates the assumption of independence of sample data imposed by extreme value statistics. Hence, a technique for filtering the maxima needs to be applied.

A probabilistic density function needs to be chosen and fitted to the measured data in order to enable extrapolation towards the upper tail and estimating the characteristic short-term extremes. A long-term response is based on the short-term responses with an additional statistical information provided, as presented in Section 2.3.

There are a few probabilistic models used to describe the short-term variability of sloshing pressures. The most commonly applied are the three-parameter Weibull distribution (Gavory, 2005; Pastoor et al., 2005; Rognebakke et al., 2006), the three-parameter log-normal distribution (Gavory, 2005) and the generalized Pareto distribution (Rognebakke et al., 2006).

The choice of the characteristic temporal parameters depends on the ratio of the load duration t_d and the natural period of the structure T_n, as further explained in Section 2.6. For a very short duration of pressure, an integrated impulse is an important parameter for the structural response. With increasing load duration, the rise time and total duration become more important. For sloshing impacts on the containment wall the load duration t_d is similar to the natural period of the structure T_n. Hence, the duration t_d and rise time t_r are the important parameters.

Choice of the characteristic spatial parameters should be based on the relationship between the loading area and the response. However, such a relationship is difficult to determine. This is due to the fact that containment systems are very complex structures made of relatively special materials within the field of marine technology. The structure is not uniform over the tank surface and the relationship between the loading area and the response is location-dependent. Moreover, many forms of response are important and for each of them a different relationship may apply, as further explained in Section 2.6.

As no explicit relationship between pressure temporal or spatial characteristics and response exists, it is difficult to determine a consistent approach for statistical post-processing of these pressure characteristics.

Some attempts to quantify the temporal and spatial distribution of the sloshing loads have been made. Lee et al. (2004) categorized sloshing peak temporal patterns as one of the three types: peaks with short rise time and relatively long decay time, symmetric peaks and peaks with long rise time and short decay time.

Pastoor et al. (2004) and Tveitnes et al. (2004) investigate temporal characteristics of pressure peaks and make a qualitative comparison of peaks' pattern in various filling levels. Furthermore, Pastoor et al. (2005) make an effort to determine impact temporal distribution in a qualitative form. A time history with $t_r = 0.4t_d$ is conservatively chosen as a representative load pattern, where t_r and t_d denote the rise time and pressure duration, respectively.

Zhao et al. (2004) propose to neglect details of pressure time history but instead integrate the pressure impulse over a small time period compared to the natural period of the membrane structure. The same approach is applied by Paik (2006).

Both temporal and spatial patterns are investigated by Rognebakke et al. (2006). Examples of relationships for pressure averaged over various time intervals and various areas are presented.

Gavory (2005) presents a relationship between average pressure and area for a chosen case.

As the relationship between pressure spatial characteristics and response in a closed form is still lacking, the pressure recorded by each sensor is commonly stored or averaged over a number of sensors. The averaging may be done by interpolating linearly the pressure between sensors. Other techniques are also reported in literature. Rosén (2005) suggests an alternative interpolation technique based on measurements in discrete points and applies the method for the slamming problem on a ship hull. A smooth pressure distribution over area may also be obtained by applying an interpolation method based on the Delaunay triangulation, as presented by Gavory (2005).

The procedures applied for post-processing experiments performed within this work are described in Appendix B.

The post-processing is carried out by separately investigating the pressure magnitude, duration of the time history and the average over various areas. This is necessary to relate the different parameters to each other for a given impact. Such a relationship may then be represented by the velocity of the pressure profile along the wall.

The short term statistics of the pressure magnitude is investigated in Paper I and Paper IV of this thesis. Paper I is focused on the accuracy of the three-parameter Weibull model and the generalized Pareto model. Parameters of the statistical models are determined by fitting the models to the measured data samples. Estimates of the extreme values are calculated based on the concept of order statistics.

The relationship between the shape parameter in the generalized Pareto model and a resulting domain of attraction of various extreme value distributions is described

in the Papers III and IV. It is found that the limiting lowest value for the shape parameter is zero.

The peak-over-threshold method is applied to fit the generalized Pareto model. The method is based on considering only the maxima exceeding a given, high threshold. Hence, the results will be sensitive to the threshold level. A too high threshold level limits the sample size and reduces the accuracy. In Paper IV the suitability of the generalized Pareto model for describing sloshing induced pressures based on the samples from 5h duration experimental tests is found to be questionable.

The largest values in each sample are very scarce, which results in a limited reliability of estimates, regardless of the model used. In order to collect samples that are more dense in the upper tail, longer runs are applied.

But even with a five-hour duration of the sample, a large variability of extreme estimates is observed. In order to obtain reliable estimates the number of test repetitions in the chosen condition should be high.

Moreover, it is observed that the pressure estimates calculated for runs with the same input (tank motion time history) and with different input (but for the same sea state) have the same variability. This shows the significance of an inherent sloshing variability.

The long-term statistics is related to additional sources of uncertainty, as described in Section 2.3, and in Paper III of this thesis.

The distribution of the temporal parameters, duration and rise time, as well as spatial distribution and the velocity of the pressure profile along the wall is investigated in Paper IV of this thesis.

It is found that pressure time histories are usually of a near-triangular shape. They include, however, small local distortions. As the load duration is similar to the natural period of the structure, other details of the pressure time histories may be important for the structural response. The studies in Paper IV, however show that these effects are relatively small for the largest pressures.

A common approach is therefore to approximate the temporal pattern with a triangle. An alternative analytical approximation by a trapezoid is introduced in Papers III and IV. This function describes time histories much more accurately. In order to fully understand the effect of choosing various approximate analytical functions the structural analysis is performed. The results are presented in Appendix B.

2.6 Structural response

The structural response does not only depend on the pressure peak magnitude, but also temporal and spatial variation of the loading.

Fluid impacts may be classified as impulsive or non-impulsive depending on the temporal characteristics of pressure in relation to the characteristic, typically the highest natural period of the structure response, T_n.

For impact duration t_d shorter than approximately 0.25 of T_n the structural response does not depend on pressure magnitude but rather on the total impulse. With a gradually increasing duration the rise time and duration become the dominant pa-

rameters. The magnitude is also important in this case. For the pressure duration t_d significantly longer than the structural natural period T_n, the loading becomes quasi-static. This means it is only the pressure magnitude which determines the maximum response.

In effect, when the pressure duration t_d is much shorter than T_n, the response is significantly lower than the response to a static loading of the same magnitude. This is caused by the fact that the inertial forces of the structure balance the pressure loads and maximum strains occur after the load has acted, in a free vibration phase. When the pressure duration is of the order of T_n, the response can be amplified by up to a factor 2, dependently on the pattern of the time history (Biggs, 1964). This relationship is often expressed by means of the dynamic load factor (DLF) factor, defined as

$$DLF = \frac{R_d^{max}}{R_s}. \tag{2.17}$$

R_d^{max} and R_s are the maximum dynamic response and the static response to the same loading, respectively.

The spatial variation of the sloshing pressure also affects the structural response. As the pressure is concentrated on a given area, an average pressure is a more meaningful parameter for a structural analysis. The average pressure over an area decreases with increasing area.

Different response quantities associated with the tank wall are of interest. They include local effects in structure of the insulation system, response of stiffened steel plate supporting the insulation system as well as the whole tank wall. The global ship response may also be affected by forces from the fluid. Different loading areas would be representative for these responses.

The insulation system that covers the steel structure has a much lower strength than steel. Therefore, the primary structural issue is the local response of the membrane system and its potential damage. However, the response of the insulation system cannot be decoupled from the response of the steel plate supporting it. A common simplification is to assume that the steel structure does not respond to the sloshing loads and hence, the insulation system is rigidly supported. This approach may with sufficient accuracy be applied in cases in which the largest natural period of the stiffened steel panel is much longer than the excitation duration. This approximation facilitates a reasonable two-dimensional modeling of a flat tank wall section. In a two-dimensional model the response is location-independent with respect to the steel panel support. This may be observed from Figure 2.8 in conjunction with the figures of the three-dimensional response in Paper V.

In reality, the insulation system is supported by a steel plate which is flexible. As the insulation layers are mechanically joined to the steel plate, the eigenfrequencies of the structure change. The loading may cause plate deflection in addition to the response of the insulation system itself. The response pattern becomes then more complex and location-dependent. In effect, the stresses are transmitted to the areas where the steel support structure is most stiff and hence concentrate over stiffener and girder supports. This issue is investigated in Paper V.

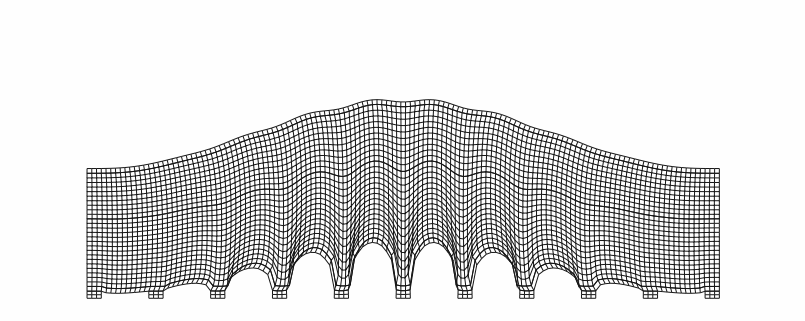

Figure 2.8: A mode of response of a two-dimensional model of the Mark III insulation system. The model represents a through-thickness cross section of the insulation system resting on rigidly supported resin ropes (lowermost in the figure) and with a fluid contact surface (membrane) on the top.

The main forms of response of the containment system are bending of the steel plate between stiffeners and girders and a vertical compression of the foam. The bending of the steel plate implies that the insulation system above the steel is compressed in the center of the panel and stretched near the edges. In addition, as the lower plywood is kept distant from the steel plate by the resin ropes, the lower plywood plate is subjected to bending between resin ropes.

In effect, the most relevant responses and failure modes include crushing of the foam in the Mark III system, buckling and through-thickness crushing of plywood plates in the No.96 system as well as shear and bending of plywood plates in both concepts.

Within these forms of response many modes may be excited. Modal composition of the response in a chosen load case is presented in Paper V. The eigenfrequency analysis is also performed. The Fast Fourier Transform of the response time series is performed and the spectra obtained are compared to the eigenfrequencies. This enables an investigation of the contribution of particular modes to the response.

In general, the structural response should be investigated by a time domain dynamic approach with an account of spatial extent, pressure time history, and added mass influence. Therefore, numerical tools are commonly applied, usually based on the finite element method.

In the linear case, however, a simplified approach, such as modal analysis and consideration of the dynamic load factor (DLF) for each mode can be applied. In Paper V the suitability of the DLF approach is investigated. It is found that due to a large number of contributing modes and local stress concentrations in rigid areas, the approach is not suitable for analyzing the response of the containment system.

The pressure excited by a fluid in a tank generates a deformation of the structure. The deformation is of an oscillatory nature and, if the structure is submerged in the fluid, causes a hydrodynamic force. The term proportional to the acceleration constitutes the added mass force. If the time scales of the excitation force and the oscillatory motion are similar the interaction between the fluid and the structure needs to be accounted for.

The problem of fluid-structure interaction gained a lot of interest in aerospace technology over many decades. Recently, due to a considerable progress in computational techniques and computer performance the problem has become investigated with increasing attention. A wide review of fluid-structure coupling algorithms as well as fluid and structure models is presented by Kamakoti and Shyy (2004) with a specific attention to aeroelasticity. The degree of coupling between the fluid flow and structural response may be classified as loosely-, closely- and fully coupled.

The fluid-structure interaction is also of concern in many ocean engineering applications. A review of hydroelastic problems associated with fluid impact is presented by Faltinsen (2000). Theoretical and experimental studies are described with a special attention to slamming on ship hulls.

Different approaches may be utilized to account for the hydroelasticity. A simple method is to model the mass by the structural mass and an added mass. Two limiting cases of added mass are determined. The upper limit corresponds to the asymptotic value of the added mass for a plate reciprocating on the fluid surface with an infinite frequency of oscillation and is expressed as (Faltinsen, 1990)

$$A = \pi \rho R^2/2. \tag{2.18}$$

The lower limit corresponds to the zero added mass. It is noted that these two limits do not necessarily result in the respective limits for the structural response. Namely, the added mass affects the eigenperiod of the structure and, as described above in this section, the dynamic response changes nonlinearly with the ratio between duration of excitation and eigenperiod.

This simple approach by using added mass is in common use as it is very cheap in application. Also rules of the majority of the classification societies utilize this concept. They are often limited to considering either *dry* response only or modeling the fluid as an acoustic medium filling the whole domain, and thus imposing a fully wetted length, accounting for *wet* response only.

For sloshing impact on the membrane structure a complex fluid flow in the impact region is observed and a number of parameters influence the added mass. Thickness of the fluid layer, its spatial extent as well as its density due to aeration can be very different for various impacts and in addition they are non-stationary during a given impact. There is a limited number of works describing influence of these parameters on the value of added mass for a rectangular plate. Among them Cheung and Zhou (2000) present a semi-analytical study dealing with vibrations of a thin plate which is a part of a container bottom, rigid beyond the plate and filled with a fluid. Results in terms of the frequency ratio of wet-to-dry oscillations are presented for different fluid depths, plate dimensions, fluid-plate density ratio and boundary conditions.

Approaches capable of determining an instantaneous value of added mass enable calculation of a coupled response. A number of approaches based on the Wagner theory have been developed. The Wagner theory describes the initial stage of a water entry problem and is valid when the penetration depth is much smaller then the body width. Hence, the methods can be applied for elastic blunt bodies impacting vertically on a fluid surface with a moderate velocity. Actually, it is not important

which of the two surfaces is curved. An important feature of these approaches is that the hydrodynamic coefficients can be calculated analytically, which makes the calculations very time efficient.

Kvålsvold and Faltinsen (1995) present a study of the water impact on a horizontal elastic plate. The authors use a two-dimensional normal mode decomposition method that combines the boundary value problem for the fluid with the Euler beam formulation for the structure of wet deck. The structural deflection is expressed in the modal form (uncoupled from the fluid). The fluid-structure interaction is accounted for by instantaneous hydrodynamic coefficients determined analytically by a decomposition of the fluid force into added mass, damping and the remaining excitation force. The method is validated by comparison to experiments by Faltinsen et al. (1997)

Korobkin et al. (2006) present a two-dimensional method for the fluid-structure interaction with a coupling of the finite element (FE) method for the structural response with a similar, Wagner theory-based approach for hydrodynamics. The boundary value problem for the impacting rigid deformed wedge and the problem for the oscillating wedge in a fixed position are solved in parallel for each time step. The approach is presented for a wedge consisting of two beams. Since the FE method is applied to model the structure the method in principle can be applied to more complex problems. The method is validated by comparison with the modal method. Malenica et al. (2006) show a possible application of this method to an analysis of two-dimensional coupled response of the membrane structure to a simplified impact.

Rognebakke and Faltinsen (2006) use the normal mode decomposition method and beam theory for determining the coupled response of a flexible wall in the tank with a high filling level. A response to impact on the tank roof is investigated. Calculated strains are compared to experiments with an elastic upper part of a wall.

An experimental and numerical investigation of the elastic response of the tank wall under sloshing impact is also presented by Lee and Choi (1999). The authors apply the normal mode decomposition method with the thin plate theory and combine it with the boundary element method for the fluid solver. The results are compared to experiments with the filling level of 25% and 75% of the tank height. The tank model has one elastic wall. A qualitative agreement is observed for pressure due to impacts occurring on the tank wall and roof.

In more general cases, e.g. when the structure is very flexible and hydroelasticity becomes important also for impact with a relatively large deadrise angle, methods based on the numerical solvers, both for fluid and structure need to be used.

Lee et al. (2004) present a simplified approach for the fluid-structure interaction in the membrane LNG tank. A FE method is used for modeling both structure and fluid. The free surface flow is not modeled. Instead, a prescribed pressure field is assumed to move along the boundary while the whole structure is assumed to be wet.

Lu et al. (2000) investigate a two-dimensional problem of an impact of a wedge with thin walls. The boundary element method and the FE method are used in the fluid and the structure solvers, respectively. A fully coupled system is applied. This means that the governing equations for hydrodynamic and structural analyses are combined and are solved and integrated simultaneously in time. Fluid pressure is calculated from a linearized Bernoulli equation, the nonlinear free surface boundary

condition is satisfied and the jet formation is treated in an effective way. Linear elastic theory governs the structural response. The method is validated by comparing results for rigid body calculations to previous work and a good agreement is reported. Results for an elastic wedge with different plate thickness and deadrise angle are presented.

Nam et al. (2005) make an attempt to solve a fluid-structure interaction problem relevant for sloshing in LNG membrane tanks. The finite volume method for the fluid is combined with the FE method for a structure. A closely coupled system is applied; the fluid and structure equations are solved separately using two different solvers and are coupled into one module. Interaction is ensured by a coupling surface, which acts as a boundary for the flow and transfers the pressures. The analysis is stepwise. First, an uncoupled fluid simulation is performed in order to find time instants for sloshing impacts on the structure. Subsequently, the coupled analysis is carried out for limited temporal and spatial extent. The time range covers the fluid impact on the structure. Fluid state variables determined by the uncoupled fluid analysis constitute the initial conditions. A small part of the layered insulation structure near the tank upper corner is modeled.

The authors also perform a sensitivity study of the insulation system hydroelastic response to different parameters of the fluid impact (Nam et al., 2006). However, determining impact pressure by numerical methods is still problematic, as shown e.g. by Landrini (2006). Therefore, fluid solvers need to be properly validated by comparison with analytical or experimental results

Mutsuda et al. (2005) presents another approach. A method based on the finite difference discretization and the Constrained Interpolation Profile (CIP) is used for solving the fluid and is coupled with the particle based Extended Distinct Element Method (EDEM) for structural modeling. The CIP method is a convective scheme based on the idea that for a given quantity, not only the advection equation of this quantity, but also the advection equation of its spatial gradient is calculated. The method is a less diffusive and more stable algorithm than any other high order convective schemes of finite difference method. The EDEM method describes the motion of individual solid particles providing information about their shape, kinematics and interactions between them. The continuity between the particles is maintained by so-called pore-spring. The two formulations are solved simultaneously with a different time step. Solution of various fluid-structure interaction problems between fluid and elastic structures are shown, but the results are not compared to experiments.

Besides developing accurate, refined methods for determining the coupled sloshing response of the containment system, it is important to establish simplified and robust approaches for assessment of the hydroelastic effects.

The accuracy of a simplified method obtained by modifying the structural mass by a given, constant value of added mass, is investigated in Paper V of this thesis. The hydroelastic analysis is performed using a simplified two-dimensional method. The structure is represented by a beam model and the Wagner theory is applied for the hydrodynamic problem.

Representing the containment wall as a beam is not straightforward. In the hydroelastic analysis it is required that the model covers the fluid-structure contact surface. It is equally important that the model allows investigating the structural

response of a layer which is distant from this surface. The model is established based on the observation that there is a linear relationship between the displacement of the upper plywood and the bending stress in the lower plywood for the rigidly supported insulation system.

For this simplified model and the range of structural and hydrodynamic properties considered the effect of hydroelasticity is found to be insignificant.

Chapter 3

Concluding remarks

3.1 Original contributions

The main findings of the thesis are listed below.

The variability of the sea environment is investigated and its implications on long-term estimates of ship motion and sloshing response are demonstrated.

- By investigating ship motion characteristics, and specifically acceleration spectra, the sloshing severity may be assessed. The tank natural frequency needs to be introduced and nonlinearities in determining this frequency play an important role. This method may effectively be utilized to determine the critical operational conditions. The critical operational conditions for a tank with a high filling level may also be satisfactorily determined by the semi-analytical multimodal method.

- The method established to investigate ship motion characteristics can effectively be used to investigate a large number of conditions, hence, also to determine the long-term estimates of sloshing response.

- Sloshing response in benign sea states may contribute much to the long-term response when the excitation frequency is close to the fluid resonance in the tank. Therefore, the suitability of the contour line approach, involving the significant wave height and a typical period only, is questionable. This method is meant to approximate the long-term response based on a chosen critical condition.

Measured sloshing pressure is investigated with regard to parameters that are crucial for the structural response. Techniques for simplifying pressure time histories are investigated and typical loading patterns are determined.

- Pressures excited in tanks with a low filling level are larger than those recorded for a high filling level. Moreover, they last longer and have a larger spatial extent. Quantitative comparison of sloshing response is presented for various operational regimes and locations in tank.

- A three-parameter Weibull model is suitable for describing magnitude of sloshing pressure.

- Application of the generalized Pareto model is problematic. Less accurate estimates than by using the Weibull model are obtained when a low threshold level is chosen, while for a high threshold level a large instability of estimates is observed due to a limited sample size.

- Estimates from experiments have a large variability. To obtain reliable estimates a large number of repetitions needs to be carried out.

- Hydrodynamic sloshing impacts and impacts with entrapped gas occur randomly in a tank. Gas bubbles are also present in the impact region. The importance of gas compressible effects makes the scaling of pressure time histories not straightforward.

- The accuracy of modeling pressure time histories by linear functions may be low for small pressures; however, a satisfactory accuracy is obtained for large pressures. Three linear functions, resulting in a trapezoidal impact, model the real time histories more accurately than a triangular impulse (two linear functions). However, the inaccuracy of the structural response by using a triangular impulse is not large and may be accounted for by introducing a correction factor.

The structural response of the membrane tank wall outfitted with the Mark III containment system is analyzed by the modal method and by the time-domain direct integration scheme.

- Two forms of structural response in the containment-steel hull system are observed in the static case. The first form is governed by the steel plate deflection and consists of a two-plane bending of the steel plate together with the insulation supported by the stiffeners and girders at the plate edges. It results in compression of the containment system in the center of the plate and tension near the edges. The other form is a vertical compression of the foam and, as the insulation layers are kept distant from the steel plate by the resin ropes, a span-wise bending of the lowest layer of insulation (plywood plate) between resin ropes.

- The structural response pattern becomes even more complex when the response is dynamic due to a lengthwise propagation of the steel plate bending as well as a difference in oscillation frequency and in relative phase between modes of plywood and steel plate response.

- These effects result in a very large amplification of the dynamic response related to the static response. This makes simplified methods for dynamic structural analysis unsuitable for the investigating the response of the LNG containment system.

- The structural response has a complex multi-modal composition, including modes representing both forms. The composition depends on many factors such as added mass, location relative to a steel plate supporting the insulation system, load duration and its spatial extent. Therefore, modal methods are not suitable for analyzing the response of the structure considered.
- For a limited model and the range of structural and hydrodynamic properties considered in this study the effect of hydroelasticity is not significant. The structural response obtained by a simple method based on modifying structural mass by a constant value of added mass is conservative.

Global response of LNG membrane ship hull is investigated with respect to the effect of hull flexibility on whipping-induced tank pressures.

- Hull elasticity and nonlinear effects are important for an LNG carrier. Due to these effects, the bending moment in sagging increases by up to 60% and the hogging moment, which is dominant, by 20%. The vertical acceleration increases by up to 20%.
- When systems capable of forecasting wave climate expected by a ship are utilized, scatter diagram needs to be modified, which reduces the long-term estimate of vertical acceleration and eliminates the whipping effect.

3.2 Recommendations for further work

Further work in this area may include the following issues:

- The simplified method for identifying important sea states for sloshing based on ship motion characteristics appears to be an important tool in determining the long-term sloshing response, but requires further validation by comparing with experimental data and possibly by including nonlinearities in the response characteristics.
- By using this method a contribution from response in particular sea states to the long-term response may be assessed. A method based on considering a larger number of conditions than in the contour line approach, possibly including also more benign sea states seems to be the proper way of progressing.
- The variability of pressure estimates is large, even from tests with a 5-hour duration. In order to determine this variability in terms of a minimum required number of repetitions resulting in stable estimates, more experimental data needs to be collected.
- This variability may also be addressed by utilizing the asymptotic extreme value theory by taking advantage of samples of the largest maxima. In this approach either the Gumbel or Fréchet distribution may be used. Determining long enough samples of the largest maxima requires an extensive testing campaign.

- In order to resolve the scaling problem experiments with varying physical parameters of gas and fluid need to be performed. Another, very costly approach is to perform full-scale experiments.
- Investigations of the structural response of the containment system is still relatively limited. More sensitivity studies of structural response to varying spatial and temporal parameters are needed.
- The analytical method applied for the hydroelastic response calculations of the containment system is based on a set of assumptions. In order to obtain fully reliable estimates of hydroelastic effects a coupled numerical approach for fluid and structure needs to be developed and validated.

References

Abramson, H. N., editor (1966). *The dynamic behavior of liquids in moving containers*, number NASA SP-106. National Aeronautics and Space Administration.

Abramson, H. N., Bass, R. L., Faltinsen, O., and Olsen, H. A. (1974). Liquid slosh in LNG carriers. In *Symposium on Naval Hydrodynamics*.

ABS (2006). *Guidance notes on strength assessment of membrane-type LNG containment systems under sloshing loads*. American Bureau of Shipping.

Baarholm, G. S. and Moan, T. (2001). Application of contour line method to estimate extreme ship hull loads considering operational restrictions. *J. Ship Res.*, 45(3):228–240.

Baarholm, G. S. and Moan, T. (2002). Efficient estimation of extreme long-term stresses by considering a combination of longitudinal bending stresses. *J. Mar. Sci. Technol.*, 6:122–134.

Battjes, J. A. (1972). Long-term wave height distributions at seven stations around the british isles. *Dtsch. Hydrogr. Z.*, 25(4):179–189.

Biggs, J. M. (1964). *Introduction to structural dynamics*. New York: McGraw-Hill.

Chapot, M. K. (2002). CS1 - new containment system for LNG carriers. In *Gastech Conference*, Doha, Qatar.

Cheung, Y. K. and Zhou, D. (2000). Coupled vibratory characteristics of a rectangular container bottom plate. *J. Fluids Struct.*, 14:339–357.

Chung, J. Y., Lee, J. H., Kwon, S. H., Ha, M. K., Bang, C. S., Lee, J. N., and Kim, J. J. (2006). Wetdrop tests for LNG insulation system. In *Proceedings of The Sexteenth International Offshore and Polar Engineering Conference*.

Cox, P. A., Bowles, E. B., and Bass, R. L. (1980). Evaluation of liquid dynamic loads in slack LNG cargo tanks. Technical Report SSC-297, Ship Structure Committee.

Curt, B. (2004). Marine transportation of LNG. Presentation at the *Intertanko Conference*.

Dietz, S. J., Friis Hansen, P., and Jensen, J. J. (2004). Design wave episodes for extreme value ship responses. In *Proceedings of the 9th International Symposium on Practical Design of Ships and Other Floating Structures*, pages 286–293.

DNV (1976). *Seminar on liquid sloshing*. Det Norske Veritas.

DNV (2008). *Rules for classification of ships, Pt.5 Ch.5: Liquefied gas carriers*. Det Norske Veritas.

Faltinsen, O. M. (1974). A nonlinear theory of sloshing in rectangular tanks. *J. Ship Res.*, 18(4):224–241.

Faltinsen, O. M. (1978). A numerical nonlinear method of sloshing in tanks with two-dimensional flow. *J. Ship Res.*, 22(3):193–202.

Faltinsen, O. M. (1990). *Sea loads on ship and offshore structures*. Cambridge: Cambridge University Press.

Faltinsen, O. M. (2000). Hydroelastic slamming. *J. Mar. Sci. Technol.*, 5:49–65.

Faltinsen, O. M. (2005). *Hydrodynamics of high-speed marine vehicles*. Cambridge: Cambridge University Press.

Faltinsen, O. M. (2008). *Sloshing*. Preprint.

Faltinsen, O. M., Kvålsvold, J., and Aarsnes, J. V. (1997). Wave impact on a horizontal elastic plate. *J. Mar. Sci. Technol.*, 2:87–100.

Faltinsen, O. M. and Rognebakke, O. F. (2000). Sloshing. In *Proceedings of the International Conference on Ship and Shipping Research, NAV*, Venice, Italy.

Faltinsen, O. M., Rognebakke, O. F., Lukovsky, I. A., and Timokha, A. N. (2000). Multidimensional modal analysis of nonlinear sloshing in a rectangular tank with finite water depth. *J. Fluid Mech.*, 407:201–234.

Faltinsen, O. M., Rognebakke, O. F., and Timokha, A. N. (2003). Resonant three-dimensional nonlinear sloshing in a square-base basin. *J. Fluid Mech.*, 487:1–42.

Faltinsen, O. M. and Timokha, A. N. (2001). An adaptive multimodal approach to nonlinear sloshing in a rectangular tank. *J. Fluid Mech.*, 432:167–200.

Fathi, D. (1997). DASS project: Veres, version 3.1, User's manual. Technical report, Marintek.

Gaillarde, G., Ledoux, A., and Lynch, M. (2004). Coupling between liquefied gas and vessel's motion for partially filled tanks: effect on seakeeping. In *RINA (2004)*, pages 33–38.

Gastech (2005). *Gastech Conference*. Bilbao, Spain.

Gavory, T. (2005). Innovative tools open up new prospects for liquid motion model tests. In *Gastech (2005)*.

Gerritsma, J. and Beukelman, W. (1964). The distribution of the hydrodynamic forces on a heaving and pitching shipmodel in still water. In *Fifth Symposium on Naval Hydrodynamics*.

Graczyk, M. and Moan, T. (2007). Assessment of sloshing pressure and response in LNG tanks. In *Proceedings of the International Conference on Violent Flows, VF-2007*, Fukuoka, Japan.

Graczyk, M. and Moan, T. (2008a). A probabilistic assessment of design sloshing pressure time histories in LNG tanks. *Ocean Eng.*, 35:834–855.

Graczyk, M. and Moan, T. (2008b). Structural response to sloshing excitation in membrane LNG tank. *Submitted for publication*.

Graczyk, M., Moan, T., and Rognebakke, O. (2006). Probabilistic analysis of characteristic pressure for LNG tanks. *J. Offshore Mech. Arct. Eng. Trans. ASME*, 128:133–144.

Graczyk, M., Moan, T., and Wu, M. K. (2007). Extreme sloshing and whipping-induced pressures and structural response in membrane LNG tanks. *Ships and Offshore Structures*, 2(3):201–216.

Guedes Soares, C. (1990). Effect of heavy weather maneuvering on the wave-induced vertical bending moments in ship structures. *J. Ship Res.*, 34(1):60–68.

Harper, I., Langley, I., and Meaden, I. (2004). Future predictions for the marine transportation of natural gas. In *RINA (2004)*.

Haver, S. (1987). On the joint distribution of heights and periods of sea waves. *Ocean Eng.*, 14(5):359–376.

Hoff, J. R. (2004). Private conversation.

Hutton, R. E. (1963). An investigation of resonant, nonlinear nonplanar free surface oscillations of a fluid. Technical Report NASA TN D-1870, National Aeronautics and Space Administration.

IACS (2000). Standard wave data. Recommendation, No.34.

Ibrahim, R. A. (2005). *Liquid sloshing dynamics. Theory and applications*. Cambridge: Cambridge University Press.

IMO (1976). *Gas Carrier Code for Existing Ships*. International Maritime Organization.

Jensen, J. J. and Mansour, A. E. (2003). Estimation of the effect of green water and bow flare slamming on the wave-induced vertical bending moment using closed-form expressions. In Taylor, R. E., editor, *Proceedings of the Third International Conference on Hydroelasticity in Marine Technology*, pages 155–161, Oxford, United Kingdom.

Kamakoti, R. and Shyy, W. (2004). Fluid-structure interaction for aeroelastic applications. *Prog. Aeosp. Sci.*, 40:535–558.

Kernaghan, J. (2004). Offshore floating LNG plants. In *RINA (2004)*.

Kim, H. C. and Lee, D. Y. (2005). Core design issues of large LNG carrier. In *Gastech (2005)*.

Kim, J. W., Shin, Y. S., and Bai, K. J. (2002). A finite-element computation for the sloshing motion in LNG tank. In *Proceedings of The Twelfth International Offshore and Polar Engineering Conference*.

Kim, J. W., Sim, I. H., Shin, Y., Kim, Y. S., and Bai, K. J. (2003). A three-dimensional finite-element computation for the sloshing impact pressure in LNG tank. In *Proceedings of The Thirteenth International Offshore and Polar Engineering Conference*.

Kim, M. H., Kim, D. H., Kang, S. W., and Lee, J. M. (2006). An interlaminar strain measurement for insulation panels of LNG carriers. *Strain*, 42:97–106.

Kim, Y. (2002). A numerical study on sloshing flows coupled with ship motion - the anti-rolling tank problem. *J. Ship Res.*, 46(1):52–62.

Kim, Y., Nam, B. W., Kim, D. W., and Kim, Y. S. (2007). Study on coupling effects of ship motion and sloshing. *Ocean Eng.*, 34(16):2176–2187.

Korobkin, A., Guéret, R., and Malenica, S. (2006). Hydroelastic coupling of beam finite element model with Wagner theory of water impact. *J. Fluids Struct.*, 22:493–504.

Kvålsvold, J. and Faltinsen, O. M. (1995). Hydroelastic modeling of wet deck slamming on multihull vessels. *J. Ship Res.*, 39:225–239.

Landrini, M. (2006). Strongly nonlinear phenomena in ship hydrodynamics. *J. Ship Res.*, 50(2):99–119.

Landrini, M., Colagrossi, A., and Faltinsen, O. M. (2003). Sloshing in 2-D flows by the SPH method. In *Proceedings of the 8th International Conference on Numerical Ship Hydrodynamics*, Busan, Korea.

Lee, D. Y. and Choi, H. S. (1999). Study on sloshing in cargo tanks including hydroelastic effects. *J. Mar. Sci. Technol.*, 4:27–34.

Lee, H., Kim, J. W., and Hwang, C. (2004). Dynamic strength analysis for membrane type LNG containment system due to sloshing impact load. In *RINA (2004)*, pages 39–47.

Lee, J. M., Paik, J. K., Kim, M. H., Kim, W. S., Noh, B. J., and Choe, I. H. (2006). Dynamic strength characteristics of membrane type LNG cargo containment system. In *RINA (2006)*, pages 189–200.

Lee, S. J., Kim, M. H., Lee, D. H., Kim, J. W., and Kim, Y. H. (2007). The effects of LNG-tank sloshing on the global motions of LNG carriers. *Ocean Eng.*, 34(1):10–20.

Lindemark, T., Austefjord, H. N., Sele, H. O., Urm, H. S., Lee, K. J., and Ha, T. M. (2006). CSA-2 analysis of a 216k LNGc membrane carrier. In *RINA (2006)*, pages 121–132.

Lindemark, T., Kamsvåg, F., and Valsgård, S. (2004). Fatigue analysis of gas carriers. In *RINA (2004)*.

Loots, E., Pastoor, W., Buchner, B., and Tveitnes, T. (2004). The numerical simulation of LNG sloshing with an improved volume of fluid method. In *Proceedings of the 23rd International Conference Offshore Mechanics and Arctic Engineering*.

Lu, C. H., He, Y. S., and Wu, G. X. (2000). Coupled analysis of nonlinear interaction between fluid and structure during impact. *J. Fluids Struct.*, 14:127–146.

Magelssen, W. (2005). Issues facing the LNG-fleet, with emphasis on operational, propulsion, construction and containment. Presentation at the *24th International Conference Offshore Mechanics and Arctic Engineering*.

Mahmood, M. (2005). Issue facing the new LNG fleet. Presentation at the *24th International Conference Offshore Mechanics and Arctic Engineering*.

Malenica, S., Korobkin, A. A., Scolan, Y. M., Gueret, R., Delafosse, V., Gazzola, T., Mravak, Z., Chen, X. B., and Zalar, M. (2006). Hydroelastic impact in the tanks of LNG carriers. In *Proceedings of the Fourth International Conference on Hydroelasticity in Marine Technology*, pages 121–130, Wuxi, China.

Moan, T., Graczyk, M., Shu, Z., and Rognebakke, O. (2006). Recent developments of structural design of ships based on direct calculations - with emphasis on LNG carriers. In *Proceedings of the International Conference on Ship and Shipping Research, NAV*, Genova, Italy.

Moiseyev, N. N. (1958). On the theory of nonlinear vibrations of a liquid of finite volume. *Pmm-J. Appl. Math. Mech.*, 22(5):860–870.

Mutsuda, H., Shimizu, K., and Doi, Y. (2005). Numerical simulation for large deformation fluid-structure interaction using CIP-EDEM method. In *Proceedings of the 5th International Symposium on Ocean Wave Measurement and Analysis, WAVES2005*, Madrid, Spain.

Nam, S. K., Kim, W. S., Noh, B. J., Shin, H. C., and Choe, I. H. (2006). The parametric study on the response of membrane tanks in a Mark III type LNG carrier using coupled hydro-elastic model. In *RINA (2006)*, pages 147–154.

Nam, S. K., Kim, W. S., Noh, B. J., Shin, H. C., Choe, I. H., Park, K. H., Kim, D. E., and Rashed, S. (2005). Structural response of membrane tanks to sloshing load in a Mark III type LNG carrier. In *Proceedings of the 19th Asian Technical Exchange and Advisory Meeting on Marine Structures (TEAM)*, pages 347–352, Singapore.

Noble, P. G., Colton, T., and Levine, R. A. (2004). Planning the design, construction and operation of new LNG transportation systems. In *RINA (2004)*.

Ochi, M. K. (1990). *Applied probability and stochastic processes in engineering and physical sciences*. New York: Wiley.

Ochi, M. K. (1998). *Ocean waves: the stochastic approach*. Cambridge: Cambridge University Press.

Olsen, A. S., Schrøter, C., and Jensen, J. J. (2006). Wave height distribution observed by ships in the North Atlantic. *Ships and Offshore Structures*, 1(1):1–12.

Paik, J. K. (2006). Limit state design technology for a membrane type liquid natural gas cargo containment system under sloshing impacts. *Mar. Technol. Sname News*, 43(3):126–134.

Pastoor, W., Østvold, T. K., Byklum, E., and Valsgård, S. (2005). Sloshing load and response in LNG carriers for new designs, new operations and new trades. In *Gastech (2005)*.

Pastoor, W., Tveitnes, T., Valsgård, S., and Sele, H. O. (2004). Sloshing in partially filled LNG tanks - an experimental survey. In *Proceedings of the Offshore Technology Conference*.

Richardson, A. J., Bray, W. H., Sandström, R. E., Lokken, R. T., and Danaczko, M. A. (2005). Advances in assessment of LNG sloshing for large membrane ships. In *Gastech (2005)*.

RINA (2004). *Proceedings of the International Conference on Design & Operation of Gas Carriers*. London, United Kingdom.

RINA (2006). *Proceedings of the International Conference on Design, Constructon & Operation of Natural Gas Carriers & Offshore Systems (ICSOT)*. Busan, Korea.

Rognebakke, O. F. and Faltinsen, O. M. (2000). Damping of sloshing due to tank roof impact. In *15th International Workshop on Water Waves and Floating Bodies*.

Rognebakke, O. F. and Faltinsen, O. M. (2003). Coupling of sloshing and ship motions. *J. Ship Res.*, 47(3):208–221.

Rognebakke, O. F. and Faltinsen, O. M. (2006). Hydroelastic sloshing induced impact with entrapped air. In *Proceedings of the Fourth International Conference on Hydroelasticity in Marine Technology*, pages 169–180, Wuxi, China.

Rognebakke, O. F., Hoff, J. R., Allers, J. M., Berget, K., Berge, B. O., Zhao, R., Paik, J. K., Danaczko, M. A., Lokken, R. T., Kokkinis, T., and Sandstrom, R. E. (2006). Experimental approaches for determining sloshing loads in LNG tanks. In *Transactions 2005*, volume 113, pages 384–401. Society of Naval Architects and Marine Engineers.

Rosén, A. (2005). Impact pressure distribution reconstruction from discrete point measurements. *Int. Shipbuild. Progr.*, 52(1):91–107.

Salvesen, N., Tuck, O. E., and Faltinsen, O. (1970). Ship motions and sea loads. In *Transactions*, volume 78. Society of Naval Architects and Marine Engineers.

Sember, W. J. and Mumtaz, M. (2005). The role of classification societies in design, operation and construction of LNG carriers and terminals. In *Gastech (2005)*.

Shin, Y., Kim, J. W., Lee, H., and Hwang, C. (2003). Sloshing impact of LNG cargoes in membrane containment systems in the partially filled condition. In *Proceedings of the Thirteenth International Offshore and Polar Engineering Conference*.

Temarel, P., Chen, X. B., Enge, A., Hermanski, G., Jankowski, J., Kapsenberg, G., Kawabe, H., Kruger, S., Kukkanen, T., Mavrakos, S., Pastoor, W., Pedersen, B., Ren, H. L., Sebastiani, L., and Xia, J. (2006). Committee I.2 Loads. In Frieze, P. A. and Shenoi, R. A., editors, *Proceedings of the 16th International Ship and Offshore Structures Congress*.

Tveitnes, T., Østvold, T. K., Pastoor, L. W., and Sele, H. O. (2004). A sloshing design load procedure for membrane LNG carriers. In *9th Symposium on Practical Design of Ships and Other Floating Structures*.

Valsgård, S., Østvold, T. K., Rognebakke, O., Byklum, E., and Sele, H. O. (2006). Gas carrier development for an expanding market. In *RINA (2006)*, pages 13–28.

Videiro, P. M. and Moan, T. (1999). Efficient evaluation of long-term distributions. In *Proceedings of the 18th International Conference on Offshore Mechanics and Arctic Engineering*.

Wang, L. and Moan, T. (2004). Probabilistic analysis of nonlinear wave loads on ships using Weibull, generalized Gamma and Pareto distributions. *J. Ship Res.*, 48(3):202–217.

Winterstein, S. R., Ude, T. C., Cornell, C. A., Bjerager, P., and Haver, S. (1994). Environmental parameters for extreme response: inverse form with omission factors. In Schuëller, G. I., Shinozuka, M., and Yao, J. T. P., editors, *Structural safety and reliability, ICOSSAR'93*, volume 1, pages 551–557.

Wu, M. K. and Moan, T. (2005). Efficient calculation of wave-induced ship responses considering structural dynamic effects. *App. Ocean Res.*, 27:81–96.

www.veristar.com (2008).

Zalar, M., Cambos, P., Besse, P., Le Gallo, B., and Mravak, Z. (2005). Partial filling of membrane type LNG carriers. In *Gastech (2005)*.

Zhao, R., Rognebakke, O., and Zheng, X. (2004). Wave and impact loads in design of large and conventional LNG ships. In *RINA (2004)*, pages 75–85.

Appendix A

Sloshing experiments

Sloshing rig and tank set-up

The experiments were performed with a model that represents a cargo tank of an LNG carrier in a seaway. Pressures that are induced on a tank by the fluid were measured. The experimental set-up consists of the tank and rig as schematically shown in Figure A.1 and A.2.

The tank is filled with water and the ullage is air in atmospheric pressure and room temperature. The tank is outfitted with sensors that measure the pressure inside the tank. The tank is placed in a rig performing irregular motions in 4 degrees of freedom: surge, sway, roll and pitch.

The rig is mechanically driven with a payload of up to 1300kg. Surge and sway are excited by ball screws, while roll and pitch are excited by a custom gear system. The lowest oscillation frequency is approximately 7Hz for the roll frame, and 12Hz for the pitch frame.

Experimental procedure

Based on experiences described by Lee et al. (2004), Pastoor et al. (2004), Tveitnes et al. (2004), Gavory (2005), Pastoor et al. (2005), Zalar et al. (2005) and Rognebakke et al. (2006), the procedure for sloshing experiments is established. It includes the following steps:

- specify tank location and geometry as well as ship operational parameters (filling level, ship speed, wave heading and wave environment),
- specify tank instrumentation with regard to expected responses,
- determine ship motion to obtain irregular tank motion time histories as the input for the sloshing testing,
- screen combinations of the sea state and ship operational parameters to identify the most critical ones,
- carry out a set of experiments including a set of tests for identical conditions to check repeatability.

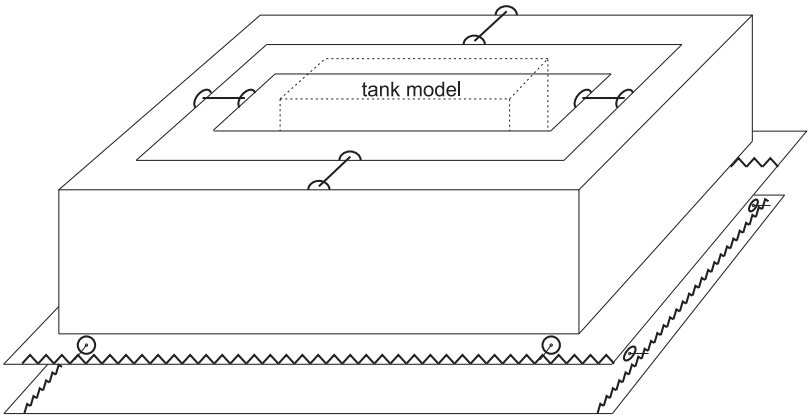

Figure A.1: Sketch of the sloshing rig.

Table A.1: LNG tank dimensions full scale for the tests with high filling level (series I) and with low filling level (series II)

dimension		series I	series II
Length	m	42.805	43.740
Breadth	m	37.400	37.898
Height	m	26.860	26.758
Upper chamfer height	m	8.289	8.638
Upper chamfer angle	deg	45	45
Lower chamfer height	m	3.869	3.778
Lower chamfer angle	deg	45	45

Tank model and ship operational parameters

Tanks used for experiments represent the second forward tank of the typical 4-tank 138000m^3 LNG tanker. The models in scale of 1:50 are made of Plexiglass. The walls are 20mm thick while the top plate is 30mm thick. The natural frequencies of vibration are sufficiently high that the tank can be assumed to be rigid in sloshing tests. The geometry and dimensions of the tanks are given in Figure A.3 and Table A.1, respectively.

Ship operational parameters are chosen to represent a real vessel behavior at the sea in two different conditions. Hence, two series of experiments are performed.

The first series simulates the tank with a high filling level. Based on literature survey of sloshing pressures occurring in tanks with filling levels of around 90%H (where H is the tank height) a 92.5%H is chosen. The conditions reflect a ship advancing in a 40-years storm with low speed (5kn) in head sea (0° wave heading angle) or in oblique sea (30° wave heading angle).

The second series of tests are conducted for a tank with filling levels of 30%H. 25%H filling level is also tested as a part of screening. This condition reflect a damaged ship (with no manoeuvering ability), hence with no forward speed and in beam seas as the most unfavorable condition. A one-year storm is assumed.

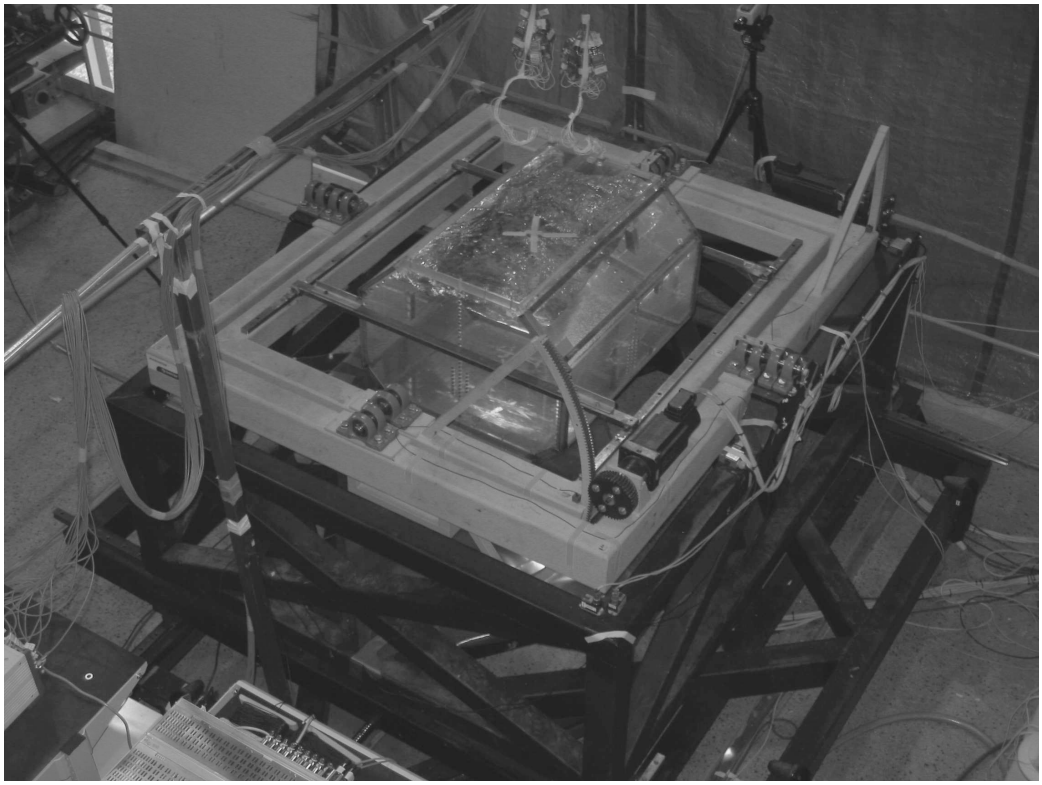

Figure A.2: Picture of the sloshing rig with the tank.

The sea environment is represented by the Pierson-Moskowitz spectrum and the scatter diagram recommended by IACS (2000). In accordance with a simplified long-term analysis based on the contour line approach (for details see Section 2.3) sea states along the 40-year contour line and the 1-year contour line are investigated for the high and low filling level, respectively.

A full scale duration is set to five-hours. A ramp of 200s is also applied. In model scale each run takes approximately 43 minutes.

Tank instrumentation

Pressure sensors are installed in the critical locations in the tank. The pressure sensors for high filling level tests (series I) are located in the upper port forward tank corner and in the middle of the edge between the tank ceiling and the forward bulkhead, Figure A.3a.

32 piezo-resistive pressure sensors of Kulite type with a round sensitive area of a 2mm diameter are arranged in two arrays of 4×4 sensors, Figure A.3b. The sensors in the outermost rows are located 2.5mm away from the wall and/or the chamfer edge, measured from the center of the sensor in model scale.

The pressure sensors for low filling level (series II) are located along the edge between the starboard wall and the aft bulkhead, Figure A.3a. Kulite pressure sensors with a 5mm diameter are arranged with a coarser spatial resolution, Figure A.3c.

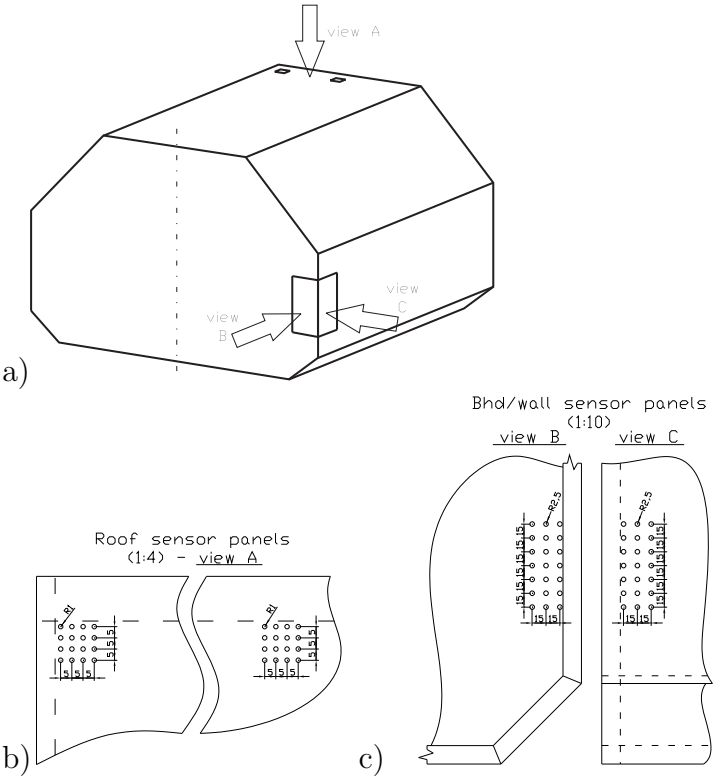

Figure A.3: Tank model and sensor panels, dimensions in model scale.

A number of sensor sockets exceeds the expected number of sensors to be used, hence the set-up allows for rearrangement of sensors in the course of experiments. In the 8 first runs (screening for the critical sea states) a 2×7 sensor array is applied on the wall and a 2×7 array on the bulkhead. After studying the results from the first 8 runs, the sensors are rearranged in order to capture the highest pressures. A 2×6 sensor array is applied on the bulkhead and a 3×6 array on the wall.

The sensors in the outermost rows are located 3.5mm away from the wall/bulkhead, measured from the center of the sensor in model scale. The lowest row of sensors is located 150mm above the bottom, i.e. 10.5mm below the mean water level.

The position of the rig is controlled by four potentiometer position gauges and four accelerometers. The signal for each degree of freedom is saved. This enables comparing the motion performed with the input signal. Video recording from two video cameras is also taken.

Pressure measurements are acquired with a sampling frequency of 19200Hz. A separate system with 400Hz sampling frequency is used to log rig motions. Each run with a 43min duration (corresponding to a 1:50 Froude scaled duration of 5 hours) provides a binary output pressure data file of almost 0.5GB for each pressure sensor.

Ship motion analysis

The ship motion is analyzed in the frequency domain by a commercial software Veres based on the linear potential strip theory (Fathi, 1997). Given sea state and ship

operational parameters motion spectra are obtained. The tank motion realizations are generated by the inverse Fourier transform of the motion spectra.

Worst case screening

Even when employing the contour line approach for determining the long-term response, the number of critical conditions is large and needs to be further limited. The choice of the critical sea states is performed by three methods: comparing short term characteristics of tank acceleration with account of the sloshing natural period, analytically-based multimodal approach (only for high filling level) and single runs of experiments.

The first method is applied for the tests of both filling levels, as described in Section 2.3 and in Papers I, II and III.

The second method is based on the adaptive multimodal approach presented by Faltinsen et al. (2000) and Faltinsen and Timokha (2001) and combined with local slamming analysis as presented by Rognebakke and Faltinsen (2000). Application of this method is limited to relatively deep water (typical patterns for low filling level, as hydraulic bores, are not represented). Thus the approach is only utilized for the screening analysis in the high filling case.

In the third method single experimental runs are utilized. Within the first test series 5 sea states along the contour line are tested with some repetitions for two heading angles (0° and 30°) while 4 sea states in two filling levels (25% and 30%) are tested for the second series.

Testing design case

Experimental runs are repeated in the sea state that gives the largest pressures estimates. This is H_s=15.10m, T_z=10.5s for both headings for high filling level and H_s=11.05m, T_z=9.5s for low filling level. Testing scheme within the first series (high filling) includes 5 runs for each heading angle with different motion samples and 10 runs for each heading with identical samples. In the second series (low filling) 10 runs are performed with different samples and 10 with identical ones.

Appendix B

Post-processing of experimental results

Pressure maxima are determined from the measured time histories. A threshold value is imposed on the logged pressure time histories as the lower bound of the maxima subject to analysis. The threshold is set to the level that efficiently reduces the number of insignificant peaks and consequently limits the disc space requirements. A threshold in the range of 150kPa to 250kPa full scale is applied.

A time window is applied in order to distinguish between pressure maxima caused directly by the fluid impacts and maxima due to secondary oscillations. The latter are caused by the compressible pressure oscillations of the gas entrapped in the impact region. The size of the time window is set to 1.1s full scale.

In order to determine the parameters important for the structural response the post-processing procedure provides also an information about spatial distribution and temporal pattern of the pressures.

The maximum pressure among all the sensors in a given panel for each impact are stored as well as the averages over different combinations of neighboring sensors. Spatial pattern of the loading is simplified by a linear interpolation of pressure between sensors.

The temporal pattern of pressure maxima is simplified. As the sloshing load duration is similar to the longest natural periods of the structure, the details of the pressure time history may be important. Commonly the temporal pattern is approximated with a triangle. Two different methods of approximating the temporal pattern of pressure time histories are applied herein: by 2 linear functions (as a triangle) and by 3 linear functions (as a trapezoid). The methods are described in the Paper IV of this thesis.

The accuracy of these two methods is investigated by comparing a response of the membrane structure to the respective two approximations for a number of real time histories with different duration.

The structure is modeled by finite elements as presented in Paper V of this thesis. Representative time histories with the largest pressure measured for the filling level equal $30\%H$ and different durations are investigated, see Figure B.1.

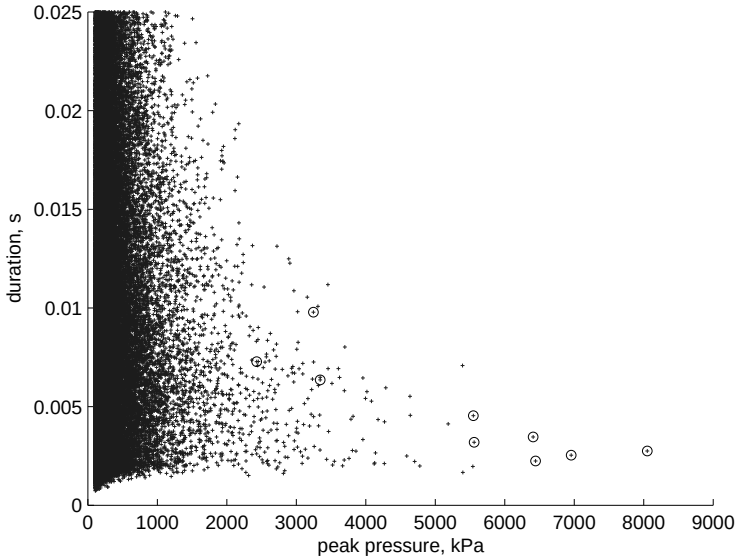

Figure B.1: Duration of the pressures time histories measured experimentally for 30%H filling level; the maxima investigated marked with a circle.

Structural response of the lowest fiber of the lower plywood plate is investigated. Location above a mid-span of the girder is considered; this location is referred to as location II in Paper V. In-plane stresses in the plywood plate (perpendicular to the resin ropes) are calculated.

The ratio between the stresses obtained for the approximate time histories and for the original time histories is presented in Table B.1. The maximum pressure is also presented for reference but as the analysis is linear it does not influence the results.

The fitting of the triangular function is made by using a threshold that determines the crossing of the original time series with the linear approximation, see Fig. 4 in Paper IV. It is found that when the triangular approximation is applied results are scattered depending on how the function is fitted. Seeking a consistent trend for the estimates two or three triangular functions are fitted to each original time history.

Increase of this threshold increases the duration of the approximate time history. It is found that for time histories with a short duration (below 4ms for dry model and below 5-6ms for wet model) an increase of the threshold (and consequently increase of duration) increases the response. For loading with a longer duration the response decreases with increasing threshold. Hence, it is difficult to determine a fitting method resulting in consistent estimates. Moreover the estimates are non-conservative in most cases.

When applying the trapezoidal approximation a slight overestimation of the in-plane stresses in the plywood plate (perpendicular to the resin ropes) is observed. This method enables an accurate modeling of time histories of different durations. However, it requires one additional parameter. Therefore it may be better to apply the triangular impulse model together with a correction factor.

Table B.1: The ratio of the maximum horizontal stress (lowest fiber of the lower plywood above a girder) for time histories approximated by a triangle ($\bigwedge$) to the original time history ($\bigcap$) and by a trapezoid ($\prod$) to the original time history ($\bigcap$); t_d is the approximate duration of the time history and p_{max} is the maximum pressure.

No	t_d,	p_{max},	Dry model		Wet model	
	ms	kPa	$\bigwedge$ / $\bigcap$	$\prod$ / $\bigcap$	$\bigwedge$ / $\bigcap$	$\prod$ / $\bigcap$
1	2.25	6444	0.95 - 1.11	0.98	0.89 - 0.95	1.01
2	2.54	6958	0.92 - 0.96	1.02	0.93 - 0.95	1.02
3	2.75	8051	0.99 - 1.04	1.01	0.90 - 0.93	1.03
4	3.19	5561	0.90 - 0.98	1.06	0.95 - 0.97	1.03
5	3.45	6409	1.03 - 1.16	1.05	0.95 - 0.97	1.04
6	4.53	5548	0.84 - 0.85	0.92	0.96	0.99
7	6.34	3345	1.04 - 1.05	1.10	0.94	1.01
8	7.28	2429	0.86 - 0.90	1.05	0.88 - 0.90	1.03
9	9.78	3246	0.94 - 0.96	0.98	0.88 - 0.93	1.01

A uniform loading is applied in this analysis. The results may be sensitive to the loading area because the eigenfrequencies of the structure change due to added mass variation and the fact that the localized loading may excite higher modes.

Appendix C

Frequency of compressible oscillations of a gas pocket

One of the assumptions of the hydroelastic analysis is that the fluid is incompressible. The speed of sound in LNG is so high that for events longer than a few milliseconds the fluid may be assumed incompressible. The compressibility may become important if responses with high frequencies, say above 1000Hz occur. For realistic loading durations, the natural frequencies of modes contributing to the structural response of a membrane containment system are in most cases well below this value.

The compressibility becomes important when a gas is present in the impact region, either in form of bubbles or an entrapped pocket. This lowers significantly the speed of sound.

Different gas cushioning effects may be observed in a tank. A primary effect is related to a situation when a gas cushion is created during an impact of the fluid on the tank wall. Gas pockets may have a large effect on excited pressures and structural response; compressible effects of the entrapped gas limit the maximum pressure. This problem is investigated e.g. by Rognebakke and Faltinsen (2006).

In order to ensure the tightness against the fluid and gas the containment system is covered with a membrane. The membrane may be corrugated (as in the Mark III system). A secondary cushioning effect is observed when during a fluid impact small gas pockets are created in these corrugations. How the compressible effects of the entrapped gas decrease the maximum pressure is investigated by Shin et al. (2003) and Chung et al. (2006). Other effects of the gas compressible oscillations may also be expected. The frequency of these oscillations may affect the significance of particular modes of the structural response or, if the frequency is high enough, also the importance of compressibility of the fluid in the impact area.

The natural frequency of the compressible oscillations is studied here in order to estimate the time scale of this phenomenon. The effect of gas cushions creation on the pressure magnitude is not investigated.

Faltinsen (2008) investigates a gas cavity created during the fluid impact on the structure near a tank corner in a two-dimensional case. It is shown that the non-dimensional eigenfrequency $\sigma\sqrt{\frac{\Omega_0\rho_l}{\lambda p_a}}$ for the compressible oscillations of the gas cavity is dependent only on the pocket shape in the contact region and specifically on the

ratio of wetted length to the extent of the gas pocket in the impact area. The non-dimensional eigenfrequency is formulated as

$$\sigma\sqrt{\frac{\Omega_0\rho_l}{\lambda p_a}} = \left(\frac{K\left(\frac{b}{a}\right)}{K\left(\sqrt{1-\left(\frac{b}{a}\right)^2}\right)}\right)^{0.5} \tag{C.1}$$

where σ is the natural frequency, Ω_0 is the two-dimensional volume of the gas cavity, ρ_l is the density of the fluid, λ is the ratio of the specific heat and p_a is the pressure in the tank. K is the complete elliptic integral and a is the extent of the total wetted length (including gas cavity) and b the extent of the gas cavity itself.

This formulation may be generalized to determine the natural frequency of compressible oscillations of a number of local gas cushions created in the wall surface corrugations. The total wetted length of the impacting fluid is much larger than the extent of a single corrugation. Hence, a number of gas pockets may be created.

Compressible oscillations of the gas pockets may be analyzed in a simplified way by studying an equivalent gas pocket with the volume equal to the total volume of all gas pockets, cumulated wetted length $2a$ and cumulated gas cushion extent $2b = \Sigma b_i$, see Figure C.1.

The number of gas cushions created is dependent on the impact inflow conditions and the membrane geometry. The fluid density is ρ_l=420kg/m^3, ratio of the specific heat λ=1.4, and pressure in the tank p_a is equal to atmospheric pressure. The analysis is performed for a range of values of the input parameters. In Figure C.2 the oscillation frequency is presented for the total wetted length $2a$ in range 0.5-1.5m, the ratio b/a in range 0.9-1.0 and the height of the corrugation profile h in range 3-5cm.

The natural frequency of gas compressible oscillations in the cushions varies between 10 and 50Hz and is much below the lowest eigenfrequencies for the structure. No effect on structural dynamics is therefore expected. Moreover, the time scale of gas oscillations on the order of a few milliseconds means that the fluid compressibility does not matter.

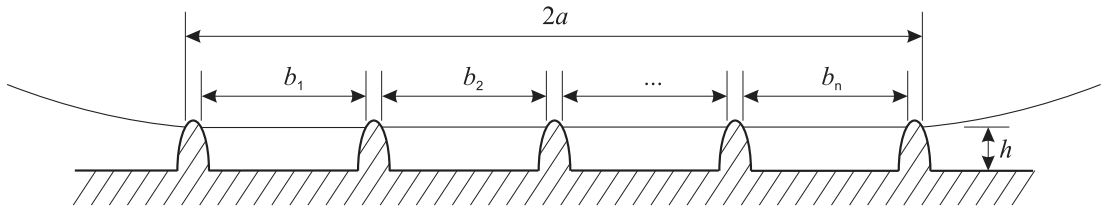

a)

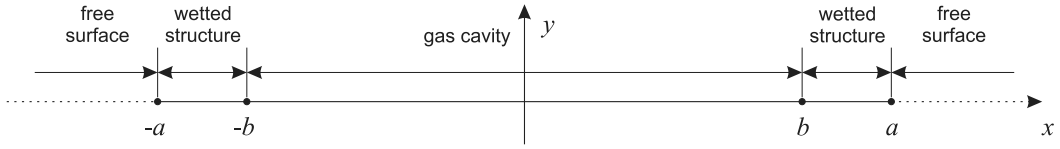

b)

Figure C.1: Fluid impact on the corrugated surface of the Mark III containment system; a) mechanism of creating n gas pockets, b) model for equivalent gas pocket with an extent $2b = \Sigma b_i$ and total wetted length $2a$.

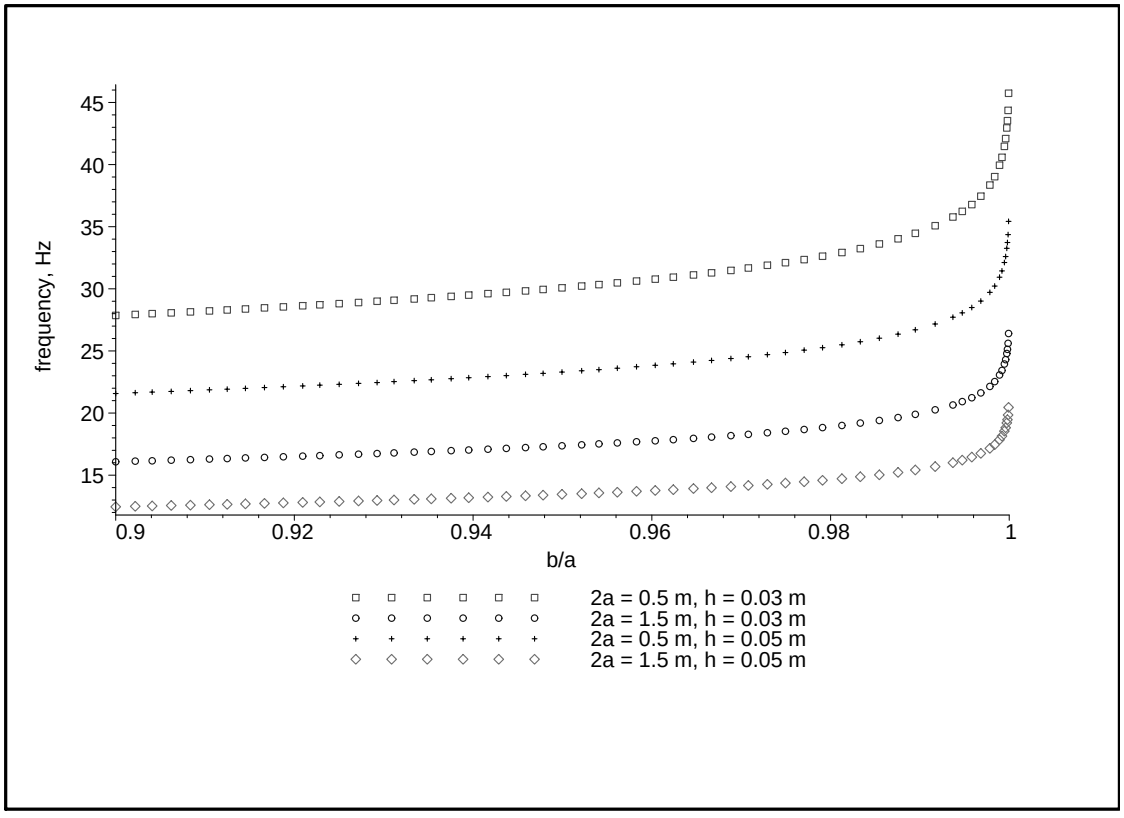

Figure C.2: The natural frequency of gas cushions' oscillation; $2a$ - total wetted length, h - height of the corrugation profile, b/a - ratio of the integrated extent of the gas pockets to the total wetted length.

Part II

Articles

Paper 1:

Graczyk M., Moan T. and Rognebakke O.

Probabilistic Analysis of Characteristic Pressure for LNG Tanks.

Journal of Offshore Mechanics and Arctic Engineering - Transactions of the ASME, 128:133-144, 2006.

Is not included due to copyright

Paper 2:

Moan T., Graczyk M., Shu Z. and Rognebakke O.

Recent Developments of Structural Design of Ships Based on Direct Calculations - with Emphasis on LNG Carriers.

Proceedings of the International Conference on Ship and Shipping Research, NAV, Genova, Italy, 2006.

Is not included due to copyright

Paper 3:

Graczyk M., Moan T. and Wu MK.

Extreme Sloshing and Whipping-Induced Pressures and Structural Response in Membrane LNG Tanks.

Ships and Offshore Structures, 2(3):201-216, 2007.

Is not included due to copyright

Paper 4:

Graczyk M. and Moan T.

A Probabilistic Assessment of Design Sloshing Pressure Time Histories in LNG Tanks.

Ocean Engineering, 35:834-855, 2008.

Available online at www.sciencedirect.com
ScienceDirect
Ocean Engineering 35 (2008) 834–855
OCEAN ENGINEERING
www.elsevier.com/locate/oceaneng

A probabilistic assessment of design sloshing pressure time histories in LNG tanks

Mateusz Graczyk*, Torgeir Moan

Centre for Ships and Ocean Structures and Department of Marine Technology, Norwegian University of Science and Technology, Otto Nielsens vei 10, 7491 Trondheim, Norway

Received 29 August 2007; accepted 22 January 2008
Available online 7 February 2008

Abstract

The violent motion (sloshing) of liquefied natural gas (LNG) in cargo tanks has attracted significant attention. Transformations of the LNG market have led to the increased transport of LNG in partially filled tanks, but established technology is mainly based on engineering experience with completely filled containers. This paper investigates a large sample of sloshing pressure measurements. It focuses on the magnitude of individual sloshing impact events, and their associated temporal and spatial patterns. The durations of these impacts are comparable to the natural frequency of an LNG container wall, so the details of their time histories are important in determining the structural response. Experiments are performed on tanks with high (92.5%) and low (30%) filling levels, for various wave headings. The common post-processing approach of representing impact pressure histories by a triangular profile is studied, and an alternative approach is presented. Two statistical models are used to describe the distribution of maximal pressures in sloshing impacts: a three-parameter Weibull model and a generalized Pareto model. The latter is found to be of questionable utility due to small sample sizes. It is observed that for low filling levels the sloshing impacts are of greater magnitude, having longer durations, smaller ratios of rise time to duration, and larger spatial extents. All these factors should in principle increase the structural response.

Keywords: Sloshing; Statistics; Pressure; Spatial distribution; Temporal distribution; LNG

1. Introduction

Liquefied natural gas (LNG) is often shipped in membrane tanks. In this tank concept the hull structure is utilized as boundaries for cargo holds. The tanks are thus limited in length by transverse bulkheads and in breadth by ship's sides. Due to the extremely low temperature of the cargo (−163 °C), the steel structure of the ship needs to be protected by load-bearing insulation. Containment systems cover all surfaces with either a layered, foam-based insulation structure (the so-called Mark III system) or mineral-filled wooden boxes (the "No. 96" system). The insulation material is protected from direct contact with the cargo by a tight membrane. In order to ensure the reliability of the system, prevent the LNG from evaporating, and protect the inner hull from low temperatures, the insulation layer and membrane are doubled; the insulation rests on resin ropes. When a few other non-continuous elements are taken into account, we see that the containment system is a very complex structure indeed.

Sloshing is a violent motion of the fluid in partially filled tanks. In LNG tankers, sloshing is currently an important problem (RINA, 2006). It has been observed that LNG carriers are needed for short-term charters, and that offshore offloading becomes desirable. Both of these applications imply operating with partially filled cargo tanks. Today, shipping LNG in partially filled tanks is not allowed. In this condition, hydraulic bores are created and very high pressure is excited when fluid impacts on tank walls. In high filling levels a standing wave pattern is observed, which is more favorable in terms of excited pressures.

The typical shipping routes have also been relocating to new sea areas such as the North Sea or Alaskan coast known for very rough conditions.

*Corresponding author. Tel.: +47 73 550654; fax: +47 73 595776.
E-mail address: Mateusz.Graczyk@marintek.sintef.no (M. Graczyk).

0029-8018/$ - see front matter © 2008 Elsevier Ltd. All rights reserved.
doi:10.1016/j.oceaneng.2008.01.020

Moreover, while LNG carriers have become larger for economic reasons, they are still designed with only four (or possibly five) tanks. This is due to the high cost of fabricating complex structural solutions, including tank insulation. Sloshing loads may significantly increase in larger tanks.

In order to determine structural load effects to sloshing excitation, an extensive, multistep approach such as that outlined in Moan et al. (2006) must be used. One must determine the long-term randomness of the sea state, the ship motion in irregular waves, the motion of the fluid in the tanks (which may couple with the ship motion), the pressures induced in critical locations, and finally the structural response. Only then is a capacity assessment possible, according to the proper limit state criteria. The focus of this work is the determination of sloshing pressure time histories, given critical tank motion histories.

By the analytical multimodal method, the most important sloshing modes along with their corresponding natural frequency ranges, as well as free surface elevations, and total hydrodynamic forces can be predicted with a fairly good accuracy (Faltinsen et al., 2005). The pressure distribution on a tank of arbitrary shape, however, still cannot be determined.

Over the last decade, there have been a large number of attempts to develop reliable numerical tools for determining the sloshing pressure in the tank. Pressure time histories in given locations in the tank have recently been presented, e.g., by Kim et al. (2004) who adopted the finite difference method, Bulgarelli (2005) based their work on smoothed particle hydrodynamics approach, Kishev et al. (2006) adopted the constraint interpolation profile method and Lee et al. (2007) used a commercial code based on the volume of fluid method. These numerical models are of course significantly cheaper than experimental methods. Due to the complexity of sloshing motions, however, much research is still required to gain a full understanding of the hydrodynamic phenomena involved. Moreover, since numerical calculations are inaccurate unless they have fine spatial and temporal resolution, and a long duration of the simulation and big spatial domain is required the computational cost is rather high.

Thus, despite their expense experiments are presently the most reliable method of determining the structural loading due to sloshing.

In determining structural response, the maximum pressure attained is not the only important factor. The spatial and temporal patterns of the sloshing pressure must also be considered. Both distributions are very complex, and for practical use they have to be described by a simplified model.

Extensive investigations of sloshing in LNG tanks have been carried out independently by research organizations, classification societies, and the maritime industry. Some recent results are closely related to the work presented in this paper. Graczyk et al. (2006) describe a procedure of performing sloshing experiments. They study sloshing pressures at a high filling level by fitting two statistical models to samples of maximum and averaged pressure and assess the models' performance.

The suitability of simplified long-term approaches such as the coefficient of contribution and the contour line approach is investigated in Graczyk et al. (2007). This work provides an analysis of the long-term response due to sloshing, by a simplified method based on a comparison of the linear hull acceleration and the tank's natural period. Valsgård et al. (2006) also discuss the long-term variability of sloshing pressures.

A number of dedicated tools have been developed to study the spatial and temporal pressure distributions of sloshing impacts and their effects on the estimated extreme values. These are discussed in Gavory (2005), Pastoor et al. (2005), Rognebakke et al. (2005), and other works.

Rosén (2005) proposes an interpolation technique for the reconstruction of pressure distributions from measurements at discrete points, and applies it to the problem of slamming on a ship's hull. This approach is especially suitable for analyses which require a complete information regarding the pressure profile in the combined form including its magnitude, spatial distribution, and temporal pattern as well as the velocity of pressure profile passing along the structure. This is contrary to, for instance, the probabilistic assessment of each separate parameter of the time history, as reported in this paper.

Sloshing pressure time histories are frequently modeled by a triangular function. The duration of the fluid impacts is close to one of the eigenfrequencies of the structure. Hence, deviations in the pressure time history from a triangular shape may have an important effect on the structural response. Attention should be devoted to determining the accuracy of such approximate models and the possible effects of simplification on the structural response.

This paper presents a probabilistic assessment of pressure time histories with regard to the structural response induced in an LNG membrane containment system. The pressure time histories are obtained from physical experiments.

In the post-processing of experimentally determined pressure histories, the pressure rise and decay are commonly represented by straight lines. This paper investigates the accuracy of such simplification. Moreover, as an alternative we propose an innovative approach to post-processing based on a trapezoidal modeling of the pressure histories.

Pressure time histories are analyzed based on the assumption that the temporal and spatial characteristics of impacts and the pressure maxima can be investigated separately. We study distributions for the pressure magnitude, duration t_d, rise time t_r, ratio of rise time and duration t_r/t_d and also investigate the spatial profiles of the impact events.

As the patterns of the fluid motion in a low and a high tank filling level are so unlike, a difference between the

characteristic parameters of the loading in these two conditions is of interest.

2. Terminology and nomenclature

The analysis of pressure time histories and their local effects on different timescales requires a specific nomenclature. To avoid confusion, some important expressions are defined below.

In this paper, the expression *sea state* refers to a combination of parameters that characterize the marine environment for the duration in which they can be considered as stationary (normally 3 h). The parameters are the significant wave height H_s and the zero-crossing period T_z.

Motion time history is a certain realization of the tank motion in a given sea state and is applied as an input to each experiment.

The pressure signals registered experimentally are of a complex shape, consisting of pressure maxima lasting on the order of a few milliseconds separated by zero pressure intervals on the order of a few seconds. A sketch of a typical long-term pressure signal is presented in Fig. 1. The expression *pressure time history* will refer to a small portion of the signal which includes a particular pressure maximum, while *the sample* will refer to the collection of pressure time histories from a given experiment.

One example of a pressure time history is presented in Fig. 2. The points are experimental measurements, and represent the real impact signal sampled at a given frequency, f. The time history consists of *rise range*, spreading out from the beginning of the time history to the peak ($\overline{AE}$), *peak value E* and *decay range*, from the peak to the end of the time history ($\overline{EF}$).

The rise range $\overline{AE}$ has the average slope $\phi_{avr} = \partial p/\partial t$. This value is referred to as the *rise rate*. The *decay rate* is defined in an analogous way.

The "regularity" of the time histories is investigated by observing *local rise cycles* and *secondary peaks*. A local rise cycle is defined as a segment of the rise range $\overline{AE}$ where the local rise rate ϕ_i is larger than the average rise rate ϕ_{avr}. Local rise cycles are therefore separated by segments where the rise rate is less than average. In the time history A–B–C–D–E–F depicted in Fig. 2, for example, the local rise cycles $\overline{BC}$ and $\overline{DE}$ have rise rates $\phi_1 > \phi_{avr}$ and $\phi_3 > \phi_{avr}$, respectively. They are separated by segment $\overline{CD}$, which has a rise rate $\phi_2 < \phi_{avr}$.

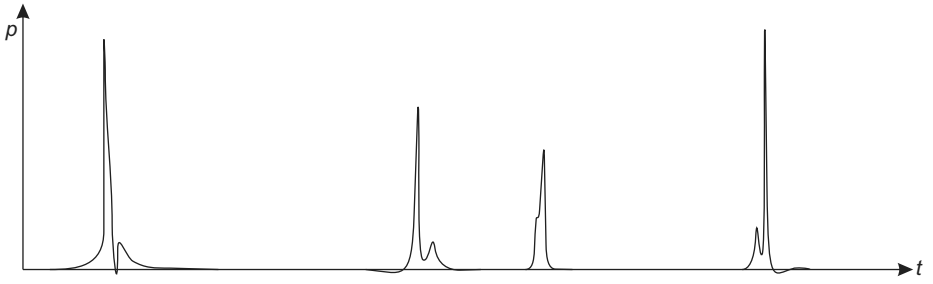

Fig. 1. A sketch of the pressure signal due to sloshing in a prismatic tank.

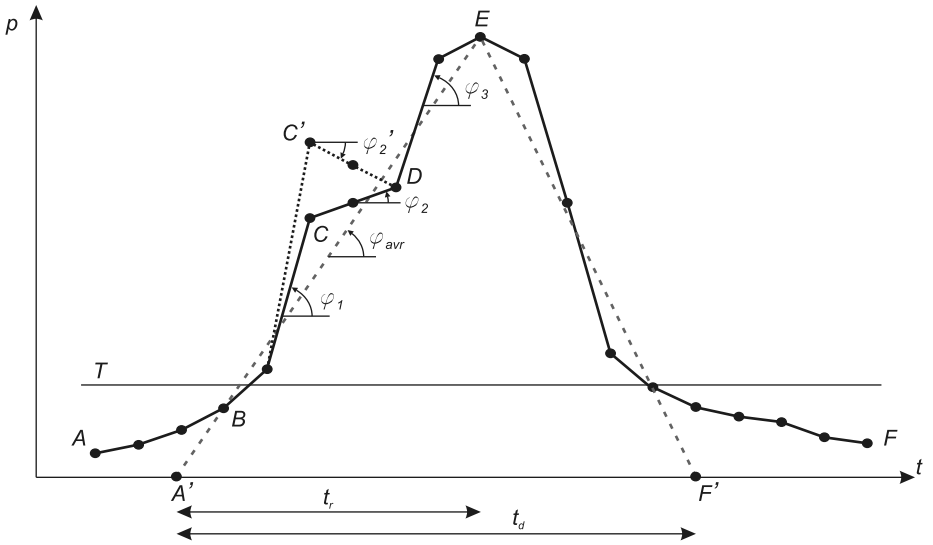

Fig. 2. A pressure time history (solid line) and its approximation by a triangle ($A'EF'$). Definition of local features: the *local rise cycles* are segments $\overline{BC}$ (or $\overline{BC'}$) and $\overline{DE}$. In an alternate time history, there is a secondary peak at C'.

Secondary peaks can be recognized when a negative rise rate is observed inside the rise range. In the alternate time history A–B–C'–D–E–F, $\overline{BC}$ and $\overline{DE}$ are still rise cycles, and $\overline{C'D}$ is found to have a rise rate $\phi_2' < 0$. C' is thus recognized as a secondary peak.

Rise time, t_r and *duration*, t_d are used to characterize a shape of time histories and relate the loading to the dynamic characteristics of the structure. These expressions are defined in Fig. 2.

Different thresholds are applied in analyses reported in the later sections. To avoid confusion, the various thresholds are listed below.

A threshold is used to determine a simplified pressure time histories (T in Fig. 2). This threshold is chosen as a fraction of the maximum pressure of the given time history.

The other thresholds are expressed as a quantile of the data set rather than in physical units. This format makes it easier to compare results. Results of analyses on how different impact characteristics change with pressure are reported either for a threshold varying in range 0.9–1.0 or for predefined set of strongest impacts. The strongest impacts are chosen to be represented by time histories with pressure maxima exceeding the 97% quantile.

Different threshold levels are applied in the peak over threshold (POT) method for a short-term description of pressure. Both stability of results and goodness of fit of a statistical model are investigated for various threshold levels. The threshold equal 87%, 92%, or 98% is often used for reporting the results.

Simplified methods for estimating long-term extreme response are applied. These methods imply that extreme short-term response may be so modified that it becomes representative for the long-term response. An important issue is a selection of the proper quantile α of the short-term pressure distribution. Based on results of Baarholm and Moan (2001) the present work adopts the quantile 90%.

Moreover, the following symbols are used: h—tank filling height, H—overall tank height, β—wave heading angle, H_s—significant wave height, T_z—zero-crossing period, μ—mean value, and σ—standard deviation.

3. Sloshing experiments

3.1. Experimental setup and testing scheme

The experiments were based on a rigid Plexiglas model of the second tank of a typical 138 000 m^3, four-tank membrane-type LNG carrier. Classification societies permit fillings below 10%L and above 70%H, where L and H are the tank length and tank height, respectively. In this work we investigate tanks at filling level of 92.5%H and 30%H.

The ship motion parameters are chosen to represent a real vessel's behavior at sea. In the high filling level tests, these conditions reflect a ship advancing in a 40-year storm at low speed (5 kn) in a head sea (0° wave heading) or an oblique sea (30° wave heading). In the low filling level tests, the conditions were designed to reflect a damaged ship (with no maneuvering ability) in a one-year storm, in beam seas (90° wave heading), the most unfavorable conditions. The most important parameters of the sloshing analysis are presented in Table 1.

Table 1
Parameters of sloshing experiments

	The high filling	The low filling
Tank dimensions	$L \times B \times H$: 42.8 × 37.4 × 26.9 m	
Longitudinal eigenperiod	7.6 s	10.2 s
Transverse eigenperiod	5.5 s	9.0 s
Model scale	1:50	
Speed	5 kn	0 kn
Wave heading	0°, 30°	90°
Contour line	40 yr	1 yr
Tank filling level	92.5%	30%
Sea state (H_s, T_z)	15.10 m, 10.5 s	11.05 m, 9.5 s
Sensors' location	Roof/fwd bulkhead	Wall/aft bulkhead
Test duration	5 h	
Logging frequency	19 200 Hz	
Fluid	Water	

Sloshing pressures were obtained by manipulating a test rig with four degrees of freedom. Effect of incorporating also heave and yaw motion is investigated in Gavory (2005); both an increase and decrease of the pressure is reported depending on the tank filling level. A more detailed description of the sloshing rig may be found in Graczyk (2008).

Irregular tank motion time histories were first simulated from assumed ship response spectra in a given sea state and input to the test rig. The testing scheme consists of (a) runs at the sea states located along the appropriate contour line; (b) repetitions at the critical sea state with varied motion time histories; and (c) repetitions at the critical sea state with identical motion time histories.

We perform eight runs with sea states along the 40-year contour line at the high filling level for each of the wave headings considered, and seven runs along the one-year contour line at the low filling level. The purpose of these test series is to determine the sea states resulting in the most severe sloshing response.

Repeated runs of model tests were performed for the critical sea state, for each filling level and wave heading angle considered. The test series at 92.5% filling includes 5 runs for each heading angle with varied motion time histories, and 10 runs for each heading with identical time histories. Ten runs were performed for the 30% filling case with different time histories, and 10 runs were performed with identical time histories.

The experimental data consist of pressure levels measured at a sampling frequency of around 20 kHz, and thus accurately reflect the real time histories of sloshing impacts. The pressure level is measured inside the tank at the locations given in Table 1 and in Fig. 3. Each location listed is a critical area for the given combination of filling

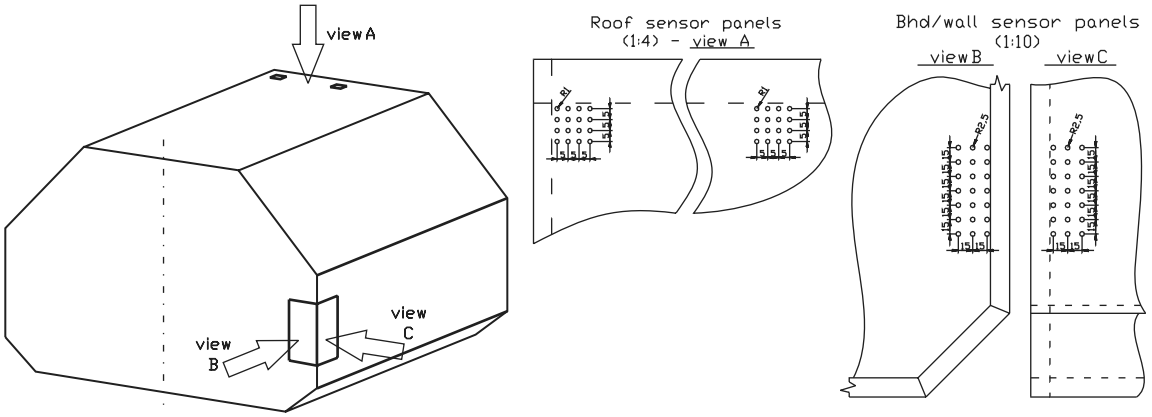

Fig. 3. Diagram of the tank, with the location of sensor panels and the arrangement of sensors indicated. The wall and bulkhead panels are located by the aft bulkhead, and the roof panels are located by the forward bulkhead.

level and wave heading, as described by Pastoor et al. (2005), Zalar et al. (2005), and others. Two panels of pressure sensors are installed for each test: two squares of 4×4 sensors for the high filling level (center of the outermost sensors is distant from the wall and the chamfer by 2.5 mm, model scale), and two rectangular panels of $2 \times 7 + 2 \times 7$ or $2 \times 6 + 3 \times 6$ for the low filling level. (Not all sensors in the bulkhead and wall panels are utilized simultaneously.) Here, center of the outermost sensors is distant from the wall/bulkhead by 3.5 mm in model scale. The lowest row of sensors is located 150 mm above the bottom, i.e. 10.5 mm below the mean water level. The tank and the sensor panels are presented in Fig. 3.

3.2. Post-processing of experimental data

As sloshing impacts may have a duration comparable to the natural period of the structure, their temporal structure must be taken into consideration. As the pressure may be exerted on a different region of the tank each time, the spatial characteristics of the signal are also important.

The spatial and temporal patterns of the sloshing pressure are very complex and for any practical use they have to be expressed quantitatively. It means that the time histories have to be simplified both in space and time and a "typical" loading parameters have to be determined. Moreover, the pressure data logged for a single 5-h run occupy 20 GB of disk space. Hence, the data need to be efficiently compressed. In this analysis, only those pressure time histories whose maxima exceed a threshold of 250 kPa are registered. Each sensor is also treated separately. Furthermore, in order to determine the typical loading, it is assumed that the maximum pressure of a time history, its temporal and spatial characteristics can be investigated independently.

The first and most obvious characteristic of each time history is the maximum pressure attained. This magnitude is extracted from each time history and each sensor. To characterize a given pressure surge, however, we consider only the largest magnitude registered by all the sensors in the panel. Based on statistical models that have been found to provide a suitable description of the sloshing pressure (Graczyk et al., 2006), we estimate the extreme pressure for all experimentally tested combinations of filling level and wave heading. The variability of the results is discussed in a later section, where all relevant samples are included to reduce the uncertainty in the tails of the distributions as much as possible.

The temporal characteristics of each pressure history must also be determined. A common approach is to approximate each time history as a triangle, as depicted in Fig. 4 by the dashed line. The measured time history passes through points A–B–D–E (among others); point C will be referred to later. Point A is the pressure measurement immediately preceding the first data point crossing a given threshold T_1, and defines the beginning of the line approximating the rise range. The other end of the line is set to the peak value and time (D). In order to obtain the lower corner of the triangle, this line is simply extrapolated to zero pressure. The decay range is found by an analogous procedure.

Real time histories, however, are often of a more complex, non-triangular shape; small local irregularities and/or oscillations are common. The "regularity" of the time histories is characterized by the number of local rise cycles and secondary peaks in the rise range, as well as the number of local decay cycles and secondary peaks in the decay range. The relationship between the regularity of impact time histories and the magnitudes of their pressure maxima is investigated in Section 3.3.

An alternative means of modeling the pressure time history ($A-B-D-E$) is presented in Fig. 4. In the triangular method, the rise range is approximated simply by the line $\overline{AD}$. A much improved fit can be obtained by fixing the upper end of the straight line to an earlier point.

That is, the second point of the rise range (B) can be set to the point just preceding the peak (D) as long as two conditions are met. First, the pressure at point B must lie above a given (high) threshold T_2. Second, the extrapolated line $\overline{AB}$ must reach the peak pressure level

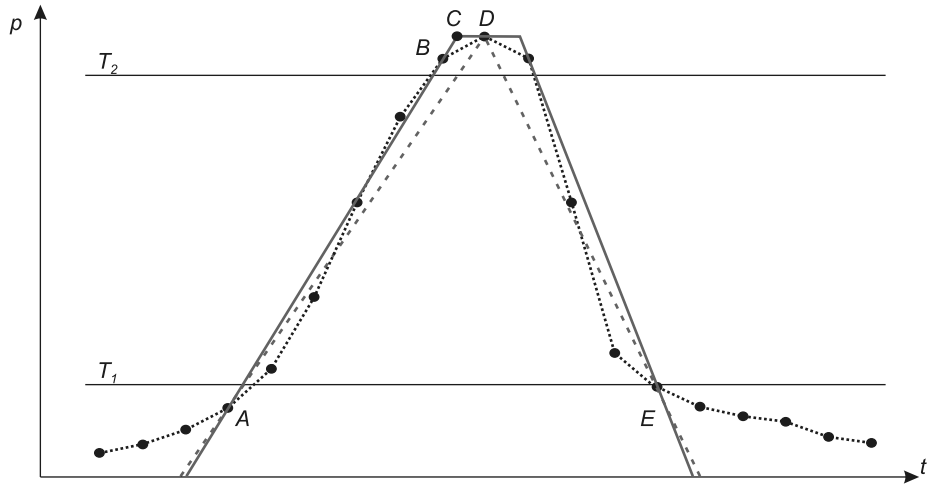

Fig. 4. A pressure time history (points) and its triangular (dashed line) and trapezoidal (solid line) approximations.

(point C) before the peak itself. If both these conditions are met, then point C is inserted into the approximation and the rise range now follows lines $\overline{AC}$ and $\overline{CD}$.

An analogous procedure is applied to find the approximate decay range. If either or both of the ranges are modeled by two lines, the approximate time history has a shape of a trapezoid. Otherwise, it is a triangle.

The structural response to both approximations is investigated in Graczyk et al. (2007). More accurate results were obtained for a few selected pressure time histories approximated by a trapezoid than by a triangular function. This issue needs to be investigated in more detail, however.

Approximating the pressure time histories by simple functions such as these enables us to apply the dynamic load factor (DLF) approach. The dynamic structural response can be characterized by a static response multiplied by the DLF, which is dependent on the load history and is a fuction of the ratio of the loading duration t_d to a characteristic natural period of the structure T_n (Biggs, 1964).

The spatial pattern of the sloshing pressure is also investigated in this paper. As previously described, the pressure level is measured by a panel containing several sensors in a grid. In Section 4.3 the sloshing loading during a given fluid impact is averaged over an area of variable size determined by the number of contributing sensors, and compared to the highest pressure registered. The ratio of average pressure to highest pressure gives information on the shape of the pressure profile, which may depend on the intensity of the impact.

As the temporal and spatial characteristics are investigated separately, it is necessary to establish a relation between the two distributions. This relation can be represented by the velocity of the pressure profile along the wall. The velocity is indirectly investigated by calculating the time lag between the time histories registered by neighboring sensors. This time lag is calculated along two perpendicular directions for all combinations of tank filling level and wave heading.

The dependence of all these parameters on the magnitude of the pressure maxima is investigated in Section 4. All results presented in subsequent sections are expressed in full-scale quantities. This applies in particular to the pressure magnitude, time history duration, and rise time as well as the distance between pressure sensors and the representative area of a group of sensors.

3.3. Accuracy of the post-processing

For an LNG tank structure consisting of steel plating covered with insulation, the longest natural period of lateral vibration, T_n, is similar to the duration of a typical impact pressure surge. Hence, the details of the impact time history may be important to the structural response. The traditional approach of approximating pressure time histories as triangular functions is based on experience gained in the operation of oil tankers, where the impacts have very small durations compared to the natural period of the structure. In this case only the integrated impulse is of interest, so it is sufficient to assign a triangular time history to experimentally determined sloshing impacts as described in Section 3.2.

It has been observed, however, that the time histories are often more complex: there may be significant local variations including multiple rise and decay cycles and/or secondary peaks (for the definition of these expressions, refer to Section 2). Such effects cannot be accurately modeled by representing rise and decay ranges by linear functions.

The dependence of impact time history regularity on the maximum pressure is investigated by studying histograms of the number of local rise cycles, decay cycles, and secondary peaks. In Fig. 5a, the fraction of time histories having the given number of local rise cycles is presented for all data from the low filling level experiments, regardless of the maximum pressure. To investigate the relationship between regularity and pressure, the time histories are first sorted from lowest to highest maximum pressure x_m.

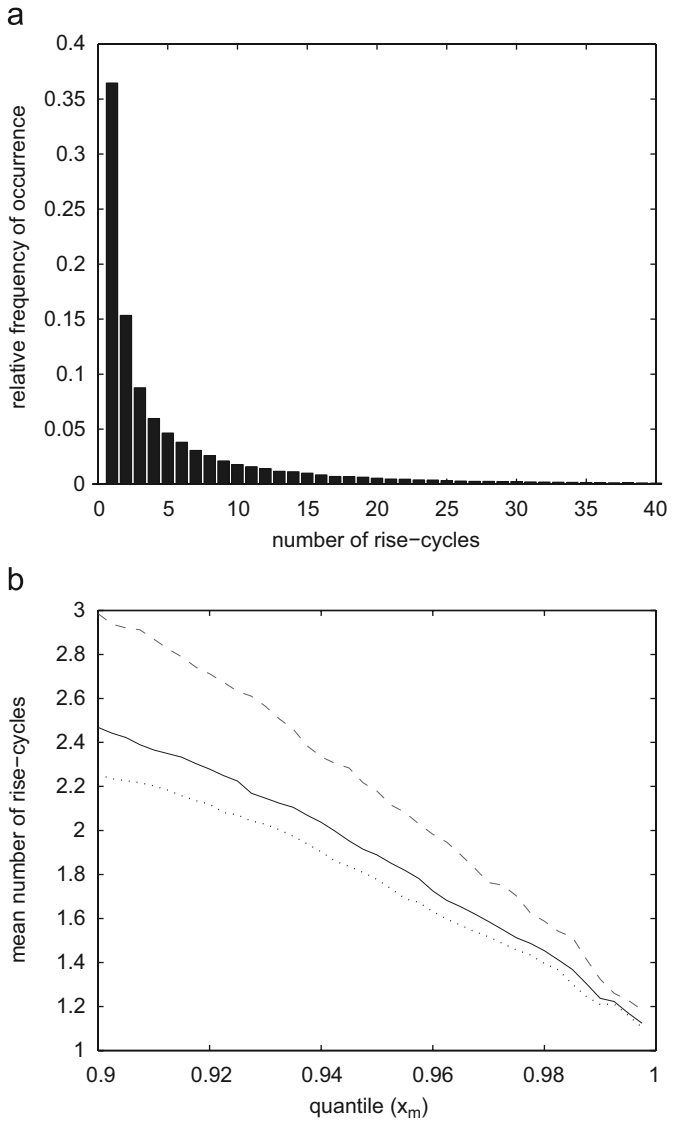

Fig. 5. (a) Histogram plotting the fraction of time histories with the given number of local rise cycles in the rise range for $h/H = 30\%$ and $\beta = 90^\circ$. All time histories for this experimental arrangement are included, regardless of their maximum pressure. (b) The mean number of local rise cycles in the rise range for time histories with maxima exceeding the threshold x_m; both panels (solid line), wall panel (dotted line), bulkhead panel (dashed line). For terminology see Section 2.

Fig. 5b plots the mean number of rise cycles for time histories having maxima greater than or equal to a given value of x_m, which is expressed as a quantile of the data set rather than in physical units. (The 97% quantile corresponds to a cut in x_m that includes only time histories with maximum pressures in the top 3%.) This format will make it easier to compare the three experimental situations. Impacts registered on the wall and bulkhead panels are plotted together in the solid curve, and separately in the dotted and dashed curves. A relatively heavy tail is observed in Fig. 5a when all the time histories are considered. Fig. 5b shows that the mean number of local rise cycles decreases steadily as the maximum pressure threshold is increased; for the highest quantiles, the number of cycles approaches 1. This indicates that the strongest impacts have the least complex histories. The numerical results of this analysis for both the low and high filling level experiments are presented in Table 2.

Table 2
Mean and standard deviation of the number of local rise cycles in the rise range, for all time histories and for those histories with maxima exceeding the 97% quantile

Condition	Panel location	All maxima		Max > 0.97q	
		μ	σ	μ	σ
$h/H = 30\%$,	Wall	5.56	9.31	1.52	1.10
$\beta = 90^\circ$	Bulkhead	6.63	9.80	1.76	1.43
$h/H = 92.5\%$,	Center	2.87	3.60	1.07	0.28
$\beta = 0^\circ$	Corner	4.51	7.77	1.14	0.44
$h/H = 92.5\%$,	Center	2.53	2.83	1.06	0.26
$\beta = 30^\circ$	Corner	3.89	4.00	1.16	0.50

For terminology see Section 2.

Some instability in the average number of local rise cycles is observed for the very highest quantiles (larger than 99%); this is an artifact caused by the limited sample size. Time histories with pressure maxima exceeding the 97% quantile are chosen to represent the characteristics of the strongest impacts in Table 2.

Fig. 6 and Table 3 present data on the number of secondary peaks in the same manner. A large fraction of impacts have many secondary peaks when all the time histories are considered, but in the highest quantiles a much lower number is observed with the mean approaching zero.

The same analysis is applied to investigate local decay cycles and secondary peaks in the decay range. Here too we find that a large fraction of impacts have many local rise cycles and secondary peaks when all the time histories are considered, but also that the highest quantiles are much more regular.

Judging from Tables 2 and 3, it appears that sloshing impacts in the low filling level experiments have more complex time histories than those in the high filling level experiments. For both filling levels, however, the time histories with a large maximum pressure can be accurately approximated by linear rise and decay ranges.

In order to investigate the accuracy of the triangular approximation in modeling time history of sloshing impacts, the ratio between the pressure rise and rise time is calculated as $\phi = \partial p/\partial t$ and referred to as the rise rate (see Section 2).

This rise rate calculated for the triangular approximation is compared with the rise rate calculated for the rise cycle of the exact time history (this analysis is only performed for "regular" time histories having only one rise cycle). The ratio between the exact and approximate rise rates observed in the low filling level experiments is presented in Fig. 7.

Fig. 7a includes all time histories, regardless of their maximum pressure. The mean value of this ratio among

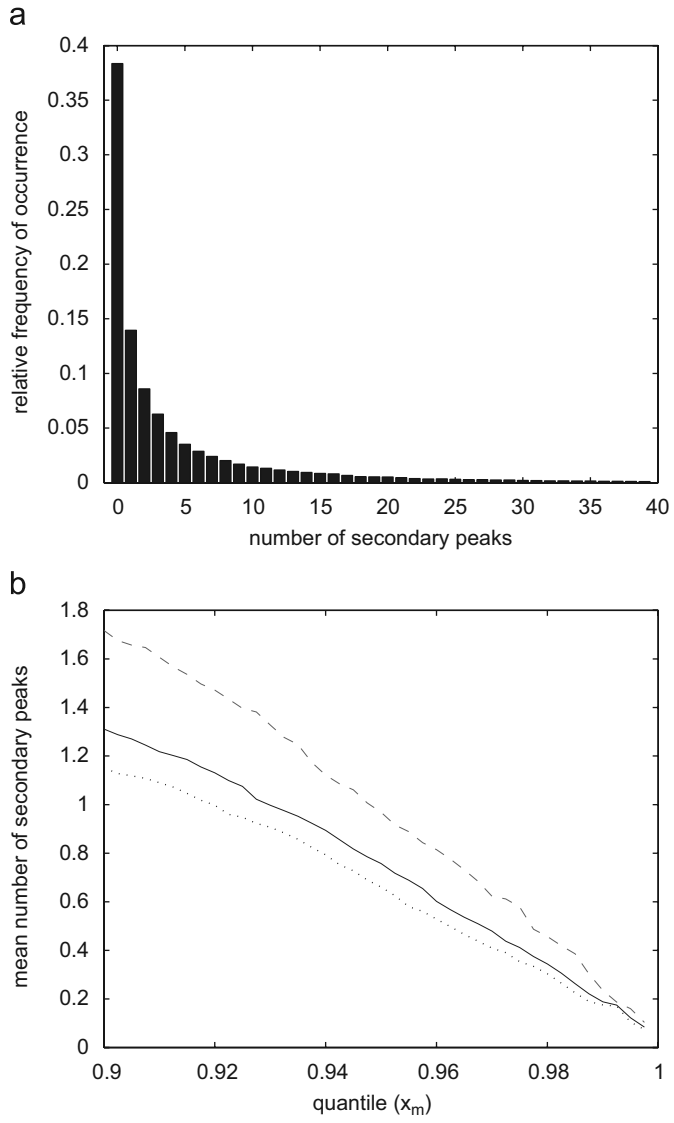

Fig. 6. (a) Histogram plotting the fraction of time histories with the given number of secondary peaks in the rise range for $h/H = 30\%$ and $\beta = 90^\circ$. All time histories for this experimental arrangement are included, regardless of their maximum pressure. (b) The mean number of secondary peaks in the rise range for time histories with maxima exceeding the threshold x_m; both panels (solid line), wall panel (dotted line), bulkhead panel (dashed line).

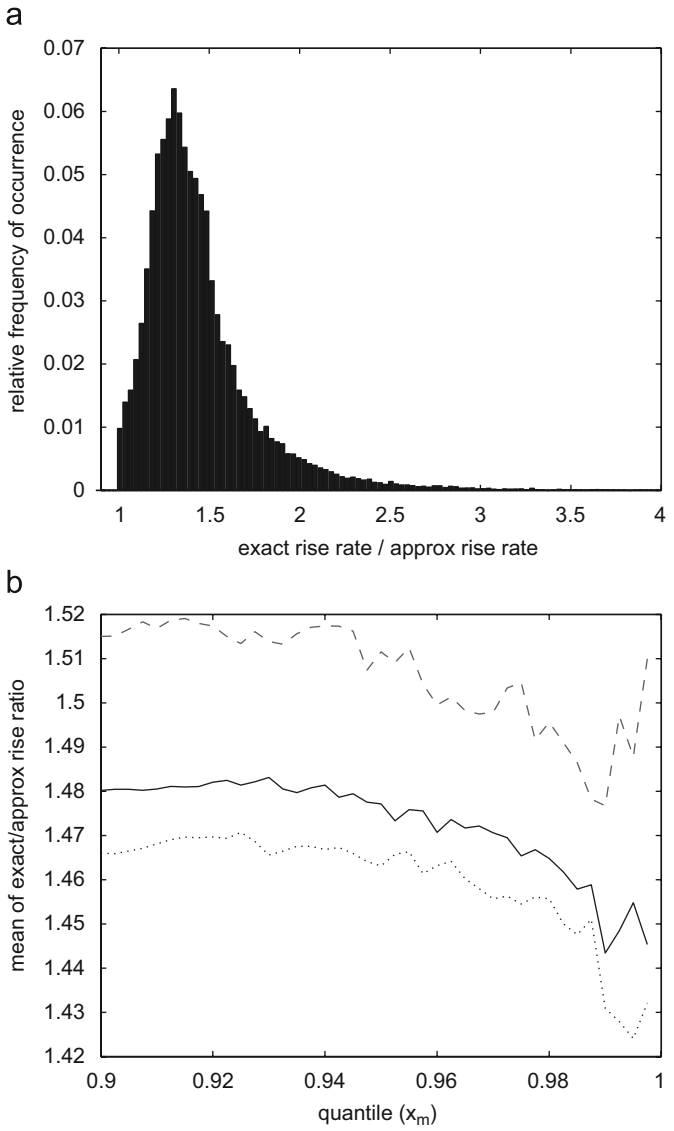

Fig. 7. (a) Histogram of the ratio of exact to approximate rise rate for $h/H = 30\%$ and $\beta = 90^\circ$ (triangular approximation). All time histories for this experimental arrangement are included, regardless of their maximum pressure. (b) The mean ratio of rise rates for time histories with maxima exceeding the threshold x_m; both panels (solid line), wall panel (dotted line), bulkhead panel (dashed line).

Table 3
Mean and standard deviation of the number of secondary peaks in the rise range, for all time histories and for those histories with maxima exceeding the 97% quantile

Condition	Panel location	All maxima		Max $> 0.97q$	
		μ	σ	μ	σ
$h/H = 30\%$, $\beta = 90^\circ$	Wall	4.59	9.62	0.41	0.94
	Bulkhead	5.89	10.43	0.62	1.33
$h/H = 92.5\%$, $\beta = 0^\circ$	Center	1.67	3.53	0.07	0.30
	Corner	3.20	7.91	0.10	0.42
$h/H = 92.5\%$, $\beta = 30^\circ$	Center	1.34	2.75	0.05	0.25
	Corner	2.55	4.00	0.14	0.53

time histories whose maximum pressure exceeds a given threshold x_m is presented in Fig. 7b. The solid line includes time histories from both panels, while the dotted and dashed lines consider the wall and bulkhead panels, respectively.

The mean and standard deviation of the rise rate are presented in Table 4, for all impacts and for those impacts with pressure maxima exceeding the 97% quantile. The relatively high value of this ratio in both categories indicates that the triangular approximation is not a very good fit to the pressure time history.

A similar analysis is performed for the new trapezoidal approximation suggested earlier. Table 5 presents the mean and standard deviation of the ratio between the

Table 4
Mean and standard deviation of the ratio between the exact rise rate and its triangular approximation, for all time histories and for those with maxima exceeding the 97% quantile

Condition	Panel location	All maxima		Max > 0.97q	
		μ	σ	μ	σ
$h/H = 30\%$, $\beta = 90^\circ$	Wall	1.44	0.32	1.46	0.32
	Bulkhead	1.45	0.34	1.50	0.39
$h/H = 92.5\%$, $\beta = 0^\circ$	Center	1.41	0.28	1.40	0.29
	Corner	1.44	0.30	1.40	0.24
$h/H = 92.5\%$, $\beta = 30^\circ$	Center	1.42	0.29	1.41	0.26
	Corner	1.44	0.29	1.41	0.24

Table 5
Mean and standard deviation of the ratio between the exact rise rate and its trapezoidal approximation, for all time histories and for those with maxima exceeding the 97% quantile

Condition	Panel location	All maxima		Max > 0.97q	
		μ	σ	μ	σ
$h/H = 30\%$, $\beta = 90^\circ$	Wall	1.29	0.32	1.30	0.34
	Bulkhead	1.30	0.34	1.36	0.41
$h/H = 92.5\%$, $\beta = 0^\circ$	Center	1.25	0.29	1.28	0.28
	Corner	1.30	0.31	1.28	0.23
$h/H = 92.5\%$, $\beta = 30^\circ$	Center	1.26	0.29	1.26	0.25
	Corner	1.29	0.29	1.28	0.22

exact and trapezoidal rise rates, in the same format as Table 4.

The ratios observed are lower, so we may conclude that the trapezoidal approach more accurately describes real time histories. A similar tendency is observed for the decay rates. Even better fit might be achieved by further tuning the method.

4. Typical loading

4.1. Pressure magnitude

In this section, the magnitude of the sloshing impact pressure is investigated by studying the expected extreme values with a given return period. Graczyk et al. (2006) investigated the relevance of two statistical models describing sloshing-excited pressures.

The three-parameter Weibull distribution is given by

$$F(x) = 1 - \mathrm{e}^{-((x-\delta)/a)^c}, \tag{1}$$

where c and a are the shape and scale parameters, respectively ($c>0$, $a>0$). δ is the location parameter, and $x \geqslant \delta$.

The generalized Pareto distribution is the limiting distribution of maxima X exceeding a threshold u, and its application is related to the POT approach (Pickands, 1975). The generalized Pareto distribution of excesses $X-u$ is formulated

$$G(x-u) = 1 - (1 + c(x-u)/a)^{-1/c} \quad \text{for } c \neq 0, \tag{2}$$

$$G(x-u) = 1 - \mathrm{e}^{-(x-u)/a} \quad \text{for } c = 0, \tag{3}$$

where c and a are the shape and scale parameters, respectively, and $a>0$. The allowed excesses are $x-u \in (0,\infty)$ for $c \geqslant 0$ and $x-u \in (0,-a/c)$ for $c<0$. The distribution of individual maxima is given by

$$F(x) = G(x-u)(1-F(u)) + F(u), \tag{4}$$

where $1-F(u)$ is the probability that X exceeds the threshold u.

The value of the shape parameter (c) in the generalized Pareto model should be commented on. Provided that the number of maxima exceeding the threshold is Poisson distributed, the probability distribution of the maximum of generalized Pareto distributed variables becomes the generalized extreme value distribution. The shape parameter of the generalized Pareto distribution determines the domain of attraction and the particular extreme value distribution. The cases $c=0$, $c>0$, and $c<0$ correspond to the Gumbel (Type I), Fréchet (Type II) and Weibull (Type III) domains of attraction, respectively.

The Type III extreme value distribution has a bounded upper tail. Such a distinct upper limit on extreme values is very unusual among natural phenomena; sloshing pressures, for example, are believed to be unbounded. In a number of experimental samples, however, the shape parameter of the generalized Pareto distribution has been found to be negative (perhaps due to limited sample sizes). Naess (1998) showed that if the distribution F_X belongs to the domain of attraction of the Type III extreme value distribution then, for a transformed process $Y = \delta(X)$, where δ is a strictly increasing function, the domain of attraction and the c parameter are both preserved. It was shown by Graczyk et al. (2007) that the negative values of c are not preserved for the samples of sloshing pressure. Thus, in principle the Type III distribution is not suitable for describing the extreme values of sloshing-excited pressures. In the present analysis, we thus take c to be zero when negative values are obtained from the sample of time histories produced by a run. When c is found to be positive, however, we retain the sample value.

Neves et al. (2006) investigate this issue in the context of significant wave height. Three different test statistics described in the literature are applied. The hypothesis that the wave height distribution belongs to the domain of attraction of the Type I distribution is tested against the alternative Type II and Type III distributions.

The parameters of both models are estimated from experimental samples by the method of moments, as described in Graczyk et al. (2006). In all cases the full-scale pressures are considered.

Long-term extreme response may be obtained as a combination of short-term responses. For linear phenomena, the response in short-term periods can be determined

in the frequency domain. Consequently, the long-term response distribution can very effectively be obtained by summing up the conditional short-term distributions multiplied by the probability of occurrence of the sea state and distribution of operational parameters such as heading and forward speed.

Long-term analysis is much more time consuming for nonlinear responses, such as that due to slamming, green water, or sloshing phenomena. Determining the variability of the largest response during a given sea state is much more challenging than the description of the randomness of the slowly varying parameters that define the sea states and which rests on the availability of a sufficient amount of data. For complicated response problems, the determination of the conditional distribution of the largest response given the sea states characteristics requires an extensive number of time domain simulations or, as in case of sloshing, experiments. In such cases simplified methods need to be utilized. One alternative is a contour line approach that decouples the environmental problem and the response problem.

Contour lines are created as the combinations of environmental characteristics (commonly H_s and T_z) that result in a constant probability of exceeding a given response level. Extreme values may then be predicted by investigating the response for sea states along the contour with a given probability of exceedance (Haver, 1980).

The inherent randomness of the largest response during a given short-term event cannot be neglected. In order to not need to include the short-term extreme response as a random variable in the analysis one may artificially increase the values of the slowly varying parameters, introduce a correction factor on the predicted response, or select a high quantile of the extreme value distribution, see for instance Baarholm and Moan (2001).

The approach may be extended by including other variables that are important for the response. For a ship this includes velocity or wave heading.

The contour lines may accurately be obtained by an approach adopted from the reliability theory, the first order reliability method (FORM), Madsen et al. (1986), or more effectively by the inverse first order reliability method (IFORM), Winterstein et al. (1994). The two-dimensional (H_s-T_z) contour lines created by IFORM with an assumed deterministic relationship between ship speed and H_s are used in this analysis.

Based on the order statistics concept the short-term characteristic extreme value x_α is calculated, as defined by the cumulative distribution function

$$F(x_\alpha) = \alpha^{1/n}. \tag{5}$$

The characteristic extreme value in 3-h duration is sought. An important issue is a selection of the proper quantile α of the sloshing pressure distribution to use in calculating the extreme pressure x_α. The literature provides little guidance regarding the proper quantile for novel problems. Graczyk et al. (2007) investigate the long-term sloshing response by a simplified method based on the analysis of the linear hull acceleration modified with respect to the natural period of the tank, and found that quantiles in the range of 50–75% were appropriate. The nonlinear effects of sloshing are difficult to estimate, however, and more study is required to determine a truly representative quantile. Baarholm and Moan (2001) analyze the nonlinear bending moment due to steady-state waves as well as slamming loading on ships, concluding that a quantile in the range of 85–90% is more appropriate. Based on these results, which may be taken as representative of other nonlinear phenomena, the present work adopts the conservative quantile $\alpha = 90\%$.

The POT approach is meant to accurately model the tail of a distribution. Hence, a better fit is to be expected than that provided by common order statistics, as applied to fit the three-parameter Weibull model is applied.

Pickand's theorem implies that the distribution is valid at high thresholds, but choosing a too high level limits the sample size and reduces the accuracy of the fit. We therefore investigate the sensitivity of the model fit to the choice of threshold. In this analysis, the uncertainty due to limited sample size is reduced by considering a large sample consisting of the maxima collected from all test runs with a given experimental setup.

The large sample for the low filling level experiment is composed of all maxima from 19 runs, and hence, the runs both with identical and different motion time histories. This in principle violates the assumption of independence of the maxima. However, it will be shown later, in relation to Tables 7–9, that the inherent variability of the results is comparable to the variability due to different input (tank motion time history), and hence, for practical purpose the maxima can be assumed independent.

The large sample composed of maxima from 14 samples registered for each of the two wave heading angles in the high filling level experiments is also investigated.

Fig. 8 presents the best-fit generalized Pareto model for two different choices of the threshold. When the threshold is relatively low (the 87% quantile), the generalized Pareto model sometimes provides a worse fit than even the Weibull model, e.g. in Fig. 8a, c, and f. Increasing the threshold to 98%, however, improves the fit greatly in most cases. It should be noted that even for such a high threshold as 98% the sample size is of an order of 100 or larger.

In Fig. 8 and in the following discussion, the expression "oblique sea" refers to experiments with the 30° wave heading.

The sensitivity of the estimated extreme pressures to the choice of threshold also needs to be investigated. In Fig. 9a, 3-h estimates of the extreme pressure x_α are plotted against the threshold for panels in tank with a low filling level. It is apparent that the estimated x_α is stable for very high thresholds (up to 99%). In Fig. 9b the relative change in consecutive estimates is plotted. The relative change is defined as

$$\Delta(x_\alpha) = \frac{|x_\alpha^{(i)} - x_\alpha^{(i-1)}|}{x_\alpha^{(i-1)}}. \tag{6}$$

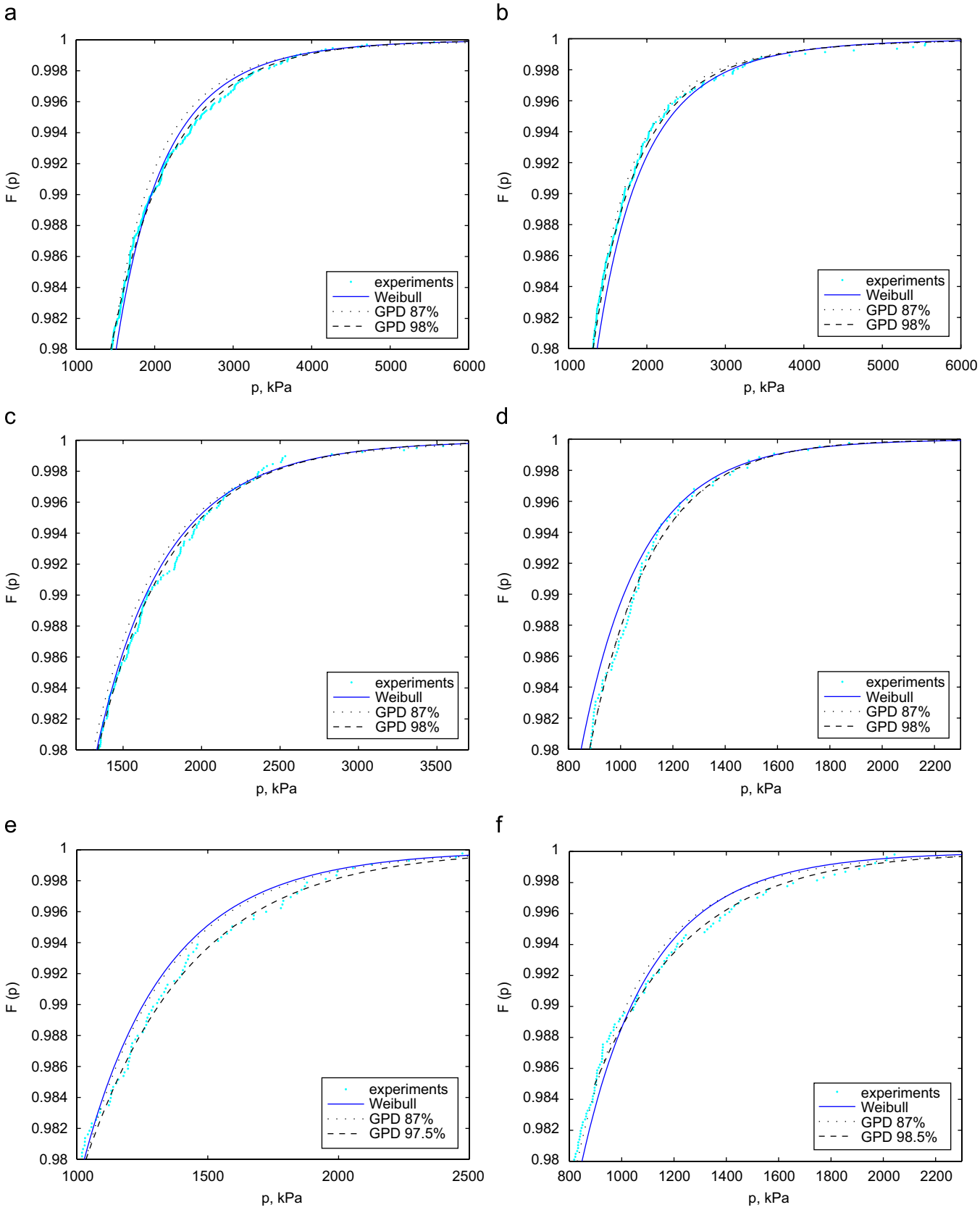

Fig. 8. The generalized Pareto model is fit to the tail of the distribution for different threshold levels: (a) wall panel for the low filling level; (b) bulkhead panel for the low filling level; (c) center panel for the high filling level in a head sea; (d) corner panel for the high filling level in a head sea; (e) center panel for the high filling level in an oblique sea; (f) corner panel for the high filling level in an oblique sea. The three-parameter Weibull model is also plotted for reference.

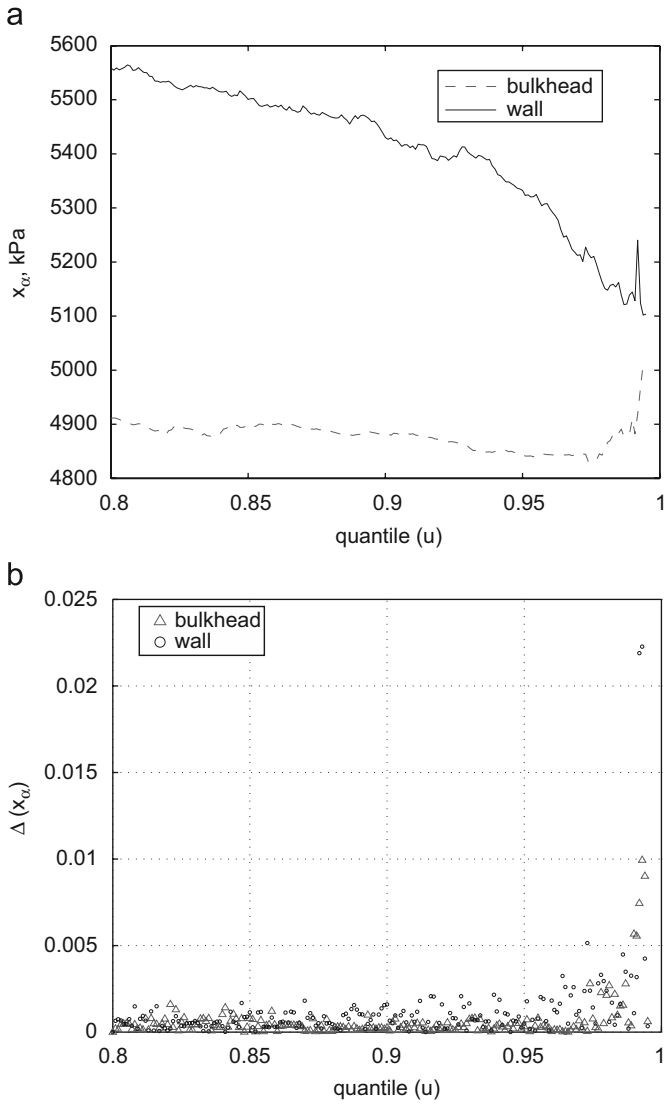

Fig. 9. (a) Estimates of the extreme pressure for threshold levels (quantiles) in the range 80–99.5%, for the wall and bulkhead panels in the low filling level experiments. (b) The relative change in the extreme pressure estimates obtained at consecutive threshold levels.

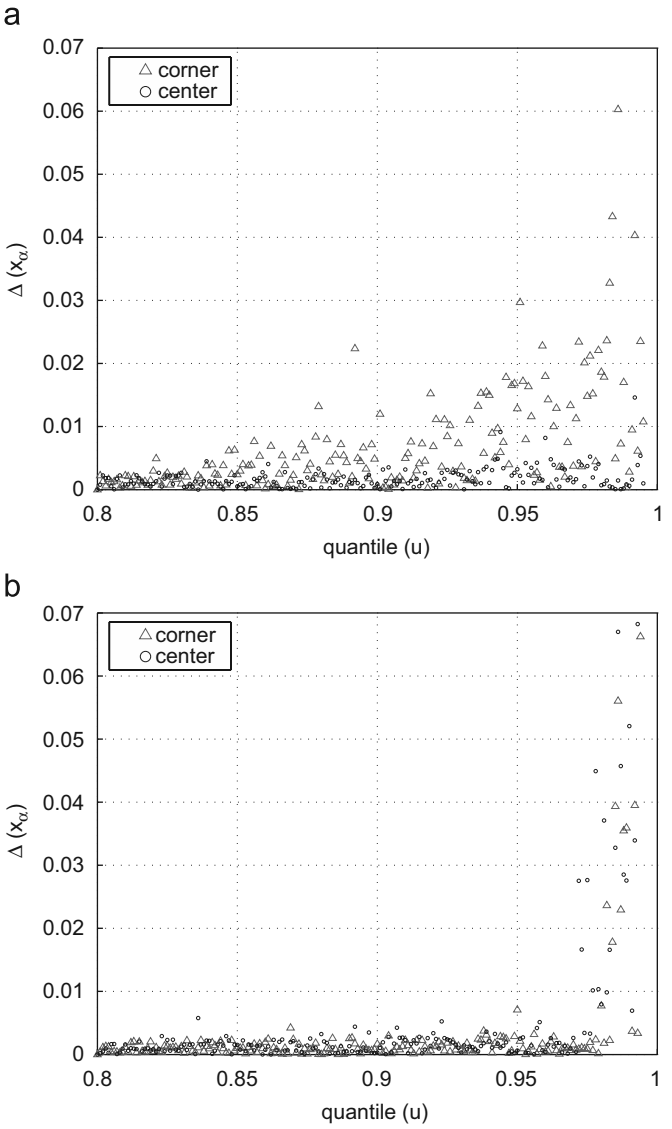

Fig. 10. The relative change in the extreme pressure estimates obtained at consecutive threshold levels (quantiles) in the range 80–99.5%, for the center and corner panels in the high filling level experiments: (a) head sea; (b) oblique sea.

In other words, the threshold level i is discretized (with step size 0.001) and the x_α obtained for each value i is compared to the previous estimate $i-1$. The relative changes in experiments with a low tank filling level are very small, even at very high thresholds. $\Delta(x_\alpha)$ increases somewhat as the threshold approaches the 99% quantile, reaching values of 1% for the bulkhead panel and 2.2% for the wall panel.

In Fig. 10a and b the relative changes $\Delta(x_\alpha)$ for consecutive thresholds are presented for the high tank filling level experiments, in head sea and oblique sea conditions, respectively. Much higher values of $\Delta(x_\alpha)$ are observed for the highest threshold levels in these data. $\Delta(x_\alpha)$ is especially unstable at the head sea corner panel, showing significant variations even at low quantiles.

These results agree well with the 98% threshold level needed for a good model fit, as discussed in relation to Fig. 8.

As mentioned above, the uncertainty resulting from limited sample sizes is reduced by collecting pressure data from many runs. The influence of the threshold level on the fit is also investigated in the smaller samples associated with each individual experiment.

The relative change in consecutive pressure estimates $\Delta(x_\alpha)$ is found to be significantly larger for separate runs that for big samples of combined runs. $\Delta(x_\alpha)$ reaches usually a few percent for thresholds in the 80–90% range. Ideally, the threshold level adopted should keep the variations $\Delta(x_\alpha)$ below the reasonable level. Here a range of 2–3% is chosen. The results of this investigation are presented in Table 6.

For the low filling level experiments the relative change in consecutive estimates exceeds 2% at thresholds around the 92% quantile. This threshold level will be utilized later

Table 6
Maximum thresholds for which the relative change in consecutive pressure estimates $\Delta(x_\alpha)$ does not exceed the range of 2–3%

$\Delta(x_\alpha) =$	0.02	0.03	0.02	0.03
$h/H = 30\%$, $\beta = 90^\circ$	Wall panel		Bulkhead panel	
max	0.995	0.995	0.993	0.993
min	0.805	0.821	0.809	0.824
μ	0.923	0.955	0.922	0.943
σ	0.060	0.045	0.061	0.060
$h/H = 92.5\%$, $\beta = 0^\circ$	Center panel		Corner panel	
max	0.950	0.992	0.877	0.942
min	0.807	0.807	0.802	0.802
μ	0.851	0.874	0.823	0.858
σ	0.045	0.062	0.025	0.043
$h/H = 92.5\%$, $\beta = 30^\circ$	Center panel		Corner panel	
max	0.979	0.979	0.988	0.988
min	0.813	0.823	0.806	0.813
μ	0.886	0.904	0.876	0.925
σ	0.069	0.058	0.064	0.063

Maximum, minimum, average value, and standard deviation for all runs of a given experiment.

in this paper, in applying the POT method for assessment of the sloshing extreme pressure for low filling levels.

For a vessel with high filling level, especially in the case of a head sea, a large variability is evident. $\Delta(x_\alpha)$ in consecutive center panel estimates exceed 2% for thresholds around and above the 85% quantile. In the corner panel high relative changes start even sooner, at a threshold of around 82%. As these thresholds are very low, we investigate the threshold at which the relative changes begin to exceed 3% instead. For both panels in the head sea experiments a reasonable cutoff seems to lie around 87%. This quantile also corresponds to the threshold where relative changes begin to exceed 2% in oblique sea conditions. We thus adopt a uniform 87% threshold in applying the POT method for assessment of the sloshing extreme pressure for the high filling level.

A higher threshold is more appropriate with regard to improving the model fit, as discussed in relation to Fig. 8; recall that the 87% threshold produces a generalized Pareto model that does only as well as the Weibull model. The stability limit of 87% thus calls into question the suitability of generalized Pareto model for describing sloshing induced pressures, at least in samples based on experiments of 5-h duration.

The extreme values x_α are estimated based on experimental runs with a 5-h duration as the 90% quantile of the maximum pressure in 3-h. All extreme values are calculated based on samples including only the highest pressure signals in a given sensor panel; i.e., for a given impact only the sensor with the highest pressure signal in a given panel is considered.

As described in Section 3.1, certain test runs within each experimental condition are given identical tank motion histories, while others are given different motion histories. The estimated extreme pressures of samples in both groups are reported for the low filling level in Table 7, and for the high filling level in Tables 8 (head sea) and 9 (oblique sea).

The scatter in the extreme pressures can now be investigated. The coefficient of variance (CoV) of a sample is defined as σ/μ, where σ and μ are standard deviation and mean, respectively. Tables 7–9 report the CoV for each experiment. In order to obtain reliable pressure estimates the number of test repetitions in each experimental condition should be high. The sample runs with identical and varied motion histories are characterized by similar maximal pressure distributions, both in their mean and their variability.

More reliable estimates of the pressure can be determined by combining the samples from all test runs with a given experimental setup, as mentioned in the discussion of Fig. 8.

Table 7
Estimated extreme values of the sloshing-induced pressure (MPa) for all runs of the low filling experiment

	Wall panel		Bulkhead panel	
	Weibull	Pareto	Weibull	Pareto
Identical sample				
max	8.17	8.51	6.76	7.20
min	2.95	2.86	2.63	2.57
μ	4.87	5.13	4.06	4.21
σ	1.55	1.67	1.35	1.45
CoV	0.32	0.32	0.33	0.34
Various samples				
max	8.17	8.51	8.00	8.72
min	3.89	4.31	2.44	1.76
μ	5.10	5.48	4.53	4.70
σ	1.28	1.33	1.79	2.11
CoV	0.25	0.24	0.40	0.45

Table 8
Estimated extreme values of the sloshing-induced pressure (MPa) for all runs of the high filling level experiment, $\beta = 0^\circ$

	Center panel		Corner panel	
	Weibull	Pareto	Weibull	Pareto
Identical sample sample				
max	4.46	4.78	1.98	2.03
min	2.75	2.83	1.39	1.20
μ	3.49	3.71	1.72	1.66
σ	0.65	0.67	0.20	0.26
CoV	0.19	0.18	0.12	0.16
Various samples				
max	4.18	4.49	1.99	2.03
min	2.90	2.42	1.52	1.34
μ	3.24	3.30	1.76	1.71
σ	0.54	0.81	0.25	0.33
CoV	0.17	0.25	0.14	0.20

Table 9
Estimated extreme values of the sloshing-induced pressure (MPa) for all runs of the high filling level experiment, $\beta = 30^\circ$

	Center panel		Corner panel	
	Weibull	Pareto	Weibull	Pareto
Identical sample				
max	2.72	2.99	2.81	3.21
min	1.56	1.52	1.45	1.39
μ	2.24	2.32	1.95	2.04
σ	0.38	0.50	0.39	0.52
CoV	0.17	0.21	0.20	0.25
Various samples				
max	2.72	2.99	2.15	2.21
min	2.11	1.99	1.42	1.40
μ	2.35	2.44	1.87	1.92
σ	0.25	0.39	0.31	0.35
CoV	0.11	0.16	0.16	0.18

A large number of sloshing motion patterns may be observed. This results in a chaotic fluid motion in the tank; for an identical tank motion time history the fluid motion does not appear to be the same. Occurrence of an impact in a given location and time is dependent on an instantaneous fluid position, velocity and acceleration field. Therefore, inspection of samples obtained for the runs repeated for a given motion time history show no correlation in time; impact events do not only have very different maximum pressure, but they also occur in different time instants and often in other locations in the tank. The two experimental groups described above (with identical and different input) have also similar variability of extreme estimates.

Therefore, maxima from runs with identical input (tank motion time history) can practically be assumed to be independent. All 95 h (19 samples) of runs registered during the low filling level tests can be analyzed as a single sample. Each data set of 70 h (14 samples) registered for each of the two wave heading angles in the high filling level experiments is also investigated.

Estimates of the extreme pressure 3-h values corresponding to the 90% quantile and the parameters of the stochastic models are presented in Table 10 for the three-parameter Weibull model and in Table 11 for the generalized Pareto model with the threshold 98%.

Fig. 11 shows the probability of exceedance (POE) for the combined set of 19 low filling samples and two combined sets of 14 high filling samples for each of the heading considered. It can immediately be seen that the expected maximum pressure is higher in the low filling case. Moreover, the POE curves are flatter for the lower filling level. This means that if the extreme pressure with a longer return period is of interest, the difference between the estimates in investigated conditions may be even larger. This is shown in Fig. 11 by indicating the POE corresponding to a 3-h and a 30-h return period with two horizontal lines.

Table 10
Weibull model estimates of the extreme sloshing-induced pressures, and the parameters of the model

Condition	Panel location	p (kPa)	Parameters		
			c	a	δ
$h/H = 30\%$, $\beta = 90^\circ$	Wall	5149	0.576	128.1	140.8
	Bulkhead	4769	0.531	93.6	145.6
$h/H = 92.5\%$, $\beta = 0^\circ$	Center	3466	0.710	176.7	125.7
	Corner	1740	0.827	143.9	100.7
$h/H = 92.5\%$, $\beta = 30^\circ$	Center	2302	0.738	143.9	114.6
	Corner	1999	0.714	108.0	118.4

All runs for a given experiment are combined.

Table 11
Generalized Pareto model estimates of the extreme sloshing-induced pressures, and the parameters of the model

Condition	Panel location	p (kPa)	Parameters	
			c	a
$h/H = 30\%$, $\beta = 90^\circ$	Wall	5153	0.051	762.9
	Bulkhead	4858	0.198	575.8
$h/H = 92.5\%$, $\beta = 0^\circ$	Center	3446	0.046	461.9
	Corner	1731	0	238.7
$h/H = 92.5\%$, $\beta = 30^\circ$	Center	2596	0	444.6
	Corner	2061	0	330.1

All runs for a given experiment are combined.

4.2. Temporal characteristics

The dependence of the structural dynamic response on the temporal pattern of a fluid impact can be characterized by the ratio of an appropriate temporal parameter to the natural period of the structure. For very short impacts, the characteristic parameter is the impulse. For longer impacts whose duration is comparable to the natural period of the structure, additional details of the time history have to be considered and in particular the rise time and duration. For very long impacts, the structural response is quasi-static.

The first natural period of an LNG membrane containment system supported by steel plating is on the order of 5–10 ms. A large number of vibration modes contribute to the structural response.

Even if the triangular approximation does not seem to be the most accurate approach in all cases, as indicated in Section 3.3, this is still commonly applied due to its simplicity and robustness. In this section the "typical" duration t_d, rise time t_r, and ratio t_r/t_d of a triangle-shaped time history are investigated.

It is observed that the distribution of these temporal parameters depends to a large extent on the pressure magnitude. For this reason we have investigated the dependence of these parameters on pressure. Restricting the analysis to the data available from each run, however,

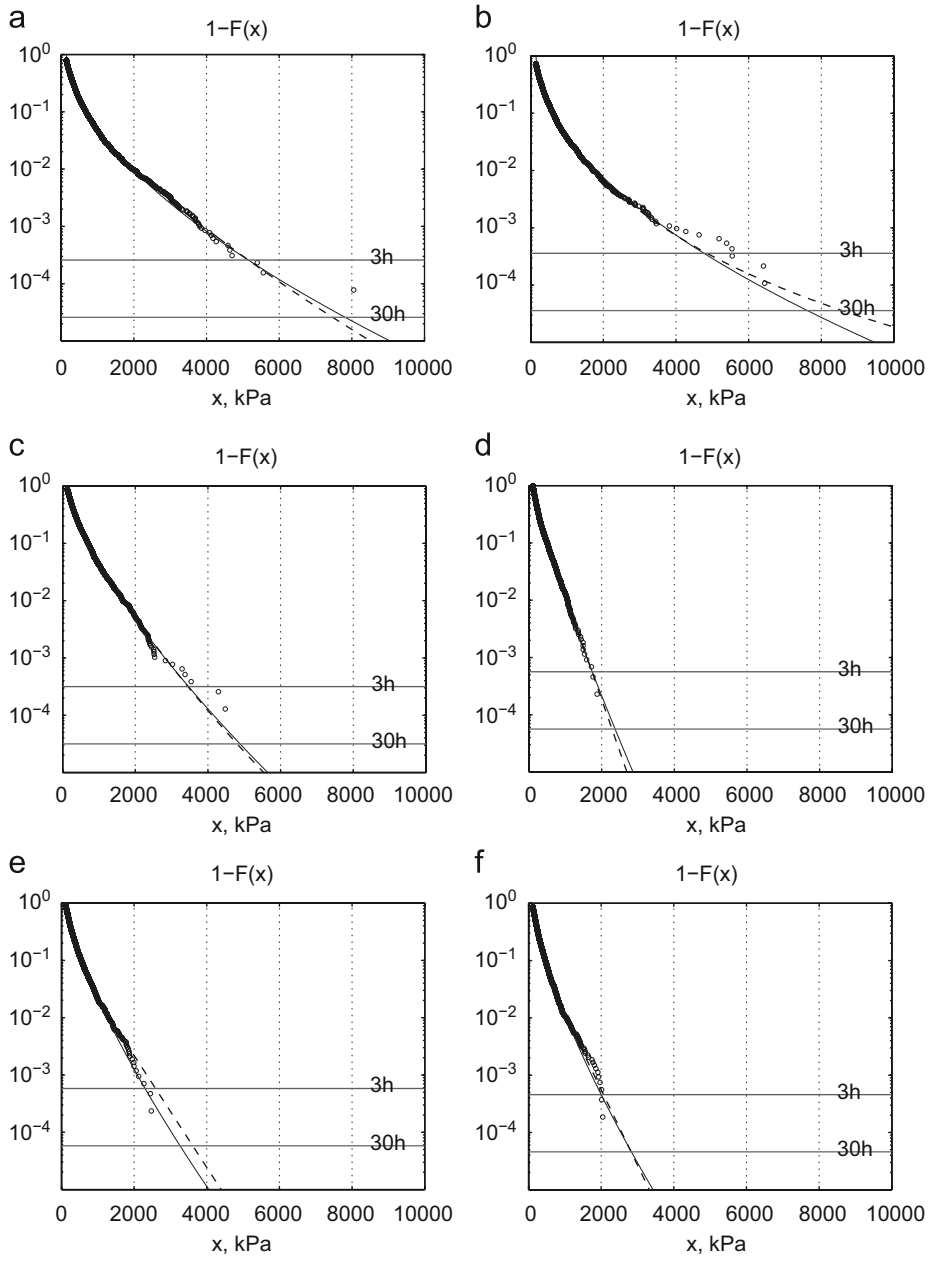

Fig. 11. Probability of exceedance for various data samples: (a) 19 runs at the low filling level, wall panel; (b) 19 runs at the low filling level, bulkhead panel; (c) 14 runs at the high filling level with $\beta = 0^\circ$, center panel; (d) 14 runs at the high filling level with $\beta = 0^\circ$, corner panel; (e) 14 runs at the high filling level with $\beta = 30^\circ$, center panel; (f) 14 runs at the high filling level with $\beta = 30^\circ$, corner panel.

might introduce a bias due to a small sample size. For this reason, as previously, all the relevant samples registered during the tests in each condition are analyzed as a single sample.

Histograms of the impact duration are presented in Fig. 12. The histograms in Fig. 12a and c include all impacts, regardless of the maximum pressure attained, in both of the sensor panels. Fig. 12a collects all impacts from the low filling level experiment, and Fig. 12c collects all impacts from one of the high filling level experiments (head sea).

Whenever all impacts are considered (Fig. 12a and c), a very heavy tail of long-duration events is apparent. This reflects the complex time histories of the smallest impacts and the fact that such time histories are not accurately modeled by the triangular function (see Sections 3.2 and 3.3).

To illustrate the distribution of durations for impacts with high pressure maxima, Fig. 12b and d include only events with maxima exceeding the 97% quantile. These two distributions are clearly much narrower; a much larger fraction of pressure time histories with short duration is observed.

It is also apparent that the durations are significantly shorter for the high filling level than for the low filling level. This is a case both for all impacts, regardless of the maximum pressure attained (compare Fig. 12a and c) as well as for the strongest impacts (Fig. 12b and d).

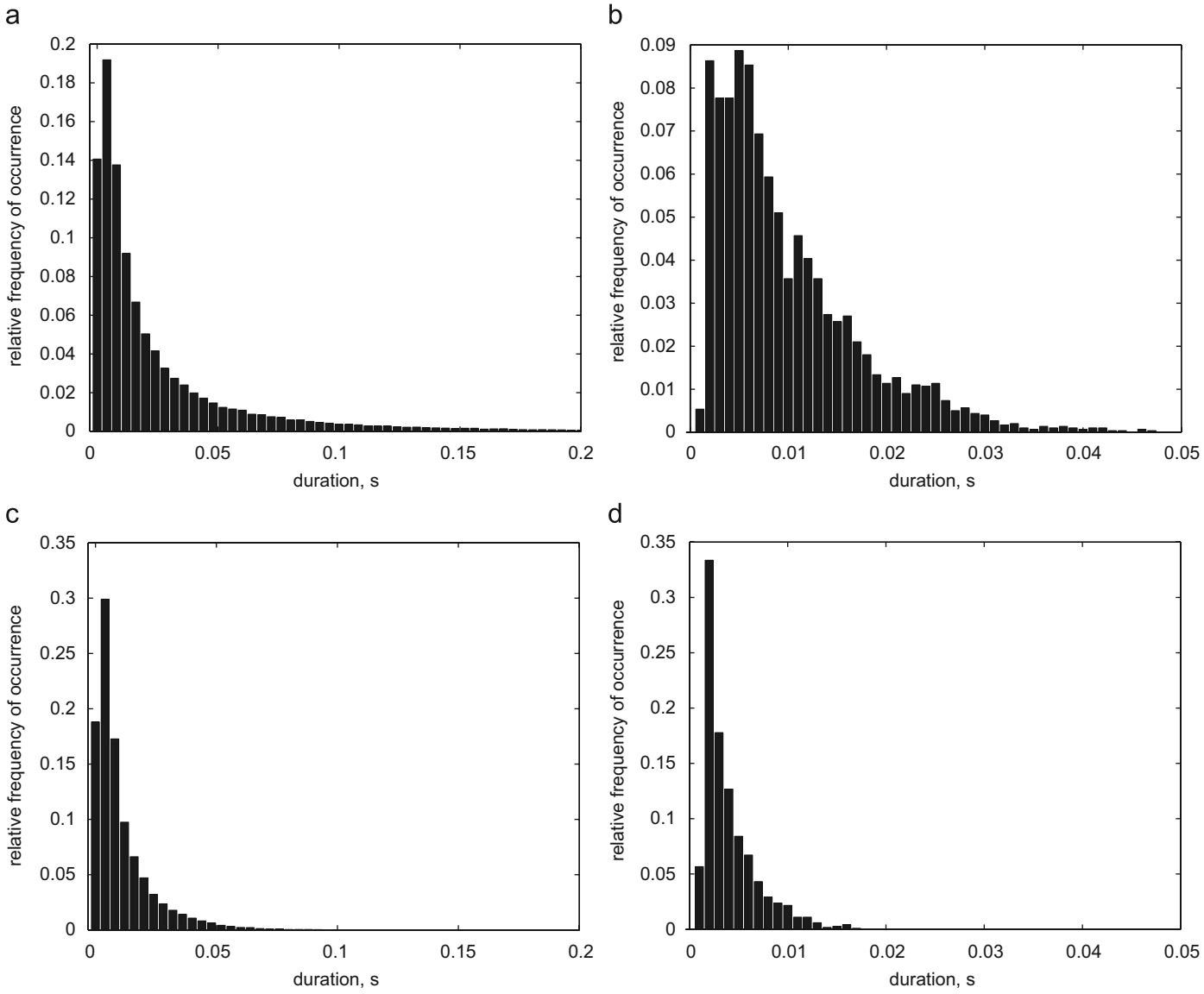

Fig. 12. Histograms of the sloshing impact duration, considering the time histories registered in both panels: (a) all time histories for $h/H = 30\%$ and $\beta = 90^\circ$; (b) time histories whose pressure maxima exceed the 97% quantile for $h/H = 30\%$ and $\beta = 90^\circ$; (c) all time histories for $h/H = 92.5\%$ and $\beta = 0^\circ$; (d) time histories whose pressure maxima exceed the 97% quantile for $h/H = 92.5\%$ and $\beta = 0^\circ$.

The means and standard deviations of all four histograms are presented in Table 12, along with data for the high filling level in an oblique sea (for which no histogram is given).

The mean and standard deviation of the rise time is presented in Table 13 for all time histories and for those whose pressure maxima exceed the 97% quantile. The rise times follow a similar tendency: they are significantly shorter in events exceeding the 97% quantile, and longer rise times are observed for the low filling level.

We now consider the ratio of rise time to duration, which may be considered a parameter indicating the overall shape of the time history. As certain differences are observed in the time histories of sloshing impacts at different locations in the tank, these results are presented as separate samples for each sensor panel. Fig. 13 shows histograms of this ratio for four different cases.

Table 12
Mean and standard deviation of the sloshing pressure durations (ms), considering all time histories and those histories with pressure maxima exceeding the 0.97 quantile

Condition	All maxima		Max > 0.97q	
	μ	σ	μ	σ
$h/H = 30\%$, $\beta = 90^\circ$	27.4	41.0	10.1	7.4
$h/H = 92.5\%$, $\beta = 0^\circ$	12.4	15.7	4.3	2.7
$h/H = 92.5\%$, $\beta = 30^\circ$	11.7	10.8	4.4	2.7

The means and standard deviations of this ratio for each experiment and sensor panel are presented in Table 14. For

the strongest impacts (above the 97% quantile), it can be seen that the mean ratios of rise time to duration lie in the approximate range 0.40–0.55. The mean ratio calculated for the high quantile time histories always differs slightly from that calculated for all time histories. For the low filling level, the ratio decreases with increasing magnitude; the opposite trend occurs for the high filling level.

It is also apparent that the ratios are smaller for the low filling level than for the high filling level.

For the very strongest sloshing impacts (e.g., when the maximum pressure exceeds the 99% quantile) the ratio is unstable for all cases due to limited sample size.

Table 13
Mean and standard deviation of the sloshing pressure rise time (ms), considering all time histories and those histories with pressure maxima exceeding the 0.97 quantile

Condition	All maxima		Max $>0.97q$	
	μ	σ	μ	σ
$h/H = 30\%$, $\beta = 90^\circ$	11.4	17.6	4.0	3.8
$h/H = 92.5\%$, $\beta = 0^\circ$	6.4	12.0	2.2	1.6
$h/H = 92.5\%$, $\beta = 30^\circ$	6.0	6.4	2.2	1.5

4.3. Spatial characteristics

Pressure variations are always measured by multiple sensors in each of the locations considered (see Fig. 3). The overall loading on the structure at one of these locations can be obtained by combining the pressures registered by relevant sensors. The general trend is that the spatially

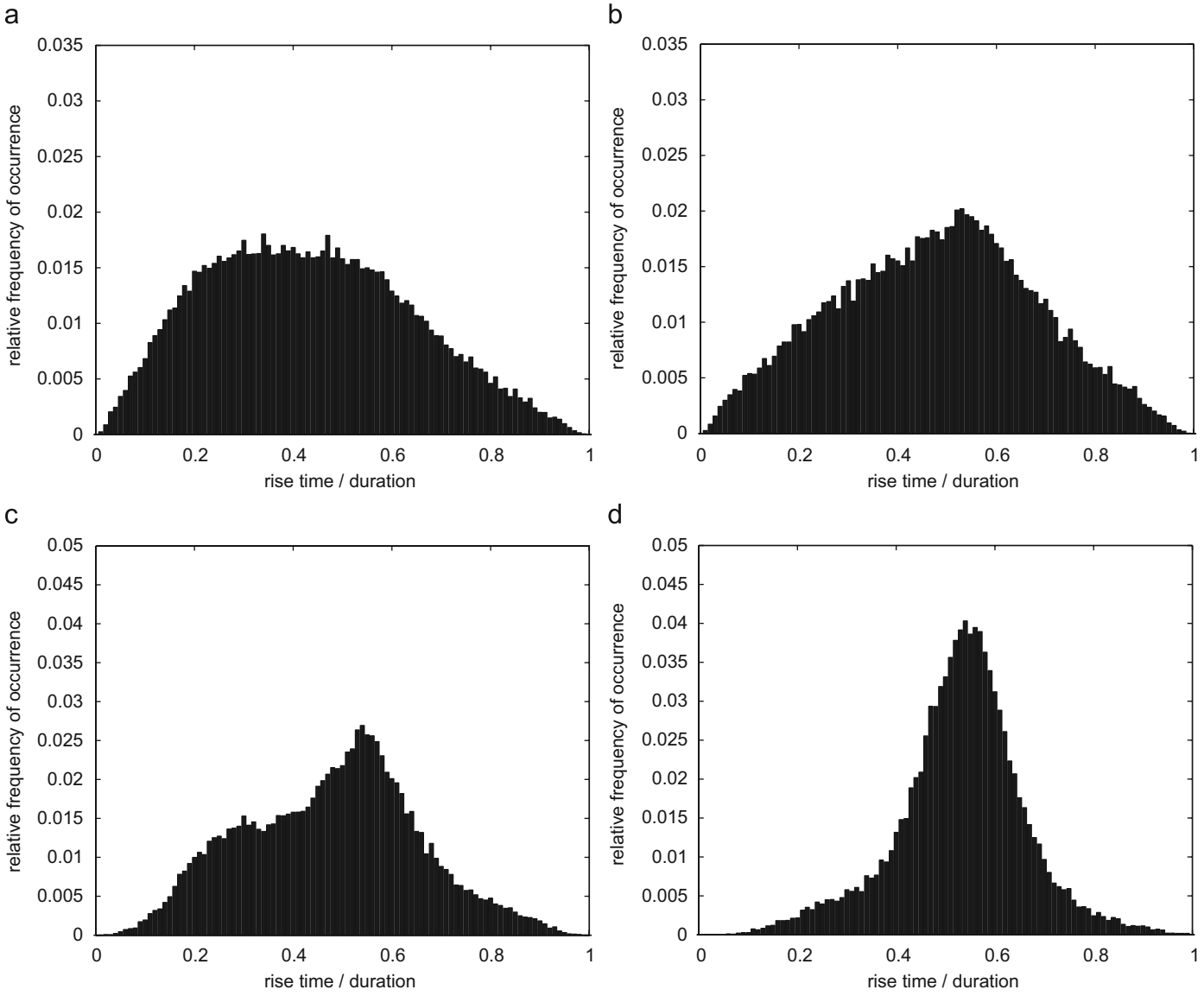

Fig. 13. Histograms of the ratio between rise time and duration for all time histories observed in the following sensor panels and experiments: (a) wall panel, $h/H = 30\%$ and $\beta = 90^\circ$; (b) bulkhead panel for $h/H = 30\%$ and $\beta = 90^\circ$; (c) center panel for $h/H = 92.5\%$ and $\beta = 0^\circ$; (d) corner panel for $h/H = 92.5\%$ and $\beta = 0^\circ$.

Table 14
Mean and standard deviation of the ratio between rise time and duration, considering all time histories and those histories with pressure maxima exceeding the 0.97 quantile

Condition	Panel location	All maxima		Max > 0.97q	
		μ	σ	μ	σ
$h/H = 30\%$, $\beta = 90^\circ$	Wall	0.43	0.21	0.39	0.18
	Bulkhead	0.48	0.20	0.45	0.18
$h/H = 92.5\%$, $\beta = 0^\circ$	Center	0.48	0.17	0.51	0.14
	Corner	0.53	0.13	0.52	0.13
$h/H = 92.5\%$, $\beta = 30^\circ$	Center	0.47	0.17	0.49	0.14
	Corner	0.53	0.13	0.54	0.13

averaged maximum pressure decreases as the area affected increases.

When the layered structure of an LNG containment system is supported by a conventional steel structure, there are various regimes of the structural response that are of interest. These include local effects on the containment system itself, such as crushing of the foam in the foam-based insulation system, buckling and indentation of the plywood plates in a box-based insulation system, shear and bending of plywood plates in both concepts, as well as bending of steel plates and stiffened panels. Various loading areas are representative for each of these responses.

In order to investigate the spatial distribution of sloshing pressure, the sensor panels must have a reasonably fine resolution. The 4×4 square panels used for the high filling tests are satisfactory in this respect, but a low filling condition needs to be further tested. It may be that a finer sensor arrangement than the rectangular panels used herein is necessary to properly discern the spatial structure of impacts in this experiment.

The spatially averaged pressure of an impact event is the arithmetic mean of the maximum pressure values obtained by all contributing sensors. Pressure measured by each sensor is assumed to be representative for an area d^2, where d is the distance between neighboring sensors (0.75 m in the wall and bulkhead panels, and 0.25 m in the center and corner panels, full scale). In the following the pressure over $n = 4$, 9, and 16 sensors is investigated for the high filling level and the average over four sensors for the low filling level.

When the loading at a particular location is of interest (e.g. in a tank corner), the pressure–area relationship is typically established for a specific combination of sensors. Then the relationship between average pressure and maximum pressure is calculated based on varying area in this predefined location.

This paper adopts another approach: the sloshing pressures are measured over a region of variable size assuming that the structure is continuous and "uniform", i.e. there is no account to any special structural arrangements due to tank corners and edges between walls. The relationship between average pressure and maximum pressure is investigated throughout the entire panel; the pressure is averaged over several combinations of n adjacent sensors. The number of adjacent sensors may be 4, 9, or 16 and the combination resulting in the *highest* average pressure is investigated regardless of the location in the panel where the highest pressure is measured.

Fig. 14a presents a histogram of the ratio between the average pressure of four neighboring sensors and the highest measured pressure, for all sloshing impacts on a wall panel in the low filling level experiments. Fig. 14c presents the mean ratio for all events with pressure maxima exceeding the threshold x_m (for quantiles above 90%), providing an indication of how this ratio depends on the peak pressure.

There is a strong peak at the ratio 0.25 in Fig. 14a, which corresponds to impacts where the pressure was registered only in one sensor. This can occur because pressures below 250 kPa are not registered by the sensors. The peaks at ratios just below 0.5 and 0.75 are also caused by untriggered sensors; they correspond to events where the pressure is registered by only two or three sensors out of four, respectively.

The histogram for high filling level events (head sea; Fig. 14b and d) displays similar features: a high peak at a ratio of 0.25, and lower peaks at ratios of 0.5 and 0.75. The high filling level histogram clearly has the heavier tail.

The results for different cases are summarized in Table 15 for all time histories, and in Table 16 for time histories whose pressure maxima exceed the 97% quantile. It can be observed that for a given number of sensors, the ratio between spatially averaged pressure and highest measured pressure increases significantly when only the strong impacts are considered.

Although this ratio cannot be quantitatively compared for the two filling levels considered, due to the different arrangements and sizes of the sensor panels, it can still be concluded that sloshing impacts in the high filling level experiment are more concentrated in space. This fact can be seen, for example by comparing case "a" for $n = 4$ to cases "b" and "c" for $n = 16$. The high filling level ratios are nearly twice as small as the low filling level ratios.

4.4. Combined temporal–spatial characteristics

So far our treatment of sloshing impacts has only provided information about the distribution of pressure in time and space individually. The temporal and spatial characteristics need to be combined. By comparing the time lag Δt between pressure time histories in neighboring sensors, we can also indirectly measure the velocity V of the pressure profile as it passes along the wall. The velocity may be estimated as $V = d/\Delta t$, where d is the known distance between sensors (typically a few tens of centimeters). The time lag is measured in two perpendicular directions simultaneously. This analysis is performed for all

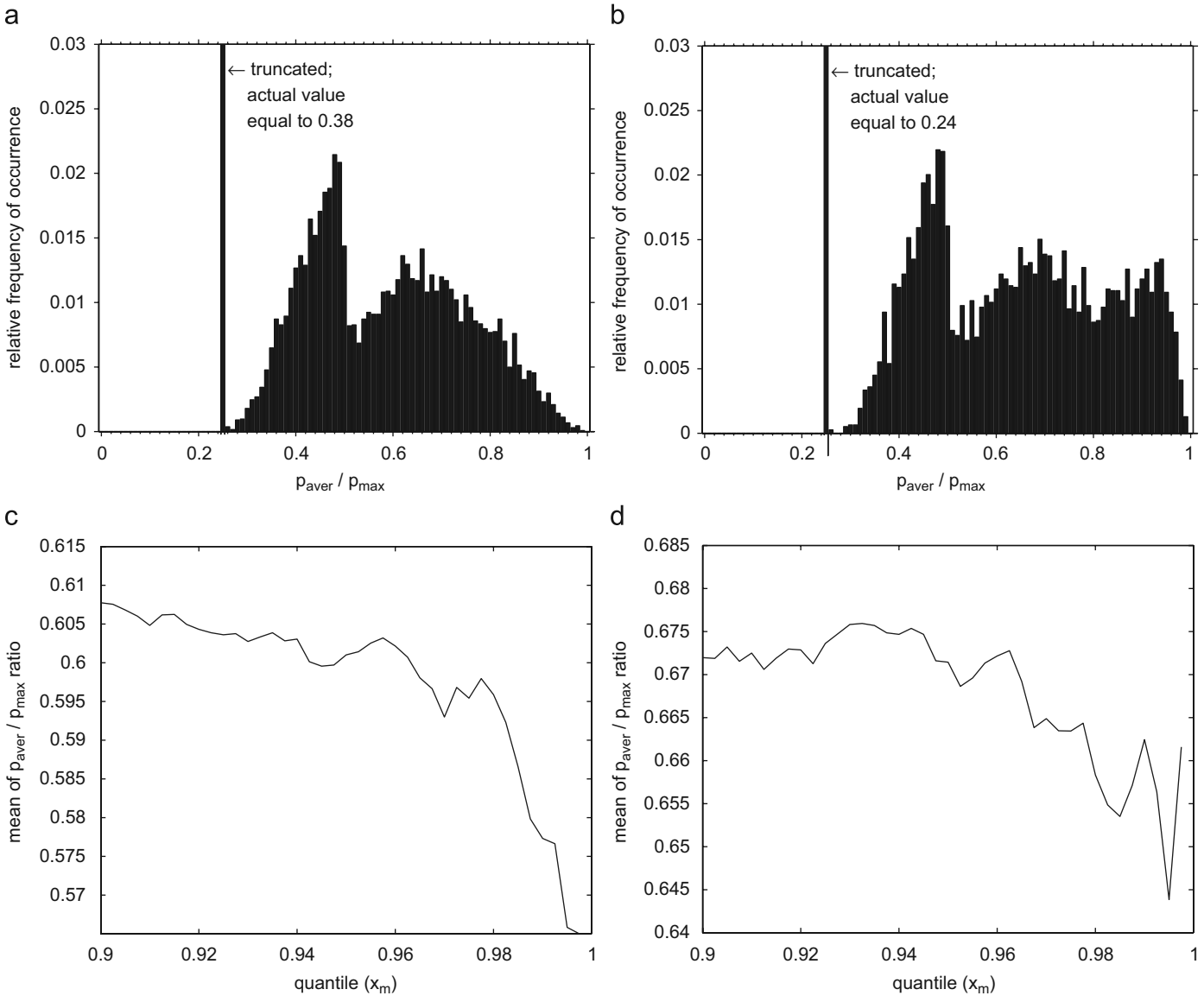

Fig. 14. Histograms of the ratio between the average pressure of four neighboring sensors and the highest measured pressure for all sloshing impacts: (a) wall panel, $h/H = 30\%$ and $\beta = 90^\circ$; (b) center panel, $h/H = 92.5\%$ and $\beta = 0^\circ$. The mean ratio for time histories with maxima exceeding the threshold x_m: (c) wall panel, $h/H = 30\%$ and $\beta = 90^\circ$; (d) center panel, $h/H = 92.5\%$ and $\beta = 0^\circ$.

Table 15
Mean and standard deviation of the ratio between spatially averaged pressure and the highest pressure measured, p_{aver}/p_{max}, considering all impact events

Case	Condition	Panel location	$n = 4$		$n = 9$		$n = 16$	
			μ	σ	μ	σ	μ	σ
a	$h/H = 30\%$,	Wall	0.46	0.21				
	$\beta = 90^\circ$	Bulkhead	0.44	0.20				
b	$h/H = 92.5\%$,	Center	0.55	0.23	0.37	0.24	0.27	0.22
	$\beta = 0^\circ$	Corner	0.56	0.25	0.38	0.26	0.28	0.25
c	$h/H = 92.5\%$,	Center	0.54	0.23	0.36	0.23	0.25	0.21
	$\beta = 30^\circ$	Corner	0.55	0.25	0.38	0.26	0.28	0.25

experimental combinations of tank filling level and wave heading angle.

As previously, the pressure maxima from repeated runs are collected into a single sample in order to reduce the uncertainty. Fig. 15 presents the time lag between the occurrences of the peak pressure in neighboring sensors for the wall panel in the low filling level experiment ($h/H = 30\%$, $\beta = 90^\circ$; for the panel's location and dimensions, see Fig. 3). Fig. 15a reports the time lags collected for all pairs of adjacent sensors along the vertical direction, and Fig. 15b reports the time lags for horizontal pairs.

The dependence of the mean time lag on the maximum pressure of the impact is also investigated, as usual by comparing the entire sample to the sample of impacts

Table 16
Mean and standard deviation of the ratio between spatially averaged pressure and the highest measured pressure, p_{aver}/p_{max}, , considering only pressure maxima exceeding the 0.97 quantile

Case	Condition	Panel location	$n=4$		$n=9$		$n=16$	
			μ	σ	μ	σ	μ	σ
a	$h/H=30\%$,	Wall	0.59	0.14				
	$\beta=90^\circ$	Bulkhead	0.51	0.13				
b	$h/H=92.5\%$,	Center	0.66	0.13	0.49	0.15	0.36	0.14
	$\beta=0^\circ$	Corner	0.63	0.15	0.44	0.16	0.32	0.15
c	$h/H=92.5\%$,	Center	0.69	0.12	0.50	0.14	0.37	0.14
	$\beta=30^\circ$	Corner	0.64	0.16	0.44	0.17	0.32	0.16

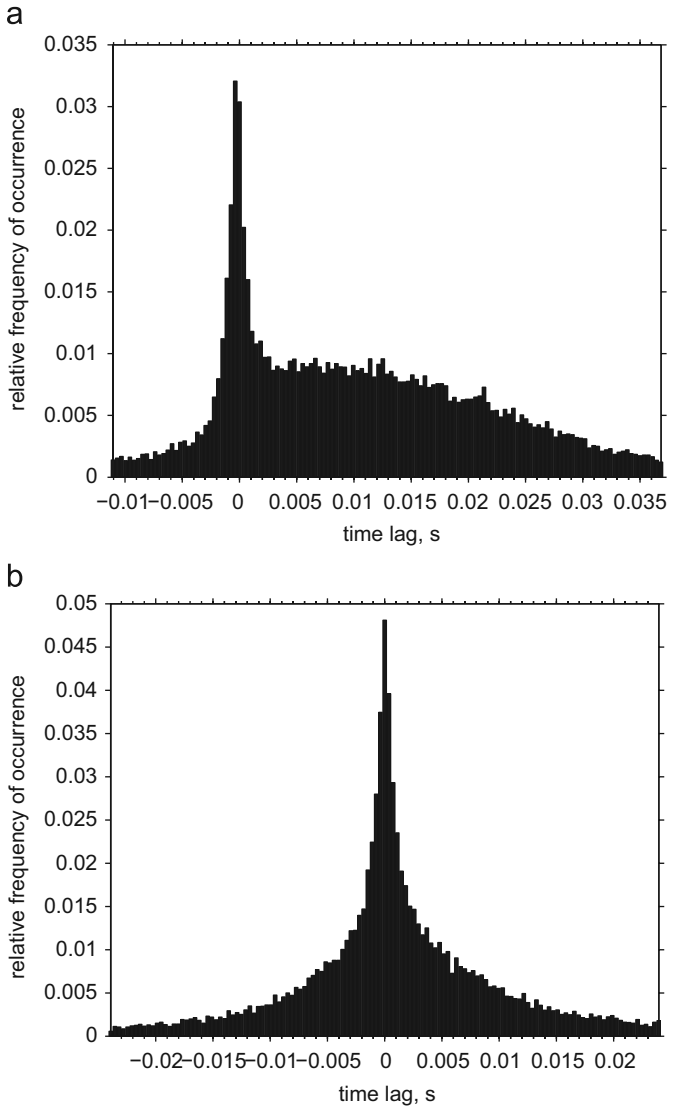

Fig. 15. Histograms of the time lag between any pair of adjacent sensors in the wall panel for $h/H=30\%$ and $\beta=90^\circ$: (a) vertical direction; (b) longitudinal direction. All time histories are considered, regardless of their pressure maxima.

whose pressure maxima exceed the 97% quantile. These results are presented for the wall panel and bulkhead panel of the low filling level experiment in Tables 17 and 18.

In the wall panel, positive values correspond to profiles moving upwards and backwards. In the bulkhead panel, positive values correspond to profiles moving upwards and outwards (toward the starboard side).

Similar results for the high filling level experiments are given for both wave headings in Tables 19 and 20 for the center and the corner panel, respectively. In this case positive values correspond to profiles passing backwards and to starboard.

For the applied time histories of the tank motion and in the investigated locations the dominant direction of pressure profile propagation is vertical for low filling level experiments, and longitudinal for high filling level experiments in a head sea. For high filling level experiments in an oblique sea, the pressure profile tends to move along a diagonal.

As mentioned in previous sections, the distance between adjacent sensors is 0.25 m in the center and corner panels

Table 17
Mean and standard deviation of the time lag (ms) between any pair of adjacent sensors along a vertical and longitudinal direction in wall panel for $h/H=30\%$ and $\beta=90^\circ$

Time histories	Vertical		Longitudinal	
	μ	σ	μ	σ
All magnitudes	10.6	50.3	2.8	46.4
>0.97 quantile	5.5	7.6	0.7	5.7

Table 18
Mean and standard deviation of the time lag (ms) between any pair of adjacent sensors along a vertical and transverse direction in bulkhead panel for $h/H=30\%$ and $\beta=90^\circ$

Time histories	Vertical		Transverse	
	μ	σ	μ	σ
All magnitudes	8.3	35.1	−6.0	37.4
>0.97 quantile	5.3	8.4	−1.4	5.2

Table 19
Mean and standard deviation of the time lag (ms) between any pair of adjacent sensors along a longitudinal and transverse direction in center panel for the high filling level

Condition	Panel location	Longitudinal		Transverse	
		μ	σ	μ	σ
$h/H=92.5\%$,	All magnitudes	1.0	9.2	0.1	8.8
$\beta=0^\circ$	>0.97 quantile	0.6	7.9	0.0	1.6
$h/H=92.5\%$,	All magnitudes	1.1	5.3	0.2	6.5
$\beta=30^\circ$	>0.97 quantile	0.4	1.0	0.3	2.4

Table 20
Mean and standard deviation of the time lag (ms) between any pair of adjacent sensors along a longitudinal and transverse direction in corner panel for the high filling level

Condition	Panel location	Longitudinal		Transverse	
		μ	σ	μ	σ
$h/H = 92.5\%$, $\beta = 0^\circ$	All magnitudes	0.4	4.2	0.0	5.6
	>0.97 quantile	0.7	1.4	0.1	1.4
$h/H = 92.5\%$, $\beta = 30^\circ$	All magnitudes	0.3	7.2	0.2	8.0
	>0.97 quantile	0.6	2.9	0.2	2.0

used for the high filling level, and 0.75 m in the wall and bulkhead panels used for the low filling level. Examining only those time histories with the largest pressure maxima, we find that velocities are lowest in the low filling level experiment. The mean velocity of these pressure maxima is 136 m/s.

For the high filling level experiments in a head sea the corresponding mean velocity is 357 m/s in the longitudinal direction and on the order of 10 000 m/s in the transverse direction, which in practice is effectively infinite; the pressure is exerted almost simultaneously over the entire sensor panel.

The effect of the pressure profile velocity on the structural response remains to be investigated.

5. Conclusions

This work provides a probabilistic assessment of the pressures due to sloshing in partially filled tanks. Several features of the pressure time histories relevant to a structural response analysis of the LNG membrane containment system are characterized.

The data used in this paper were provided by sloshing experiments in a movable tank. The most commonly applied post-processing method consists of representing the rise and decay of pressure by a triangular time history. The accuracy of this method is investigated. It is found that while weaker sloshing impacts may produce very complex time histories, the number of local distortions (such as secondary peaks) decreases significantly for those impacts with the highest pressure maxima.

By comparing the slopes of real (measured) time histories to the approximate (triangular) time histories, it is shown that the rise time is often not modeled properly. A more accurate alternative to post-processing based on a trapezoidal profile is thus presented. How the alternative approach affects predictions of the structural response has yet to be investigated.

The pressure magnitude as well as the spatial and temporal patterns of the sloshing pressure are important factors for the structural response. Their statistical distribution is investigated. It is assumed that the characteristic pressure magnitudes, temporal profiles, and spatial profiles of the sloshing impacts can be investigated separately.

The Weibull and generalized Pareto models are used to describe the distribution of sloshing pressure maxima. Suitability of the latter is investigated with respect to goodness of fit in the tail of the distribution, and the stability of its estimated extreme value for various quantile thresholds. When considering only those time histories with a maximum pressure exceeding the 87% quantile, the Pareto model's fit to the tail is no more accurate than the Weibull model. The fit improves significantly, however, when the threshold is increased to the 98% quantile.

For a very large sample of pressure maxima combining data from all relevant runs (19 for the low filling level experiment, and 14 each for the two high filling level experiments), the estimated extreme values are very stable near such a high threshold level.

In reality, however, sample sizes are usually much smaller. The stability of the estimated extreme value is therefore also investigated separately for each run. The threshold resulting in reasonable stability of the estimated extreme value is much lower in this case, sometimes far below the 90% quantile. The generalized Pareto model may thus be unsuitable for describing the sloshing-induced pressures in a sample drawn from only a 5-h experiment.

The uncertainty in determining extreme value estimates from limited samples is also addressed. In order to obtain reliable estimates the number of test repetitions in a given experiment should be high. Moreover, it is found that estimates obtained for samples with identical tank motion time histories have approximately the same scatter as estimates obtained for samples with varied tank motions.

The pressure maxima registered in the low filling level experiment are significantly higher than those recorded for a high filling level. Moreover, the slope of the POE curve is flatter in the low filling level, which means that the extreme pressure value will increase more when a longer return period is examined.

The duration t_d, rise time t_r, and ratio t_r/t_d of triangular impacts are investigated, and their dependence on the maximum pressure of the impact is analyzed.

When all time histories are considered, regardless of their magnitude, the duration and rise time distributions both exhibit a pronounced upper tail. This tail is caused by the many small impacts with more complex time histories, and reflects an important shortcoming of applying the triangular time history. When the sample is restricted to the largest impacts, both the mean duration and the mean rise time decrease significantly and the tail disappears. The sloshing impacts at a low filling level have a longer duration and smaller t_r/t_d ratio, on average, than those occurring at a high filling level.

The pressure is also averaged over adjacent sensors and compared to the highest pressure. In the high filling level experiments, blocks of 4, 9, and 16 sensors were considered; for the low filling level experiments, only blocks of 4 sensors were considered. It is found that sloshing impacts in the high filling level experiments are more concentrated in space than those found for a low

filling level. Moreover, the ratio of spatially averaged pressure to highest observed pressure increases significantly as impacts with a higher maximum pressure are considered.

It can be concluded that sloshing impacts in tanks with a low filling level generally have larger magnitudes, longer durations, a smaller ratio of rise time to duration, and greater spatial extent. All these factors should in principle increase the structural response.

The information about the distribution of pressure in time and space is combined by analyzing the velocity of the pressure profiles. This velocity is estimated by measuring the time lag between maximum pressure signals in neighboring sensors in two perpendicular directions.

For the applied time histories of the tank motion and in considered locations the dominant direction of the pressure profile is vertical (upward) in the low filling level experiments and longitudinal (backward) in the high filling level experiments (head sea). For the high filling level in an oblique sea, the pressure profile travels along the diagonal.

The mean profile velocity observed for the low filling level is over 2.5 times smaller than the mean profile velocity of the high filling level. The effect of profile velocity on the structural response should be investigated in future research.

Acknowledgments

The authors wish to express their gratitude to the Research Council of Norway for providing financial support to the Centre for Ships and Ocean Structures.

References

Baarholm, G.S., Moan, T., 2001. Application of contour line method to estimate extreme ship hull loads considering operational restrictions. Journal of Ship Research 45 (3), 228–240.

Biggs, J.M., 1964. Introduction to Structural Dynamics. McGraw-Hill, New York.

Bulgarelli, U.P., 2005. The application of numerical methods for the solution of some problems in free-surface hydrodynamics. Journal of Ship Research 49 (4), 288–301.

Faltinsen, O.M., Rognebakke, O.F., Timokha, A.N., 2005. Classification of three-dimensional nonlinear sloshing in a square-base tank with finite depth. Journal of Fluids and Structures 20, 81–103.

Gavory, T., 2005. Innovative tools open up new prospects for liquid motion model tests. In: Proceedings of Gastech, Bilbao, Spain.

Graczyk, M., 2008. Experimental investigation of sloshing loading and load effects in membrane LNG tanks subject to random excitation. Ph.D. Thesis, Norwegian University of Science and Technology, Trondheim, Norway.

Graczyk, M., Moan, T., Rognebakke, O., 2006. Probabilistic analysis of characteristic pressure for LNG tanks. Journal of Offshore Mechanics and Arctic Engineering Transactions of the ASME 128, 133–144.

Graczyk, M., Moan, T., Wu, M.K., 2007. Extreme sloshing and whipping-induced pressures and structural response in membrane LNG tanks. Ships and Offshore Structures 2 (3), 201–216.

Haver, S., 1980. Analysis of uncertainties related to the stochastic modeling of ocean waves. Ph.D. Thesis, Division of Marine Structures, The University of Trondheim, Norway.

Kim, Y., Shin, Y.S., Lee, K.H., 2004. Numerical study on slosh-induced impact pressures on three-dimensional prismatic tanks. Applied Ocean Research 26, 213–226.

Kishev, Z.R., Hu, C., Kashiwagi, M., 2006. Numerical simulation of violent sloshing by a CIP-based method. Journal of Marine Science and Technology 11, 111–122.

Lee, D.H., Kim, M.H., Kwon, S.H., Kim, J.W., Lee, Y.B., 2007. A parametric sensitivity study on LNG tank sloshing loads by numerical simulations. Ocean Engineering 34 (1), 3–9.

Madsen, H.O., Krenk, S., Lind, N.C., 1986. Methods of Structural Safety. Prentice-Hall International Inc., New Jersey.

Moan, T., Graczyk, M., Shu, Z., Rognebakke, O., 2006. Recent developments of structural design of ships based on direct calculations—with emphasis on LNG carriers. In: Proceedings of the International Conference on Ship and Shipping Research, NAV, Genova, Italy.

Naess, A., 1998. Estimation of long return period design values for wind speeds. Journal of Engineering Mechanics 3, 252–259.

Neves, C., Scotto, M.G., Guedes Soares, C., 2006. On the statistical choice of extreme domains of attraction in long-term predictions of significant wave height. In: Proceedings of OMAE, Hamburg, Germany.

Pastoor, W., Østvold, T.K., Byklum, E., Valsgård, S., 2005. Sloshing load and response in LNG carriers for new designs, new operations and new trades. In: Proceedings of Gastech, Bilbao, Spain.

Pickands III, J., 1975. Statistical inference using extreme order statistics. Annals of Statistics 3 (1), 119–131.

RINA, 2006. Proceedings of the International Conference on Design, Construction & Operation on Natural Gas Carriers & Offshore Systems, ICSOT, Busan, Korea. The Royal Institution of Naval Architects.

Rognebakke, O.F., Hoff, J.R., Allers, J.M., Berget, K., Berge, B.O., Zhao, R., 2005. Experimental approaches for determining sloshing loads in LNG tanks. In: Proceedings of SNAME Annual Meeting, Houston, Texas, USA.

Rosén, A., 2005. Impact pressure distribution reconstruction from discrete point measurements. International Shipbuilding Progress 52 (1), 91–107.

Valsgård, S., Østvold, T.K., Rognebakke, O., Byklum, E., Sele, H.O., 2006. Gas carrier development for an expanding market. In: RINA.

Winterstein, S.R., Ude, T.C., Cornell, C.A., Bjerager, P., Haver, S., 1994. Environmental parameters for extreme response: inverse form with omission factors. In: Schuëller, G.I., Shinozuka, M., Yao, J.T.P. (Eds.), Structural Safety and Reliability. Balkema, Rotterdam, pp. 551–557.

Zalar, M., Cambos, P., Besse, P., Le Gallo, B., Mravak, Z., 2005. Partial filling of membrane type LNG carriers. In: Proceedings of Gastech, Bilbao, Spain.

Paper 5:

Graczyk M. and Moan T.

Structural Response to Sloshing Excitation in Membrane LNG Tank.

Submitted for publication.

Is not included due to copyright

R A P P O R T E R
UTGITT VED
INSTITUTT FOR MARIN TEKNIKK
(tidligere: FAKULTET FOR MARIN TEKNIKK)
NORGES TEKNISK-NATURVITENSKAPELIGE UNIVERSITET

UR-79-01 Brigt Hatlestad, MK:	The finite element method used in a fatigue evaluation of fixed offshore platforms. (Dr.Ing. Thesis)
UR-79-02 Erik Pettersen, MK:	Analysis and design of cellular structures. (Dr.Ing. Thesis)
UR-79-03 Sverre Valsgård, MK:	Finite difference and finite element methods applied to nonlinear analysis of plated structures. (Dr.Ing. Thesis)
UR-79-04 Nils T. Nordsve, MK:	Finite element collapse analysis of structural members considering imperfections and stresses due to fabrication. (Dr.Ing. Thesis)
UR-79-05 Ivar J. Fylling, MK:	Analysis of towline forces in ocean towing systems. (Dr.Ing. Thesis)
UR-80-06 Nils Sandsmark, MM:	Analysis of Stationary and Transient Heat Conduction by the Use of the Finite Element Method. (Dr.Ing. Thesis)
UR-80-09 Sverre Haver, MK:	Analysis of uncertainties related to the stochastic modelling of ocean waves. (Dr.Ing. Thesis)
UR-85-46 Alf G. Engseth, MK:	Finite element collapse analysis of tubular steel offshore structures. (Dr.Ing. Thesis)
UR-86-47 Dengody Sheshappa, MP:	A Computer Design Model for Optimizing Fishing Vessel Designs Based on Techno-Economic Analysis. (Dr.Ing. Thesis)
UR-86-48 Vidar Aanesland, MH:	A Theoretical and Numerical Study of Ship Wave Resistance. (Dr.Ing. Thesis)
UR-86-49 Heinz-Joachim Wessel, MK:	Fracture Mechanics Analysis of Crack Growth in Plate Girders. (Dr.Ing. Thesis)
UR-86-50 Jon Taby, MK:	Ultimate and Post-ultimate Strength of Dented Tubular Members. (Dr.Ing. Thesis)

UR-86-51 Walter Lian, MH:	A Numerical Study of Two-Dimensional Separated Flow Past Bluff Bodies at Moderate KC-Numbers. (Dr.Ing. Thesis)
UR-86-52 Bjørn Sortland, MH:	Force Measurements in Oscillating Flow on Ship Sections and Circular Cylinders in a U-Tube Water Tank. (Dr.Ing. Thesis)
UR-86-53 Kurt Strand, MM:	A System Dynamic Approach to One-dimensional Fluid Flow. (Dr.Ing. Thesis)
UR-86-54 Arne Edvin Løken, MH:	Three Dimensional Second Order Hydrodynamic Effects on Ocean Structures in Waves. (Dr.Ing. Thesis)
UR-86-55 Sigurd Falch, MH:	A Numerical Study of Slamming of Two-Dimensional Bodies. (Dr.Ing. Thesis)
UR-87-56 Arne Braathen, MH:	Application of a Vortex Tracking Method to the Prediction of Roll Damping of a Two-Dimension Floating Body. (Dr.Ing. Thesis)
UR-87-57 Bernt Leira, MR:	Gaussian Vector Processes for Reliability Analysis involving Wave-Induced Load Effects. (Dr.Ing. Thesis)
UR-87-58 Magnus Småvik, MM:	Thermal Load and Process Characteristics in a Two-Stroke Diesel Engine with Thermal Barriers (in Norwegian). (Dr.Ing. Thesis)
MTA-88-59 Bernt Arild Bremdal, MP:	An Investigation of Marine Installation Processes - A Knowledge - Based Planning Approach. (Dr.Ing. Thesis)
MTA-88-60 Xu Jun, MK:	Non-linear Dynamic Analysis of Space-framed Offshore Structures. (Dr.Ing. Thesis)
MTA-89-61 Gang Miao, MH:	Hydrodynamic Forces and Dynamic Responses of Circular Cylinders in Wave Zones. (Dr.Ing. Thesis)
MTA-89-62 Martin Greenhow, MH:	Linear and Non-Linear Studies of Waves and Floating Bodies. Part I and Part II. (Dr.Techn. Thesis)
MTA-89-63 Chang Li, MH:	Force Coefficients of Spheres and Cubes in Oscillatory Flow with and without Current. (Dr.Ing. Thesis)
MTA-89-64 Hu Ying, MP:	A Study of Marketing and Design in

	Development of Marine Transport Systems. (Dr.Ing. Thesis)
MTA-89-65 Arild Jæger, MH:	Seakeeping, Dynamic Stability and Performance of a Wedge Shaped Planing Hull. (Dr.Ing. Thesis)
MTA-89-66 Chan Siu Hung, MM:	The dynamic characteristics of tilting-pad bearings.
MTA-89-67 Kim Wikstrøm, MP:	Analysis av projekteringen for ett offshore projekt. (Licenciat-avhandling)
MTA-89-68 Jiao Guoyang, MR:	Reliability Analysis of Crack Growth under Random Loading, considering Model Updating. (Dr.Ing. Thesis)
MTA-89-69 Arnt Olufsen, MK:	Uncertainty and Reliability Analysis of Fixed Offshore Structures. (Dr.Ing. Thesis)
MTA-89-70 Wu Yu-Lin, MR:	System Reliability Analyses of Offshore Structures using improved Truss and Beam Models. (Dr.Ing. Thesis)
MTA-90-71 Jan Roger Hoff, MH:	Three-dimensional Green function of a vessel with forward speed in waves. (Dr.Ing. Thesis)
MTA-90-72 Rong Zhao, MH:	Slow-Drift Motions of a Moored Two-Dimensional Body in Irregular Waves. (Dr.Ing. Thesis)
MTA-90-73 Atle Minsaas, MP:	Economical Risk Analysis. (Dr.Ing. Thesis)
MTA-90-74 Knut-Aril Farnes, MK:	Long-term Statistics of Response in Non-linear Marine Structures. (Dr.Ing. Thesis)
MTA-90-75 Torbjørn Sotberg, MK:	Application of Reliability Methods for Safety Assessment of Submarine Pipelines. (Dr.Ing. Thesis)
MTA-90-76 Zeuthen, Steffen, MP:	SEAMAID. A computational model of the design process in a constraint-based logic programming environment. An example from the offshore domain. (Dr.Ing. Thesis)
MTA-91-77 Haagensen, Sven, MM:	Fuel Dependant Cyclic Variability in a Spark Ignition Engine - An Optical Approach. (Dr.Ing. Thesis)
MTA-91-78 Løland, Geir, MH:	Current forces on and flow through fish farms.

	(Dr.Ing. Thesis)
MTA-91-79 Hoen, Christopher, MK:	System Identification of Structures Excited by Stochastic Load Processes. (Dr.Ing. Thesis)
MTA-91-80 Haugen, Stein, MK:	Probabilistic Evaluation of Frequency of Collision between Ships and Offshore Platforms. (Dr.Ing. Thesis)
MTA-91-81 Sødahl, Nils, MK:	Methods for Design and Analysis of Flexible Risers. (Dr.Ing. Thesis)
MTA-91-82 Ormberg, Harald, MK:	Non-linear Response Analysis of Floating Fish Farm Systems. (Dr.Ing. Thesis)
MTA-91-83 Marley, Mark J., MK:	Time Variant Reliability under Fatigue Degradation. (Dr.Ing. Thesis)
MTA-91-84 Krokstad, Jørgen R., MH:	Second-order Loads in Multidirectional Seas. (Dr.Ing. Thesis)
MTA-91-85 Molteberg, Gunnar A., MM:	The Application of System Identification Techniques to Performance Monitoring of Four Stroke Turbocharged Diesel Engines. (Dr.Ing. Thesis)
MTA-92-86 Mørch, Hans Jørgen Bjelke, MH:	Aspects of Hydrofoil Design: with Emphasis on Hydrofoil Interaction in Calm Water. (Dr.Ing. Thesis)
MTA-92-87 Chan Siu Hung, MM:	Nonlinear Analysis of Rotordynamic Instabilities in High-speed Turbomachinery. (Dr.Ing. Thesis)
MTA-92-88 Bessason, Bjarni, MK:	Assessment of Earthquake Loading and Response of Seismically Isolated Bridges. (Dr.Ing. Thesis)
MTA-92-89 Langli, Geir, MP:	Improving Operational Safety through exploitation of Design Knowledge - an investigation of offshore platform safety. (Dr.Ing. Thesis)
MTA-92-90 Sævik, Svein, MK:	On Stresses and Fatigue in Flexible Pipes. (Dr.Ing. Thesis)
MTA-92-91 Ask, Tor Ø., MM:	Ignition and Flame Growth in Lean Gas-Air Mixtures. An Experimental Study with a Schlieren System. (Dr.Ing. Thesis)

MTA-86-92 Hessen, Gunnar, MK:	Fracture Mechanics Analysis of Stiffened Tubular Members. (Dr.Ing. Thesis)
MTA-93-93 Steinebach, Christian, MM:	Knowledge Based Systems for Diagnosis of Rotating Machinery. (Dr.Ing. Thesis)
MTA-93-94 Dalane, Jan Inge, MK:	System Reliability in Design and Maintenance of Fixed Offshore Structures. (Dr.Ing. Thesis)
MTA-93-95 Steen, Sverre, MH:	Cobblestone Effect on SES. (Dr.Ing. Thesis)
MTA-93-96 Karunakaran, Daniel, MK:	Nonlinear Dynamic Response and Reliability Analysis of Drag-dominated Offshore Platforms. (Dr.Ing. Thesis)
MTA-93-97 Hagen, Arnulf, MP:	The Framework of a Design Process Language. (Dr.Ing. Thesis)
MTA-93-98 Nordrik, Rune, MM:	Investigation of Spark Ignition and Autoignition in Methane and Air Using Computational Fluid Dynamics and Chemical Reaction Kinetics. A Numerical Study of Ignition Processes in Internal Combustion Engines. (Dr.Ing. Thesis)
MTA-94-99 Passano, Elizabeth, MK:	Efficient Analysis of Nonlinear Slender Marine Structures. (Dr.Ing. Thesis)
MTA-94-100 Kvålsvold, Jan, MH:	Hydroelastic Modelling of Wetdeck Slamming on Multihull Vessels. (Dr.Ing. Thesis)
MTA-94-102 Bech, Sidsel M., MK:	Experimental and Numerical Determination of Stiffness and Strength of GRP/PVC Sandwich Structures. (Dr.Ing. Thesis)
MTA-95-103 Paulsen, Hallvard, MM:	A Study of Transient Jet and Spray using a Schlieren Method and Digital Image Processing. (Dr.Ing. Thesis)
MTA-95-104 Hovde, Geir Olav, MK:	Fatigue and Overload Reliability of Offshore Structural Systems, Considering the Effect of Inspection and Repair. (Dr.Ing. Thesis)
MTA-95-105 Wang, Xiaozhi, MK:	Reliability Analysis of Production Ships with Emphasis on Load Combination and Ultimate Strength. (Dr.Ing. Thesis)
MTA-95-106 Ulstein, Tore, MH:	Nonlinear Effects of a Flexible Stern Seal Bag on Cobblestone Oscillations of an SES. (Dr.Ing. Thesis)

MTA-95-107 Solaas, Frøydis, MH:	Analytical and Numerical Studies of Sloshing in Tanks. (Dr.Ing. Thesis)
MTA-95-108 Hellan, øyvind, MK:	Nonlinear Pushover and Cyclic Analyses in Ultimate Limit State Design and Reassessment of Tubular Steel Offshore Structures. (Dr.Ing. Thesis)
MTA-95-109 Hermundstad, Ole A., MK:	Theoretical and Experimental Hydroelastic Analysis of High Speed Vessels. (Dr.Ing. Thesis)
MTA-96-110 Bratland, Anne K., MH:	Wave-Current Interaction Effects on Large-Volume Bodies in Water of Finite Depth. (Dr.Ing. Thesis)
MTA-96-111 Herfjord, Kjell, MH:	A Study of Two-dimensional Separated Flow by a Combination of the Finite Element Method and Navier-Stokes Equations. (Dr.Ing. Thesis)
MTA-96-112 Æsøy, Vilmar, MM:	Hot Surface Assisted Compression Ignition in a Direct Injection Natural Gas Engine. (Dr.Ing. Thesis)
MTA-96-113 Eknes, Monika L., MK:	Escalation Scenarios Initiated by Gas Explosions on Offshore Installations. (Dr.Ing. Thesis)
MTA-96-114 Erikstad, Stein O., MP:	A Decision Support Model for Preliminary Ship Design. (Dr.Ing. Thesis)
MTA-96-115 Pedersen, Egil, MH:	A Nautical Study of Towed Marine Seismic Streamer Cable Configurations. (Dr.Ing. Thesis)
MTA-97-116 Moksnes, Paul O., MM:	Modelling Two-Phase Thermo-Fluid Systems Using Bond Graphs. (Dr.Ing. Thesis)
MTA-97-117 Halse, Karl H., MK:	On Vortex Shedding and Prediction of Vortex-Induced Vibrations of Circular Cylinders. (Dr.Ing. Thesis)
MTA-97-118 Igland, Ragnar T., MK:	Reliability Analysis of Pipelines during Laying, considering Ultimate Strength under Combined Loads. (Dr.Ing. Thesis)
MTA-97-119 Pedersen, Hans-P., MP:	Levendefiskteknologi for fiskefartøy. (Dr.Ing. Thesis)
MTA-98-120 Vikestad, Kyrre, MK:	Multi-Frequency Response of a Cylinder Subjected to Vortex Shedding and Support

	Motions. (Dr.Ing. Thesis)
MTA-98-121 Azadi, Mohammad R. E., MK:	Analysis of Static and Dynamic Pile-Soil-Jacket Behaviour. (Dr.Ing. Thesis)
MTA-98-122 Ulltang, Terje, MP:	A Communication Model for Product Information. (Dr.Ing. Thesis)
MTA-98-123 Torbergsen, Erik, MM:	Impeller/Diffuser Interaction Forces in Centrifugal Pumps. (Dr.Ing. Thesis)
MTA-98-124 Hansen, Edmond, MH:	A Discrete Element Model to Study Marginal Ice Zone Dynamics and the Behaviour of Vessels Moored in Broken Ice. (Dr.Ing. Thesis)
MTA-98-125 Videiro, Paulo M., MK:	Reliability Based Design of Marine Structures. (Dr.Ing. Thesis)
MTA-99-126 Mainçon, Philippe, MK:	Fatigue Reliability of Long Welds Application to Titanium Risers. (Dr.Ing. Thesis)
MTA-99-127 Haugen, Elin M., MH:	Hydroelastic Analysis of Slamming on Stiffened Plates with Application to Catamaran Wetdecks. (Dr.Ing. Thesis)
MTA-99-128 Langhelle, Nina K., MK:	Experimental Validation and Calibration of Nonlinear Finite Element Models for Use in Design of Aluminium Structures Exposed to Fire. (Dr.Ing. Thesis)
MTA-99-129 Berstad, Are J., MK:	Calculation of Fatigue Damage in Ship Structures. (Dr.Ing. Thesis)
MTA-99-130 Andersen, Trond M., MM:	Short Term Maintenance Planning. (Dr.Ing. Thesis)
MTA-99-131 Tveiten, Bård Wathne, MK:	Fatigue Assessment of Welded Aluminium Ship Details. (Dr.Ing. Thesis)
MTA-99-132 Søreide, Fredrik, MP:	Applications of underwater technology in deep water archaeology. Principles and practice. (Dr.Ing. Thesis)
MTA-99-133 Tønnessen, Rune, MH:	A Finite Element Method Applied to Unsteady Viscous Flow Around 2D Blunt Bodies With Sharp Corners. (Dr.Ing. Thesis)
MTA-99-134 Elvekrok, Dag R., MP:	Engineering Integration in Field Development Projects in the Norwegian Oil and Gas Industry. The Supplier Management of Norne. (Dr.Ing.

	Thesis)
MTA-99-135 Fagerholt, Kjetil, MP:	Optimeringsbaserte Metoder for Ruteplanlegging innen skipsfart. (Dr.Ing. Thesis)
MTA-99-136 Bysveen, Marie, MM:	Visualization in Two Directions on a Dynamic Combustion Rig for Studies of Fuel Quality. (Dr.Ing. Thesis)
MTA-2000-137 Storteig, Eskild, MM:	Dynamic characteristics and leakage performance of liquid annular seals in centrifugal pumps. (Dr.Ing. Thesis)
MTA-2000-138 Sagli, Gro, MK:	Model uncertainty and simplified estimates of long term extremes of hull girder loads in ships. (Dr.Ing. Thesis)
MTA-2000-139 Tronstad, Harald, MK:	Nonlinear analysis and design of cable net structures like fishing gear based on the finite element method. (Dr.Ing. Thesis)
MTA-2000-140 Kroneberg, André, MP:	Innovation in shipping by using scenarios. (Dr.Ing. Thesis)
MTA-2000-141 Haslum, Herbjørn Alf, MH:	Simplified methods applied to nonlinear motion of spar platforms. (Dr.Ing. Thesis)
MTA-2001-142 Samdal, Ole Johan, MM:	Modelling of Degradation Mechanisms and Stressor Interaction on Static Mechanical Equipment Residual Lifetime. (Dr.Ing. Thesis)
MTA-2001-143 Baarholm, Rolf Jarle, MH:	Theoretical and experimental studies of wave impact underneath decks of offshore platforms. (Dr.Ing. Thesis)
MTA-2001-144 Wang, Lihua, MK:	Probabilistic Analysis of Nonlinear Wave-induced Loads on Ships. (Dr.Ing. Thesis)
MTA-2001-145 Kristensen, Odd H. Holt, MK:	Ultimate Capacity of Aluminium Plates under Multiple Loads, Considering HAZ Properties. (Dr.Ing. Thesis)
MTA-2001-146 Greco, Marilena, MH:	A Two-Dimensional Study of Green-Water Loading. (Dr.Ing. Thesis)
MTA-2001-147 Heggelund, Svein E., MK:	Calculation of Global Design Loads and Load Effects in Large High Speed Catamarans. (Dr.Ing. Thesis)

MTA-2001-148 Babalola, Olusegun T., MK:	Fatigue Strength of Titanium Risers - Defect Sensitivity. (Dr.Ing. Thesis)
MTA-2001-149 Mohammed, Abuu K., MK:	Nonlinear Shell Finite Elements for Ultimate Strength and Collapse Analysis of Ship Structures. (Dr.Ing. Thesis)
MTA-2002-150 Holmedal, Lars E., MH:	Wave-current interactions in the vicinity of the sea bed. (Dr.Ing. Thesis)
MTA-2002-151 Rognebakke, Olav F., MH:	Sloshing in rectangular tanks and interaction with ship motions. (Dr.Ing. Thesis)
MTA-2002-152 Lader, Pål Furset, MH:	Geometry and Kinematics of Breaking Waves. (Dr.Ing. Thesis)
MTA-2002-153 Yang, Qinzheng, MH:	Wash and wave resistance of ships in finite water depth. (Dr.Ing. Thesis)
MTA-2002-154 Melhus, Øyvin, MM:	Utilization of VOC in Diesel Engines. Ignition and combustion of VOC released by crude oil tankers. (Dr.Ing. Thesis)
MTA-2002-155 Ronæss, Marit, MH:	Wave Induced Motions of Two Ships Advancing on Parallel Course. (Dr.Ing. Thesis)
MTA-2002-156 Økland, Ole D., MK:	Numerical and experimental investigation of whipping in twin hull vessels exposed to severe wet deck slamming. (Dr.Ing. Thesis)
MTA-2002-157 Ge, Chunhua, MK:	Global Hydroelastic Response of Catamarans due to Wet Deck Slamming. (Dr.Ing. Thesis)
MTA-2002-158 Byklum, Eirik, MK:	Nonlinear Shell Finite Elements for Ultimate Strength and Collapse Analysis of Ship Structures. (Dr.Ing. Thesis)
IMT-2003-1 Chen, Haibo, MK:	Probabilistic Evaluation of FPSO-Tanker Collision in Tandem Offloading Operation. (Dr.Ing. Thesis)
IMT-2003-2 Skaugset, Kjetil Bjørn, MK:	On the Suppression of Vortex Induced Vibrations of Circular Cylinders by Radial Water Jets. (Dr.Ing. Thesis)
IMT-2003-3 Chezhian, Muthu	Three-Dimensional Analysis of Slamming. (Dr.Ing. Thesis)
IMT-2003-4 Buhaug, Øyvind	Deposit Formation on Cylinder Liner Surfaces

	in Medium Speed Engines. (Dr.Ing. Thesis)
IMT-2003-5 Tregde, Vidar	Aspects of Ship Design: Optimization of Aft Hull with Inverse Geometry Design. (Dr.Ing. Thesis)
IMT-2003-6 Wist, Hanne Therese	Statistical Properties of Successive Ocean Wave Parameters. (Dr.Ing. Thesis)
IMT-2004-7 Ransau, Samuel	Numerical Methods for Flows with Evolving Interfaces. (Dr.Ing. Thesis)
IMT-2004-8 Soma, Torkel	Blue-Chip or Sub-Standard. A data interrogation approach of identity safety characteristics of shipping organization. (Dr.Ing. Thesis)
IMT-2004-9 Ersdal, Svein	An experimental study of hydrodynamic forces on cylinders and cables in near axial flow. (Dr.Ing. Thesis)
IMT-2005-10 Brodtkorb, Per Andreas	The Probability of Occurrence of Dangerous Wave Situations at Sea. (Dr.Ing. Thesis)
IMT-2005-11 Yttervik, Rune	Ocean current variability in relation to offshore engineering. (Dr.Ing. Thesis)
IMT-2005-12 Fredheim, Arne	Current Forces on Net-Structures. (Dr.Ing. Thesis)
IMT-2005-13 Heggernes, Kjetil	Flow around marine structures. (Dr.Ing. Thesis)
IMT-2005-14 Fouques, Sebastien	Lagrangian Modelling of Ocean Surface Waves and Synthetic Aperture Radar Wave Measurements. (Dr.Ing. Thesis)
IMT-2006-15 Holm, Håvard	Numerical calculation of viscous free surface flow around marine structures. (Dr.Ing. Thesis)
IMT-2006-16 Bjørheim, Lars G.	Failure Assessment of Long Through Thickness Fatigue Cracks in Ship Hulls. (Dr.Ing. Thesis)
IMT-2006-17 Hansson, Lisbeth	Safety Management for Prevention of Occupational Accidents. (Dr.Ing. Thesis)
IMT-2006-18 Zhu, Xinying	Application of the CIP Method to Strongly Nonlinear Wave-Body Interaction Problems. (Dr.Ing. Thesis)
IMT-2006-19 Reite, Karl Johan	Modelling and Control of Trawl Systems.

	(Dr.Ing. Thesis)
IMT-2006-20 Smogeli, Øyvind Notland	Control of Marine Propellers. From Normal to Extreme Conditions. (Dr.Ing. Thesis)
IMT-2007-21 Storhaug, Gaute	Experimental Investigation of Wave Induced Vibrations and Their Effect on the Fatigue Loading of Ships. (Dr.Ing. Thesis)
IMT-2007-22 Sun, Hui	A Boundary Element Method Applied to Strongly Nonlinear Wave-Body Interaction Problems. (PhD Thesis, CeSOS)
IMT-2007-23 Rustad, Anne Marthine	Modelling and Control of Top Tensioned Risers. (PhD Thesis, CeSOS)
IMT-2007-24 Johansen, Vegar	Modelling flexible slender system for real-time simulations and control applications.
IMT-2007-25 Wroldsen, Anders Sunde	Modelling and control of tensegrity structures. (PhD Thesis, CeSOS)
IMT-2007-26 Aronsen, Kristoffer Høye	An experimental investigation of in-line and combined in-line and cross flow vortex induced vibrations. (Dr.avhandling, IMT)
IMT-2007-27 Zhen, Gao	Stochastic response analysis of mooring systems with emphasis on frequency-domain analysis of fatgue due to wide-band processes. (PhD-thesis CeSOS).
IMT-2007-28 Thorstensen, Tom Anders	Lifetime Profit Modelling of Ageing Systems Utilizing Information about Technical Condition Dr.ing. thesis, IMT.
IMT-2008-29 Berntsen, Per Ivar B.	Structural Reliability Based Position Mooring. PhD-Thesis, IMT.
IMT-2008-30 Ye, Naiquan	Fatigues Assessment of Aluminium Welded Box stiffener Joints in ships. Dr.ing.-Thesis, IMT.
IMT-2008-31 Radan, Damir	Integrated Control of Marine Electrical Power Systems. PhD-Thesis, IMT.
IMT-2008-32 Norum, Viggo L.	Analysis of Ignituin and Combustion in Otto Lean-Burn Engines with Prechambers. Dr.ing. thesis, IMT.
IMT-2008-33 Pákozdi, Csaba	A Smoothed Particle Hydrodynamics Study of Two-dimensional Nonlinear Sloshing in

	Rectangular Tanks. Dr.ing.thesis, IMT.
IMT-2008-34 Grytøyr, Guttorm	A Higher-Order Boundary Element Method and Applications to Marine Hydrodynamics. Dr.ing. Thesis, IMT.
IMT-2008-35 Drummen, Ingo	Experimental and Numerical Investigation of Nonlinear Wave-Induced Load effects in Containerships Considering Hydroelasticity. PhD-Thesis. CeSOS.
IMT-2008-36 Skejic, Renato	Maneuvering and Seakeeping of a Singel Ship and of Two Ships in Interaction. PhD-Thesis. CeSOS.
IMT-2008-37 Harlem, Alf	An Age-Based Replacement Model for Repairable Systems with Attention to High-Speed Marine Diesel Engines. PhD-Thesis, IMT.
IMT-2008-38 Alsos, Hagbart S.	Ship Grounding. Analysis of Ductile Fracture, Bottom Damage and Hull Girder Response. PhD-thesis, IMT.